

**Warsaw University of Technology**

FACULTY OF BUILDING SERVICES,  
HYDRO AND ENVIRONMENTAL ENGINEERING



# Master's diploma thesis

in the field of Urban Climate Studies

M.Sc Environmental Engineering

Urban Heat Island in Cities of Nepal

**DIPSON BHANDARI**

student record book number 330764

thesis supervisor  
Dr hab. inż. Lech Łobocki

Warsaw, 2025

**Statement of the author (authors) of thesis**  
*Oświadczenie autora (autorów) pracy dyplomowej*

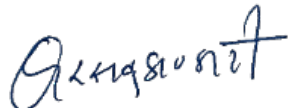
Being aware of my legal responsibility, I certify that this diploma:  
*Świadcom odpowiedzialności prawnej oświadczam, że przedstawiona praca dyplomowa:*

- has been written by me alone and does not contain any content obtained in a manner  
*została napisana przeze mnie samodzielnie i nie zawiera treści uzyskanych w sposób niezgodny*  
inconsistent with the applicable rules,  
*z obowiązującymi przepisami,*
- had not been previously subject to the procedures for obtaining professional title or  
*nie była wcześniej przedmiotem procedur związanych z uzyskaniem tytułu zawodowego lub*  
degree at the university.  
*stopnia naukowego w wyższej uczelni.*

Furthermore I declare that this version of the diploma thesis is identical with the electronic  
*Oświadczam ponadto, że niniejsza wersja pracy jest identyczna z wersją elektroniczną*  
version attached.  
*w załączniu.*

2025/01/01

date  
*data*



author ('s) signature  
*podpis autora (autorów) pracy*

## **ACKNOWLEDGEMENT**

First and foremost, I would like to express my heartfelt gratitude to my parents, my father and mother, Deepak Bhandari and Sharada Bhattarai Bhandari for their unconditional support and the values they imparted in me, which have shaped my character and achievements. I am truly grateful to my wonderful girlfriend, Uma, for standing by my side through all the highs and lows.

I extend my heartfelt appreciation to my supervisor, Dr. hab. inż. Lech Łobocki, whose lectures at Warsaw University of Technology enhanced my interest in this field of study and whose support and encouragement have been invaluable throughout my academic journey. I am also grateful to Dr. hab. inż. Joanna Strużewska and the team at the National Research Institute, Department of Atmosphere and Climate Modeling in Poland, for providing me an opportunity to work with them, as well as access to their resources, where I was able to learn and work with the WRF model.

## ABSTRACT

Nepal, a landlocked and developing country in South Asia, faces significant challenges from rapid and unplanned urbanization. The concentration of economic opportunities and resources in major cities, due to a centralized governance system, has further accelerated urban growth while neglecting the development of smaller towns and rural areas. This disparity has resulted in poorly managed urban expansion, leading to environmental, social, and infrastructural issues. One such concern is the growing impact of Urban Heat Island (UHI) effects, which exacerbate thermal discomfort in urban areas and pose risks to the sustainability of rapidly urbanizing regions.

The Urban Heat Island phenomenon, marked by elevated temperatures in urban areas compared to their rural surroundings, has emerged as a critical issue in the context of climate change and unchecked urbanization. This study examines the extent and dynamics of UHI effects in Nepal's major cities, with a focus on Kathmandu and Pokhara, both experiencing rapid urban growth. By employing satellite imagery and remote sensing techniques, the research analyzes Land Surface Temperature (LST) patterns to quantify surface-level UHI intensities. These observations provide a spatial overview of temperature distribution, highlighting the thermal hotspots associated with urban areas. To complement surface-level analyses, this research utilizes basic atmospheric modeling techniques within the Weather Research and Forecasting (WRF) framework to simulate canopy layer Urban Heat Island (UHI) effects. The WRF-Urban Canopy Model (WRF-UCM) was employed, integrating MODIS land cover datasets and Local Climate Zones (LCZ) to better represent urban surface characteristics. This approach allowed for the modeling of canopy layer temperature variations and the assessment of urban-induced microclimatic changes in Kathmandu. By combining remote sensing data with WRF-UCM simulations, the study provides insights into the UHI dynamics within Nepal's cities.

## STRESZCZENIE

Nepal, będący śródlądowym i rozwijającym się krajem w Azji Południowej, zmaga się z poważnymi wyzwaniami wynikającymi z szybkiej i nieplanowanej urbanizacji. Koncentracja możliwości ekonomicznych i zasobów w głównych miastach, spowodowana scentralizowanym systemem zarządzania, przyspieszyła wzrost urbanizacji, zaniedbując jednocześnie rozwój mniejszych miast i obszarów wiejskich. Ta dysproporcja doprowadziła do niekontrolowanego rozrostu miast, skutkując problemami środowiskowymi, społecznymi i infrastrukturalnymi. Jednym z takich problemów jest rosnący wpływ zjawiska miejskiej wyspy ciepła (Urban Heat Island, UHI), które pogłębia dyskomfort termiczny na obszarach miejskich i stanowi zagrożenie dla zrównoważonego rozwoju szybko urbanizujących się regionów.

Zjawisko miejskiej wyspy ciepła, charakteryzujące się podwyższonymi temperaturami na obszarach miejskich w porównaniu z ich wiejskimi otoczeniami, stało się kluczowym problemem w kontekście zmian klimatycznych i niekontrolowanej urbanizacji. Niniejsze badanie analizuje zakres i dynamikę efektów UHI w głównych miastach Nepalu, ze szczególnym uwzględnieniem Katmandu i Pokhary, które doświadczają szybkiego wzrostu urbanizacji. Wykorzystując zdjęcia satelitarne i techniki teledetekcji, badanie analizuje wzorce temperatury powierzchni ziemi (Land Surface Temperature, LST), aby oszacować intensywność UHI na poziomie powierzchni. Obserwacje te dostarczają przestrzennego przeglądu rozkładu temperatury, wskazując na termiczne hotspotty związane z obszarami miejskimi. W celu uzupełnienia analiz powierzchniowych, badanie wykorzystuje podstawowe techniki modelowania atmosferycznego w ramach systemu modelowania Weather Research and Forecasting (WRF), aby symulować efekty miejskiej wyspy ciepła w warstwie korony miejskiej (canopy layer). W badaniu zastosowano model WRF-Urban Canopy Model (WRF-UCM), integrując dane o pokryciu terenu z MODIS oraz lokalne strefy klimatyczne (Local Climate Zones, LCZ), aby lepiej odwzorować charakterystyki powierzchni miejskich. Takie podejście umożliwiło modelowanie zmian temperatury w warstwie korony miejskiej oraz ocenę mikroklimatycznych zmian wywołanych urbanizacją w Katmandu. Łącząc dane teledetekcyjne z symulacjami WRF-UCM, badanie dostarcza wglądu w dynamikę UHI w nepalskich miastach.

# Contents

<b>Chapter I: Introduction .....</b>	<b>1</b>
1.1. Background.....	1
1.2. Statement of Problem .....	2
1.3. Objectives of the Study.....	2
1.4. Outline of Research .....	3
<b>Chapter II: Literature Review.....</b>	<b>4</b>
2.1. Remote sensing Fundamentals.....	4
2.1.1 Application of Remote Sensing in Monitoring of Environment.....	4
2.1.2. Band Designations .....	5
2.2. Black Body radiation .....	5
2.3. Satellites .....	6
2.3.1 Landsat 8-9 OLI/TIRS.....	6
2.3.2 MODIS.....	7
2.3.3. Clustering of Satellite-Derived Data from Landsat and MODIS.....	8
2.4. Climate and meteorological factors influencing UHI.....	8
2.5. INTRODUCTION TO WRF.....	13
2.5.1. WRF terrestrial Data .....	13
2.6. WRF processing system (WPS) .....	14
2.6.1 Geogrid .....	14
2.6.2. Ungrid .....	15
2.6.3. Metgrid .....	15
2.7. WRF - URBAN ( URBAN CANOPY MODEL ) .....	16
2.8. Implementation of Local Climatic zone (LCZ) in WRF model.....	17
2.9. Computational Requirements and Challenges of running WRF simulations in High Terrain .....	18
<b>Chapter III: Data Description .....</b>	<b>19</b>
3.1. Geographic and Climatic Overview .....	19
3.1.1. Kathmandu .....	19
3.1.2. Pokhara.....	20
3.2. Selection of Cities .....	21
Criteria for Selection.....	21
3.3. Synoptic Stations .....	22
Pokhara Airport (0804) .....	22
Kathmandu Airport (1030) .....	23
3.4 Data description for Analysis based on remote sensing.....	24
3.5. Data Description for WRF-UCM ( Urban Canopy Model) .....	26
<b>Chapter IV: Methodology .....</b>	<b>27</b>
4.1. Supervised / Unsupervised land use classification .....	27
4.1.1 Unsupervised Classification .....	27
4.1.2 Supervised Classification .....	27

4.2. Normalized Difference Vegetation Index (NDVI).....	27
4.2.1. Application of NDVI for analysis of Urban Heat Island .....	28
4.2.2. Advantages and Disadvantages of remote sensing for analysis of Urban Heat Island.....	28
4.2.3. Correlation between NDVI and LST and categorization of LST based on Local Climate Zones .....	28
4.3. Methodology for WRF Simulation .....	29
4.3.1 Geogrid .....	29
4.3.2 Domain Configuration .....	30
4.3.3. Ungrib .....	32
4.3.4. Metgrid .....	32
4.4. WRF Physics Configurations .....	32
4.5. Urban Parameterization .....	33
<b>Chapter V: Analysis and Observations .....</b>	<b>34</b>
5.1. Calculation of Land Surface Temperature using Landsat .....	34
5.2. Workflow process in MODIS Metadata. ....	35
5.3. Computational Environment for WRF Simulation .....	37
5.4. Land Used Land Covered (LULC) using Unsupervised Classification.....	38
5.5. Preparation of Local Climate Zone (LCZ) Map for Area of Interest .....	40
5.6. Observation of Land Surface Temperature (LST) of Kathmandu .....	42
5.6.1. Winter Season .....	42
5.6.2 Summer Season .....	43
5.7. Observation of Land Surface Temperature (LST) of Pokhara .....	45
5.7.1. Winter Season .....	45
5.7.2. Summer Season .....	46
5.8. Findings based on Satellite based Remote Sensing.....	51
5.9. Post processing of WRF Model output .....	52
3.15.1. Initial Test Run .....	53
5.9.1. Summer Season (Kathmandu).....	55
5.9.2. Winter Season (Kathmandu) .....	56
<b>Chapter VI: Conclusion .....</b>	<b>60</b>
6.1. Urban Heat Island Dynamics in Kathmandu and Pokhara.....	60
6.2.WRF Model Simulations for Kathmandu .....	60
6.3. Comparison of UHI intensities in Kathmandu and Pokhara .....	61
<b>References .....</b>	<b>62</b>
<b>List of Figures .....</b>	<b>64</b>
<b>List of Tables .....</b>	<b>66</b>
<b>Appendices .....</b>	<b>67</b>

## Chapter I: Introduction

### 1.1. Background

Heat islands are urbanized areas that experience higher temperatures than outlying areas. Structures such as buildings, roads, and other infrastructure absorb and re-emit the sun's heat more than natural landscapes such as forests and water bodies. According to the Environmental Protection Agency, the annual air temperature of a city with 1 million people can be 1.8–5.4 degrees Fahrenheit (1–3 degrees Celsius) warmer than its surroundings. There are many reasons for the UHI to take place, some of the reasons are the use of building materials which have very high insulating capacities. Such type of materials holds the heat, this insulation makes the areas warmer (National Geographic, n.d.). When the areas are highly populated, the number of people in a small space is high and there is densely constructed buildings and infrastructures like roads which uses highly heat absorbing material like concrete. This effect generally remains high during the night because the heat coming from the concrete surfaces resists from rising to the colder temperature and it is trapped, thus making the area warmer.

Nepal is a developing country experiencing unmanaged urbanization, where the widespread use of construction materials like concrete has contributed significantly to the Urban Heat Island (UHI) effect, disrupting the thermal comfort of urban areas. Kathmandu and Pokhara are two of Nepal's most prominent cities, each with its distinct identity. Kathmandu, as the capital, attracts a large population from across the country due to its centralized development, while Pokhara serves as a major tourism hub and gateway, drawing both domestic and international visitors.

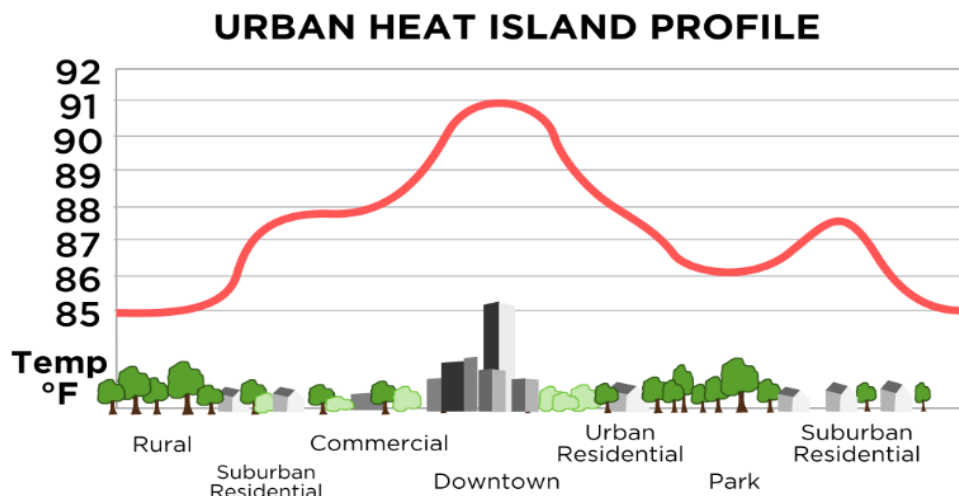


Figure 1: Urban Heat Island Profile, [Wikipedia,n.d.]

On July 14, 2021, Climate Central .United States of America released a report ,where the scientists and researchers created an index to evaluate the intensity of urban heat islands and applied it to cities across the nation. Population density was one of the top six factors that researchers considered while creating the index for the study. The others included albedo, percentage of greenery, building height and average width of streets and irregularity of the city. Out of this this albedo contributed the most. (AccuWeather, n.d.). From this we can say that it can be more rapid in underdeveloped or developing countries that has higher population growth rate and more centralized government system. Albedo

defines the intensity of heat absorbed by a particular material, it can be differ for each material. For example, the darker bodies absorb more radiation.

## **1.2. Statement of Problem**

Urbanization is rapidly transforming the landscape of Nepal, with cities experiencing unprecedented growth in population and infrastructure. However, this urban expansion brings with it a host of challenges, including the intensification of urban heat islands (UHIs). UHIs, characterized by elevated temperatures in urban areas compared to their rural surroundings, pose significant risks to public health, energy consumption, and environmental sustainability. In the context of Nepal, where cities are densely populated and often situated in geographically challenging terrain, the impact of UHIs needs an attention. The Kathmandu Valley which is the capital city of Nepal accounts for nearly about one fourth of the country's urban population (22% of urban population) and continues to sustain a fast pace of population growth. The valley is characterized by high and sustained population growth in the urban core and fast urban sprawling at the periphery.

The Central Development Region (now Bagmati Province) has the highest proportion of the urban population in Nepal, followed by Province 1 (formerly the Eastern Region) and Gandaki Province. Kathmandu Valley remains the central hub of urban development in the country. Nepal's centralized development approach has been a major driver of urbanization, resulting in the concentration of population and infrastructure in major cities. This migration contributes to reduced vegetation cover and a growing reliance on construction materials with low albedo, which amplifies Urban Heat Island (UHI) effects.

Kathmandu is also one of the most polluted cities in the world, and Pokhara, a major tourism hub experiencing rapid urbanization, are both significantly affected by the Urban Heat Island (UHI) effect because of this rapid development. In Kathmandu, UHI not only impacts thermal comfort but also traps harmful pollutants at surface and atmospheric levels, posing serious health risks to residents and disrupting the ecosystem. Similarly, the rising urbanization in Pokhara has the potential to exacerbate these challenges, threatening the city's environmental balance and appeal as a tourist destination. Monitoring and analyzing the current intensity of UHI effects in these cities is a critical first step toward raising awareness and implementing effective mitigation strategies to protect public health, the environment, and the sustainable growth of urban areas.

## **1.3. Objectives of the Study**

The primary objective of this study is to explore the extent and characteristics of Urban Heat Island (UHI) effects in major cities of Nepal which are rapidly urbanizing, with a particular emphasis on Kathmandu and Pokhara. The research focuses on quantifying surface UHI intensity through the analysis of Land Surface Temperature (LST) patterns using satellite imagery and remote sensing techniques. Additionally, it aims to simulate atmospheric-level UHI effects utilizing the Weather Research and Forecasting (WRF) model, incorporating satellite-derived land use and land cover data.

The study employs the WRF-Urban Canopy Model (WRF-UCM) to simulate canopy layer UHI effects, integrating MODIS land cover datasets and Local Climate Zones (LCZ) for enhanced representation of urban surface characteristics. By utilizing satellite imagery from both Landsat and MODIS, the research

facilitates detailed modeling of canopy layer temperature variations and evaluates urban-induced climatic changes in Nepalese cities. Through the combination of remote sensing data and WRF-UCM simulations, this study seeks to provide a comprehensive understanding of UHI dynamics and their implications for urban environments in Nepal.

#### **1.4. Outline of Research**

This study examines the Urban Heat Island (UHI) phenomenon in key urban areas of Nepal, such as Kathmandu and Pokhara. Using a combination of remote sensing techniques and the Weather Research and Forecasting (WRF) model, the research focuses on analyzing UHI intensities in both surface and canopy layers. Land Surface Temperature (LST) is calculated from satellite imagery data (LANDSAT and MODIS) to quantify surface UHI effects across various Local Climate Zones (LCZs). Concurrently, the WRF-UCM (Single layer urban canopy model) simulates atmospheric UHI dynamics, utilizing the same high-resolution land cover data of LCZ classifications. By maintaining a consistent geodata resolution for both approaches, this research provides a understanding and extent of UHI characteristics in Nepal's urban centers, highlighting the impacts of urbanization on thermal comfort in the region.

## Chapter II: Literature Review

### 2.1. Remote sensing Fundamentals

Remote sensing involves obtaining information of the distant object in the form of radiation. The earth receives electromagnetic radiation from the sun, these radiations are absorbed, reflected and emitted by earth surface or atmosphere. The electromagnetic radiation spectrum has different types which varies according to its wavelength and frequency. The spectrum can be divided into several categories.

- **Radio waves:** Radio wave is the longest wavelength (millimeters to kilometers). They are used for radio and television broadcast and communications
- **Microwaves:** The wavelength of microwaves ranges from one millimeter to one meter and is used for radar technologies
- **Infrared Radiation:** The wavelength of infrared radiation ranges from 700nanometers to 1 millimeter.it can be used for several applications such as night vision and remote control.
- **Visible Light:** This is the portion of the spectrum that human eyes can detect. It has wavelengths from 400nm (violet) to 700nm(red).
- **Ultraviolet (UV) light :** Wavelength of ultraviolet radiation ranges from 10nm to 400nm.
- **X-rays:** X-rays have shorter wavelengths, less than 0.01nm and used for medical imaging and security.
- **Gamma Rays:** These radiations have the shortest wavelength, and they are emitted by radioactive materials.

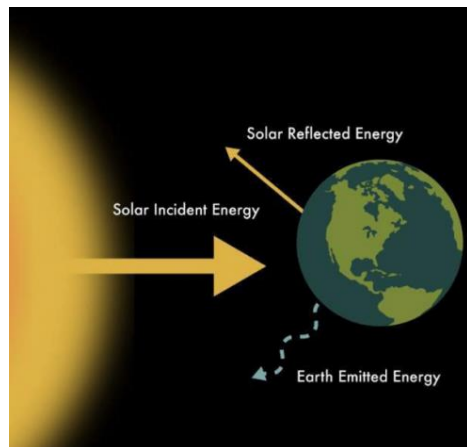


Figure 2 : Earth's Energy Budget [NASA,2022]

#### 2.1.1 Application of Remote Sensing in Monitoring of Environment

Satellites utilized various electromagnetic spectrums to capture information about the Earth's surface, ocean and atmosphere without any direct contact. It relies on the radiation like visible light, microwave and infrared to gather the information. Satellites are mounted with the sensor for detecting such type of radiation. Visible light which is used to capture images is used for vegetation analysis and urban planning. Similarly, near-infrared is used for accessing the plant health. Thermal infrared measures surface temperature which helps in climate studies. Synthetic Aperture Radar (SAR) operates

in the microwave range. It enables the observation of Earth's surface without depending on the weather conditions or sunlight. Ultraviolet light is used for monitoring atmospheric conditions like ozone levels and pollution. The data obtained from remote sensing can be used in real time analysis. It can also be used to feed the input data for various weather forecasting models. Satellites that are equipped with thermal infrared sensors can measure the surface temperature across urban and rural area. These sensors capture the heat emitted from the surface of the earth. Satellites such as Landsat and MODIS (Moderate resolution Imaging Spectroradiometer) can provide data on land surface temperatures to identify the Urban Heat Island.

### **2.1.2. Band Designations**

Band designation in remote sensing refers to the specific wavelengths or ranges of the electromagnetic spectrum that a sensor is designed to capture, typically categorized into spectral bands. These bands, such as visible, near-infrared (NIR), shortwave infrared (SWIR), and thermal infrared (TIR), are essential for various applications. For instance, visible and NIR bands are commonly used for vegetation analysis due to their sensitivity to chlorophyll absorption, while SWIR bands are effective in detecting moisture content and material composition. Thermal bands measure surface temperatures and are widely applied in environmental monitoring and urban heat island studies. The precise designation of bands depends on the sensor and its purpose, as seen in instruments like Landsat, MODIS, and Sentinel satellites, which are optimized for different scientific and practical uses (Jensen, 2015; Lillesand et al., 2015).

## **2.2. Black Body radiation**

A black body radiation is an idealized object that absorbs all the incident electromagnetic radiation, without depending on frequency or angle of incidence. It does not reflect any light and solely emits radiation based on its temperature. It is a theoretical foundation of how land surface emits thermal energy based on their temperature. This principle is essential for remote sensing for accurately estimating the land surface temperature, emissivity and analyzing the spatial and temporal temperature variation. According to the equation stated by (Planck, 1914; Tipler and Mosca, 2010),

$$I(v, t) = \frac{2hv^3}{c^2} \cdot \frac{1}{e^{hv/kT} - 1}$$

Where,

$I(v, t)$  = spectral radiance (energy per unit area per unit time per unit solid angle per unit frequency),

$h$  = Planck's constant. ( $6.626 * 10^{-34}$  Js)

$v$ =Frequency of the radiation

$c$  = Speed of light in a vacuum ( $3 * 10^8$ m/s).

$k$  = Boltzmann's constant ( $1.381 * 10^{-23}$  J/K)

$T$  = Absolute temperature of the black body in Kelvin

The total energy emitted by a blackbody across all the wavelengths can be understood by Stefan Boltzmann law

$$P = \sigma AT^4$$

Where,

$P$ = Total Power radiate

$k$  = Stefan -Boltzmann constant ( $5.67 * 10^{-8}$  W/M<sup>2</sup>K<sup>-4</sup>)

A = Surface area of the black body.

T = Absolute temperature in Kelvin

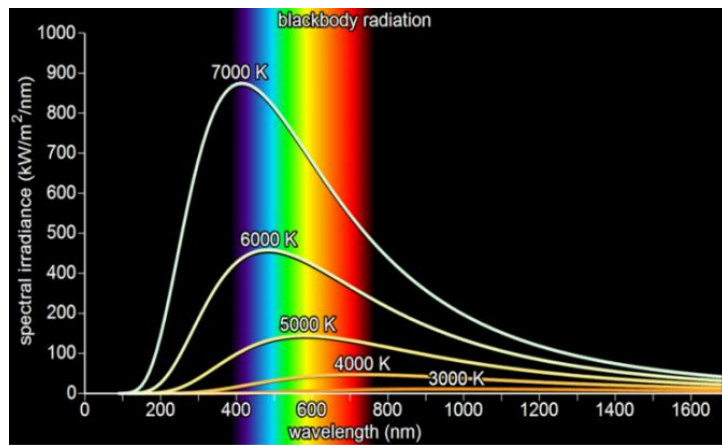


Figure 3 : Spectral Irradiance of Blackbody Radiation as a Function of Wavelength for Different Temperatures (howthingswork, n.d.)

The radiation spectrum of all the blackbodies depends on the temperature of the blackbody. The perfect blackbody does not exist. As the temperature increases, the color of the light emits changes. At lower temperatures such as room temperature, it gives the infrared light which we cannot see. As it gets hotter, it turns to yellow and then bluish-white at very high temperature. This is because the peak of its emitted light shifts toward higher frequencies. Cities have lots of dark surfaces (asphalts and buildings) that absorbs sunlight and heat up, acting like the black bodies. These surface heats up in the day and cools down during the night. As the surface heat up they emit infrared radiation, At night, the heat is released back into the atmosphere. Urban areas retain more heat than rural areas because of large number of bodies that absorb the radiation, resulting in higher temperatures during the nighttime.

### 2.3. Satellites

Satellites play an important role for monitoring the data on Earth's atmosphere, ocean and land surfaces. Satellites are released for a specific mission that involves tasks which is related to monitoring of environment which gives necessary information for analysis and observation. For the analysis of Urban heat island , Landsat 8 and Modis have been used.

#### 2.3.1 Landsat 8-9 OLI/TIRS

The Landsat mission was operated by National Aeronautics and space administration (NASA) and the Department of Interior (DOI) U.S. Geological Survey (USGS). Landsat provides the coverage of Earth's land surface. "The goal of Landsat is to continue the collection, archival, and distribution of multispectral imagery affording global, synoptic, and repetitive coverage of the Earth's land surfaces at a scale where natural and human-induced changes can be detected, differentiated, characterized, and monitored over time (USGS,2018).

Table 1 : Band Designations of Landsat OLI /TIRS

Band Number	Band Description	Band Range (nm)
1	Coastal Aerosol (Operational Land Imager (OLI))	435-451
2	Blue (OLI)	452-512
3	Green (OLI)	533-590
4	Red (OLI)	636-673
5	Near-Infrared (NIR) (OLI)	851-879
6	Short Wavelength Infrared (SWIR) 1 (OLI)	1566-1651
7	SWIR 2 (OLI)	2107-2294
8	Panchromatic (OLI)	503-676
9	Cirrus (OLI)	1363-1384
10	Thermal Infrared Sensor (TIRS) 1	10600-11190
11	TIRS 2	11500-12510

The table lists different spectral bands used by Operational Land imager (OLI) and Thermal Infrared Sensor (TIRS) . Each bands can capture different portions of the electromagnetic radiation spectrum, this allows monitoring applications. Various materials like vegetation, water, soil and clouds reflect and absorb electromagnetic radiation differently at different wavelengths. By the use of multiple spectral bands, satellites can obtain wide information from surface temperature to vegetation health and water quality. For example, for Visible light spectrum (400-700nm), red and green bands are chlorophyll sensitive in plants and used to detect healthy vegetation. This band can also be used to differentiate urban area, agricultural area and forested area by using remote sensing techniques. Once of such technique is also called Band compositing / False Band Composite. A composite can be made using the bands 2,3 and 4 which represent Blue, Green and Yellow respectively to create a difference between the surface of the earth. Similar, Technique has been used in this thesis for analysis of land coverage over the years in Urban areas which will be explained in the methodology.

The thermal infrared sensor (TIRS) 1 measures the thermal infrared radiation in the wavelength of 10600-11190 nm . This involves obtaining radiation, reflect by objects which emits heat rather than the reflected sunlight. This concept has been made clear in the theory of black body radiation. The radiation emitted by a body depends on the object's temperature. TIRS 1 detects such infrared radiation. TIRS provides 100 meter spatial resolution, providing variation of temperature across small areas . In cities, buildings, roads and other artificial or concrete surfaces absorb and retain more heat. This band is used to monitor the difference in temperature over urban and rural areas and comparing it with classified land surface obtained from False Band Composites.

### 2.3.2 MODIS

Moderate Resolution Imaging Spectroradiometer (MODIS) is a multispectral optical-mechanical scanner. Due to its large field of view, it can access the data for entire planet twice a day. MODIS is used for the study of the atmosphere and surface of the land and oceans. The Modis data product used in analysis are MOD09A1 and MOD11A2. The MOD09A1 product, Surface Reflectance 8-Day L3 Global 500m, provides atmospherically corrected surface reflectance data for visible and near-infrared wavelengths at a spatial resolution of 500 meters, aggregated over an 8-day period. This dataset is primarily used for vegetation monitoring, land cover classification, and calculating indices such as NDVI and EVI, which are critical for analyzing surface properties (NASA, 2023). Similarly, the MOD11A2 product, Land Surface Temperature and Emissivity 8-Day L3 Global 1km, delivers land surface temperature (LST) and emissivity data averaged over an 8-day period at a spatial resolution of 1 kilometer. This dataset includes daytime and nighttime temperatures and is widely used for urban

heat island studies, drought monitoring, and climate modeling (NASA, 2023). Together, these datasets are invaluable for studying the relationships between vegetation cover and surface temperature, particularly in urban-rural comparisons.

### 2.3.3. Clustering of Satellite-Derived Data from Landsat and MODIS

Satellite-derived data from platforms like Landsat and MODIS provide invaluable information for land classification and vegetation analysis when combined with clustering techniques in geospatial tools such as ArcGIS and QGIS. Clustering these datasets involves understanding how various spectral bands interact and how they can be combined to reveal distinct surface characteristics. For instance, **false-color composites**—a common technique in remote sensing—use band combinations like **Near Infrared (NIR), Red, and Green (e.g., Bands 5, 4, and 3 in Landsat 8)** to enhance vegetation analysis. In this composite, vegetation appears bright red due to its strong reflectance in the NIR band, allowing clear differentiation from other land cover types like water or urban areas. Similarly, the Normalized Difference Vegetation Index (NDVI) derived from red and NIR bands is widely used for vegetation classification and monitoring. Through clustering techniques, these spectral combinations can be analyzed over time to identify changes in land use, urban expansion, or vegetation dynamics. The integration of clustering outputs with geospatial tools enables a deeper understanding of surface processes, supporting applications like urban planning, environmental monitoring, and resource management.

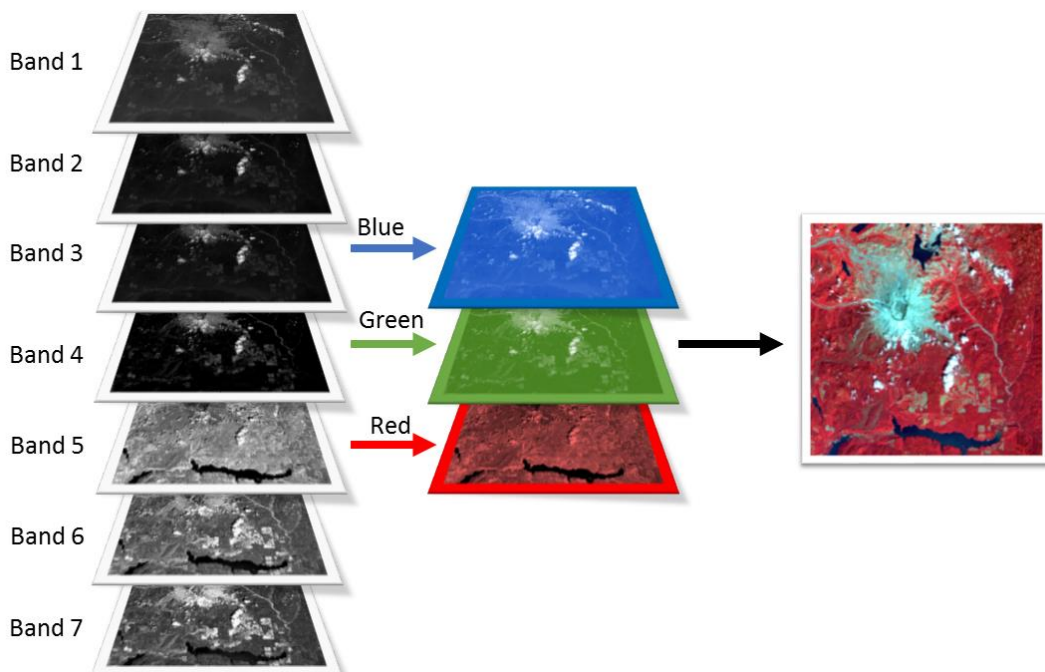


Figure 4 : Example of False-Color Composite for Land Classification. Source: Humboldt State University, Department of Geospatial Sciences

### 2.4. Climate and meteorological factors influencing UHI

Urban heat islands are significantly affected by climatic and meteorological factors. These factors include wind patterns, humidity, temperature variation and many more.

## Temperature Variation.

Urban areas often have larger difference in daytime and nighttime temperatures compared to rural areas. During the day , solar radiation are absorbed by materials with higher albedo causing significant heating . At night rural areas tends to cool more rapidly because vegetation and soil release the heat more faster than concrete surfaces that can retain the heat for longer period in the night. This can be explained clearly using the concept of boundary layers.

## Planetary and Atmospheric Boundary layers ( PBL AND ABL)

Planetary boundary layer is the lowest layer of the troposphere where wind is influenced by friction. The thickness of PBL can vary during day and night . Stronger wind causes allows more convective mixing. This mixing causes PBL to expand. During the night,the reduction of rising thermals from the surface make PBL shallower.

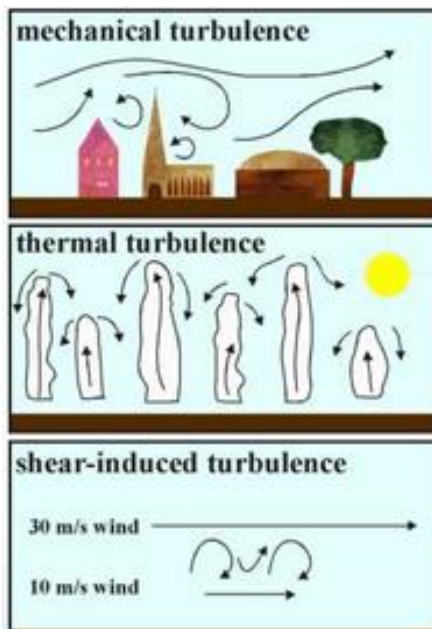


Figure 5 : Types of Turbulence (National Weather Service, n.d.)

Mechanical turbulence in the PBL is mainly by the interaction between wind and surface roughness like hills , buildings, trees etc. As wind blows , these obstacles create friction and disturbs the smooth air flow. So, the stronger the wind is more turbulence is generated. Thermal turbulence is due to uneven heating of the earth's surface by the sun which causes the convective motion. When surface is heated the warmer air rises and colder /denser air sinks down which causes turbulence. Shear induced turbulence is caused by the changing wind speed and direction with height. Significant differences between these two variables over different layers creates shear force which eventually generates turbulence. the temperature in the planetary boundary layer (PBL) is primarily influenced by advection and the thermal energy than atmospheric layers above PBL.

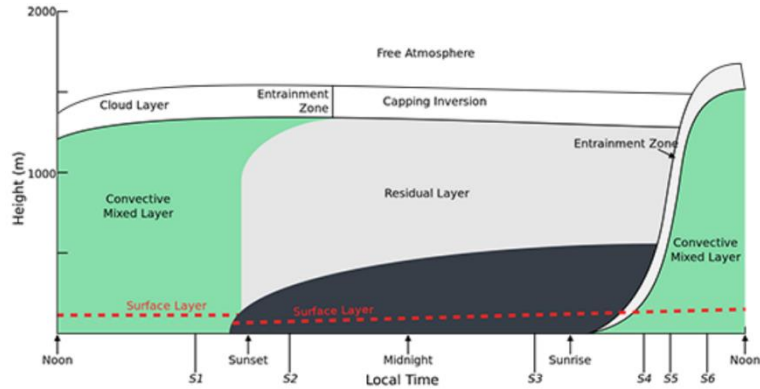


Figure 6 : Diurnal evolution of the atmospheric boundary layer (Stull,1998)

At midday, when sun is at its peak, providing the maximum solar radiation. The heating warms the surface of the earth causing the air above it to also warm up, this warm air rises because of the buoyancy. An air parcel will rise until its virtual potential temperature matches that of the surrounding air at altitude. The virtual potential temperature is a measure of the temperature of an air parcel adjusted for its moisture content. As the sun sets, there is less solar radiation to power the convective process and the boundary layer sinks leaving behind the residual layer which contains mixed air that was a leftover. When there is less turbulence in the residual layer , the air can speed up. The faster moving air above the slower moving air generates the shear to develop between two air masses. When this shear breaks down, turbulence is generated. At sunrise, solar heating begins to warm up the surface again and same process continues.

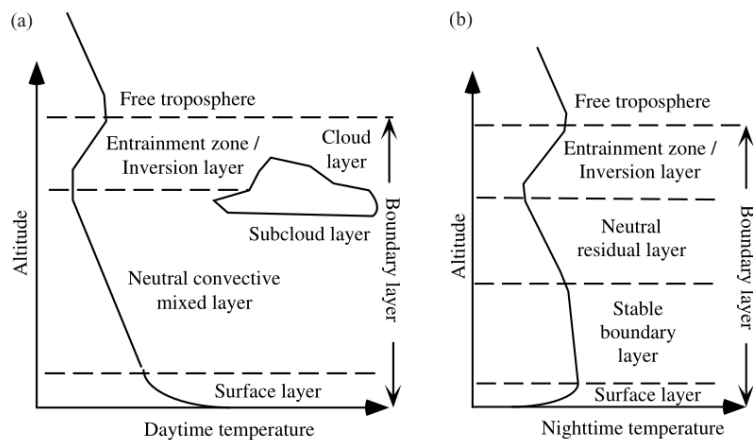


Figure 7: Variation of temperature with height during (a) Day and (b) Night in the atmospheric boundary layer over land under high pressure system Stull(1998)

Temperature in the boundary layer is also affected by the large scale pressure system. The warm air is often above the cold air which creates an inversion. Inversion is the increase in temperature with height. In low scale pressure system, air rises and cools down which creates clouds and decrease the sunlight reaching to the surface. During the day boundary layers consist of a surface layer, convective mixed layer and an entertainment zone. Since, some mixing between mixed layer and inversion layer always occur, it is called entertainment zone. Surface layer consists of 10% of the boundary layer . As the depth of boundary layer is 500 - 3000m , the surface layer is around 50 -300m thick. In the fig , during the day , the temperature decreases rapidly . As the temperature gradient is strong , it

accelerates into the mixed layer. In the mixed layer when the temperature gradient is not as strong, the air parcels mixes up and down but do not accelerate to either direction. During the night, the surface cools , causing the temperature to increase with increase in height from the ground creating an inversion. As the temperature drops, the air in the surface layer becomes more stable and denser. The cooling of surface layer cools the bottom of mixed layer making it stable. This stability is called as stable nocturnal boundary layer (NBL). The remaining portion of the mixed layer , that status neutrally stratified is called residual layer. It does not undergo significant change during the night because of less thermals.

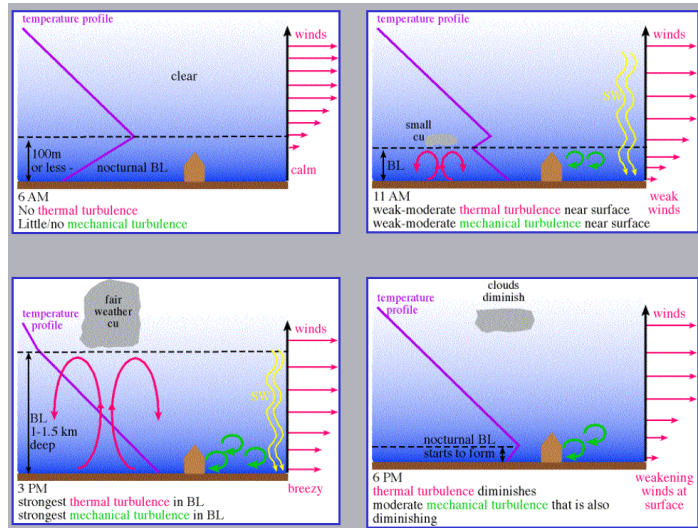


Figure 8: (National Weather Service, n.d.)

Fig shows the weather pattern when large scale weather phenomenon such as high and lows are not creating large difference in the weather. At 6AM there is no thermal turbulence and little mechanical turbulence as winds near surface are very calm. At 11 AM, the surface heating generates thermals and it mixes the stronger wind down to near grounds. At 3PM , when surface heating is maximum, thermal turbulence is strong and it mixes even the stronger wind to the surface . At 6PM, when surface heating starts to diminish, the surface temperature start to drop and nocturnal boundary starts to develop again.

### Wind patterns

Low wind speed can trap the heat in urban areas, which increases the intensity of Urban heat Island effect. This occurs when stagnant air does not allow heat to disperse and causes heat to build up around the building and streets. Stagnant air can also trap pollutants such as vehicle emission and industrial smoke. When the wind speed is high, it disperses the accumulated heat over urban areas , reducing the intensity of UHI effect. The direction of wind is also an important factor. If the wind comes from cooler region, it can bring the cooler air which reduces the urban temperature. If the wind is blowing from the warm region, such as city or industrial zone, it can carry the hot air into the area, increasing the temperature.

Cities with tall buildings often experience urban canyon effect. The streets filled with tall structure can channel the wind to the narrow path. This accelerates the speed of the wind along the corridors. It can cause localized cooling and also called as channeling effect. Large and dense building can create wind shadows, where airflows is blocked or slowed down which allows heat to accumulate. In contrast

the presence of high rise building an also cause turbulence which may mix the air later and distribute the heat.

## Humidity

Humidity refers to the amount of moisture in the air , and it can affect how the heat is absorbed and dissipated in the environment. In more humid region, the presence of water in the environment can have a cooling effect through evaporation. However, in densely built urban area where vegetation and water resource are scarce, the evaporation is minimum. Material like concrete and asphalts that covers of the city does not facilitate moisture retention or evaporation, leading to lack of cooling effect. Humid air tends to trap the heat more effectively during the night. Water vapor in the air absorbs and re-emit heat, this phenomenon is also called radiative trapping. This makes UHI effect more pronounced during nighttime hours. This is also why cities in humid climates often stay warmer during the nighttime.

## Surface Energy Balance Equation

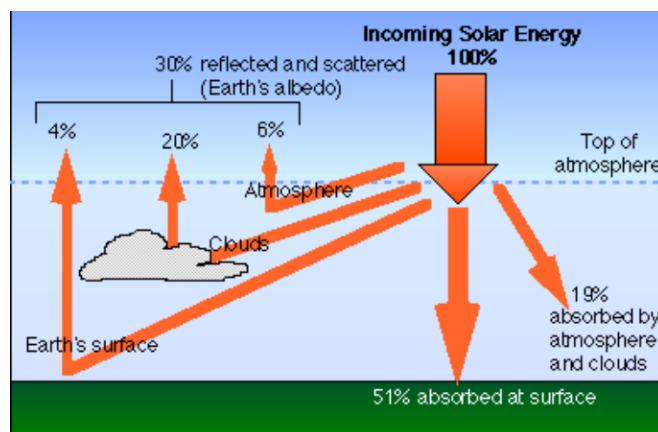


Figure 9 : Breakdown of Incoming Solar Energy (ATPI,n.d.)

The urban temperature is influenced by the energy balance at the surface, which can be represented by the Surface Energy Balance (SEB) equation. It expresses how different energy fluxes interact at the surface of the urban environment:

$$Q^{net} = Q_H + Q_E + Q_G + Q_F$$

Where,

- $Q^{net}$  = Net radiation
- $Q_H$  = Sensible heat flux
- $Q_E$  = Latent heat flux
- $Q_G$  = Ground heat flux ( $\text{W/m}^2$ )
- $Q_F$  = Anthropogenic heat flux

In urban areas , the value of  $Q_F$  is often significant and  $Q_E$  is lower due to less vegetation and water bodies , resulting in more heat retained in the surface.

## 2.5. INTRODUCTION TO WRF

WRF is a three-dimensional, nonhydrostatic model that solves a full set of mass, momentum and energy conservation equations of thermohydrodynamics, together with parametrizations of radiative energy transfer including the effects of greenhouse gases and scattering by aerosols, phase change processes, surface energy and water budgets, subgrid-scale turbulent transport using a set of specially selected approximations to ensure proper representation of individual modes, numerical stability, and an optimal balance between result accuracy and computational efficiency.

It was developed as a collaborative project between the National Center for Atmospheric Research (NCAR), the National Oceanic and Atmospheric Administration (NOAA) and other agencies. WRF provides high resolution customizable solutions of atmospheric processes. WRF can produce simulation based on actual atmospheric conditions and has a large worldwide community of registered users.

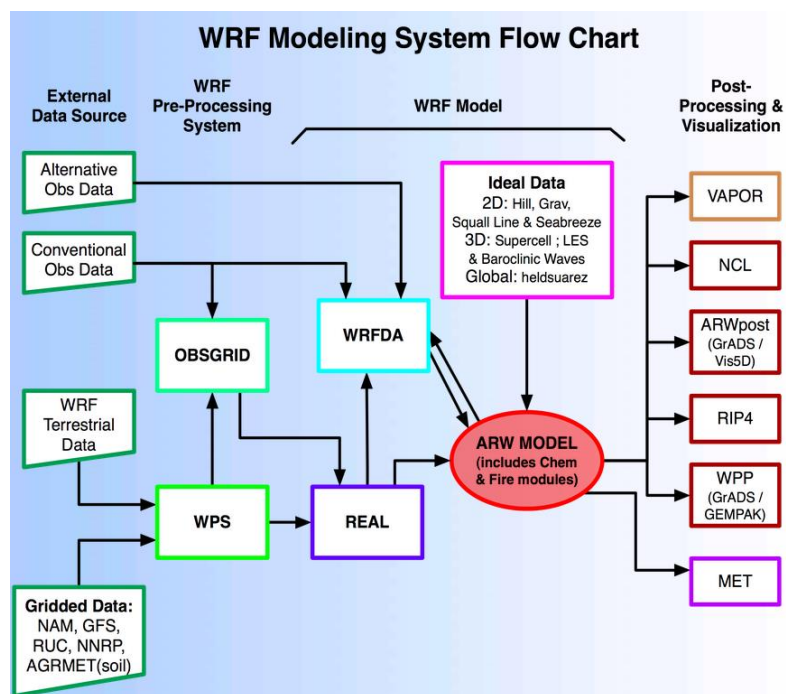


Figure 10 : WRF Modelling Flowchart (UCAR,2021)

### 2.5.1. WRF terrestrial Data

Terrestrial data refers to information that describes the Earth's surface and Topography. In WRF it includes land use data, topography, Soil type etc. This dataset is used to define the physical characteristics of region being modeled. This data is provided from various global datasets such as USGS and MODIS.

## Gridded Data

Gridded data refers to meteorological data which is distributed to the grids of points. This data includes various features such as temperature, pressure, Wind speed and direction and moisture content. Gridded data are essential for representing the initial and boundary condition to WRF model. This dataset comes from global reanalysis datasets such as GFS and ECMWF and it provided the foundation for initialization of simulations.

### OBSGRID

OBSGRID allows the assimilation of observation data into the model. After WPS processes the data, OBSGRID can cooperate with weather station data, satellite observation and Radar data. These observation data help to improve the accuracy of the initial conditions by adjusting the gridded data based on the actual measurements. It is used to improve the discrepancies between gridded data and observation for better model performance.

## 2.6. WRF processing system (WPS)

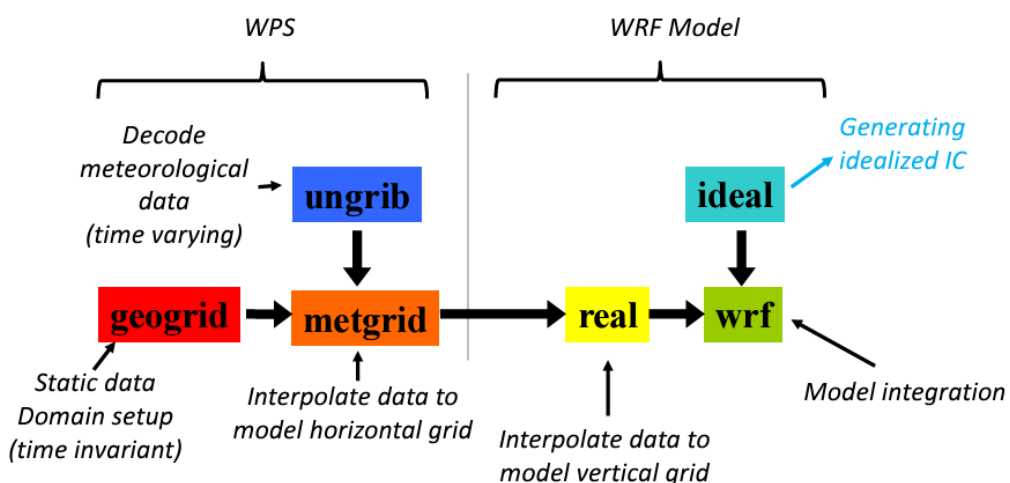


Figure 11 : WRF processing system (UCAR,2021)

WRF processing system is the key component of WRF model . It is necessary for the preparation of necessary input data for running WRF model. The WPS consists of three major modules.

- Geogrid
- Ungrib
- Metgrid

### 2.6.1 Geogrid

Geogrid defines the domain of the simulation by generated by WRF. It defines Map projections, Geographical location of the domain, Dimension of domain and Horizontal resolution of the domain. Geogrid provides the values for static (Time-invariant) fields at each grid points. It computes latitude, longitude , map scale factor and Coriolis parameter at each grid point. It horizontally interpolates the

static data such as topography, land use category, soil type, vegetation fraction, albedo and many more.

### Defining the Domain in WRF

Defining the domain in the Weather Research and Forecasting (WRF) model is a crucial step that determines the geographic area to be simulated and directly impacts the resolution and accuracy of the results (Skamarock et al., 2008). The domain encompasses both the horizontal and vertical extents of the simulation and includes specifications such as the grid spacing, number of grid points, and boundary conditions. Choosing an appropriate domain size requires balancing computational resources with the need for detailed and accurate simulations. In regions with relatively simple terrain, domain definition is more straightforward. However, in high-terrain regions like Nepal, where the Himalayan mountain range introduces extreme elevation gradients and complex microclimates, defining the domain becomes significantly more challenging (UCAR, 2021; Shodor, n.d.).

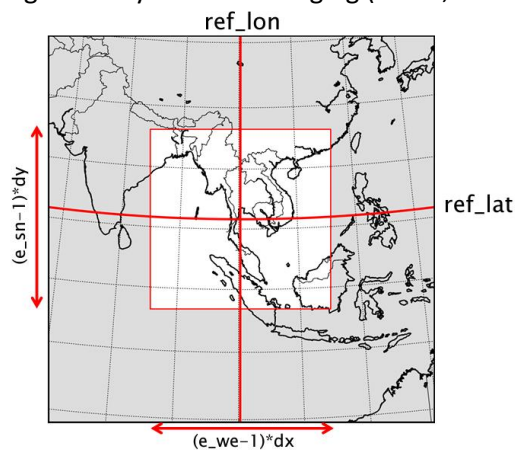


Figure 12 : Defining WRF Domain (UCAR,2021)

Where,

`RefLat`, `RefLon` : The latitude and longitude of a known location in the Domain.

`DX,DY` : Grid distance where map factor = 1

`E_WE` : Number of points in west-east direction

`E_SN` : Number of points in south-east direction.

#### 2.6.2. Ungrid

GRIB is a WMO standard file format for store regular-distributed (gridded) fields. It is a record based format. The fields present in this files are identified by code numbers, which should be referenced against an external table to determine the corresponding field. This reference tables are called as Vtables. Vtables are files that give the GRIB codes for fields to be extracted from the GRIB input file. Vtables might vary according to the source of database.

#### 2.6.3. Metgrid

Metgrid horizontally interpolates the meteorological data which is extracted by ungrid to the simulation domain defined by grogrid. It uses a staggered grid which means that the different variables such as wind components and other meteorological fields are calculated at st different positions within a grid cell. The U-component of wind is calculated at the edge of the box in the horizontal(X-axis) direction, the V-component of wind is calculated at the edge of the box in the vertical

(y-axis) direction and other meteorological variables such as temperature, pressure and humidity are calculated at the center of the grid cell. This is called the theta ( $\theta$ ) point.

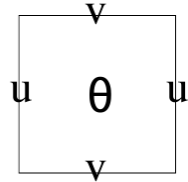


Figure 13 : Staggered Grid Structure Showing U, V, and  $\theta$  Points in METGRID

## 2.7. WRF - URBAN ( URBAN CANOPY MODEL )

Urban canopy model (UCM) coupled with WRF-Noah land surface model along with WRF routines represents the physical processes in the exchange of heat momentum in urban environment in mesoscale model. UCM is coupled to WRF model. The UCM has simplified urban geometry and it is a single layer model. Its features include shadowing from buildings, reflection of short and longwave radiation and wind profile in the canopy layer and multi-layer heat transfer equation for roof, wall and road surfaces .( Kusaka and kimura ,JAM 2004).

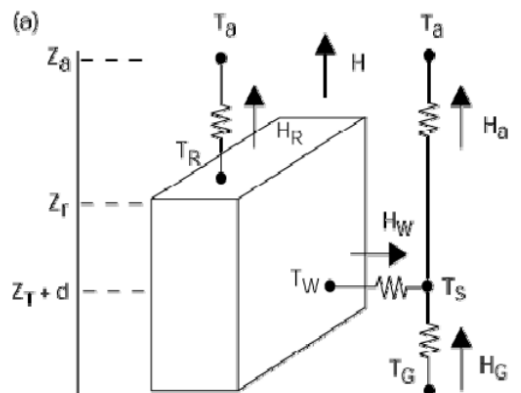


Figure 14 : Schematic of the single-layer urban canopy model.( Kusaka and kimura ,JAM 2004)

$T_a$  is the air temperature at reference height  $z_a$ ,  $T_R$  is the building roof temperature,  $T_W$  is the building wall temperature,  $T_G$  is the road temperature,  $T_S$  is the temperature defined at  $z_T + d$ ,  $H$  is the sensible heat exchange at the reference height,  $H_a$  is the sensible heat flux from the canyon space to the atmosphere,  $H_w$  is that from wall to the canyon space,  $H_g$  is that from road to the canyon space, and  $H_r$  is that from roof to the atmosphere (From Kusaka and Kimura 2004). There are buildings on either side and streets in the middle. During the day, when sun heats up the roof, walls and roads. Each surface gets its own temperature because they absorb and release heat differently. These surfaces start to give off sensible heat, which warms the air in the canyon space and some of that heat rises into the atmosphere. Sensible heat is the energy that causes a change in the temperature of a substance without changing its phase. It is the type of heat that one can “feel” and measure.

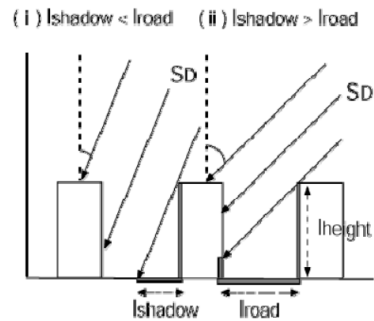


Figure 15 : Radiation of the single-layer urban canopy model (Kusaka and kimura,2004)

$SD$  is the direct solar radiation incident on a horizontal surface,  $l_{road}$  is the normalized road width,  $h_c$  is the normalized building height ( $l_{roof} + l_{road} = 1$ ), and  $l_{shadow}$  is the normalized shadow length on the road (From Kusaka and Kimura 2004).The radiation component of the single layer urban canopy model is based on how solar radiation interacts with urban surfaces and spaces between them .  $SD$  represents the direct solar radation that hits a flat, horizontal surface .  $l_{road}$  is the normalized width of the road in the model. IT means that it is expressed as a fraction of the total horizontal space, including both the road and rood tops.  $h_c$  is the normalized height of the building which represents the relative height of buildings compares to the width of the space.  $l_{roof}$  it the width of the building rooftops compared to the total horizontal area. In this model, the total width of the rooftops and roads adds up to 1 ( $l_{road} + l_{roof} =1$ ).  $l_{shadow}$  is the length of the shadow that building cast on the road due to direct solar radiation. The length of the shadow depends on the building height ( $h_c$ ) and the angle of the sunlight. As he sun changes its direction , shadows changes its length and direction too, which affects how much of the road is shaded and how direct sunlight heats it.

## 2.8. Implementation of Local Climatic zone (LCZ) in WRF model

The implementation of the CGLC-MODIS-LCZ data product into the WRF/WPS system involved several key steps. First, the raw data was converted into tiled binary files compatible with WPS, followed by the creation of an index file to map data locations across the tiles. A new entry was added to the GEOGRID.TBL table, defining the dataset path and interpolation rules using nearest neighbor averaging, prioritizing the CGLC-MODIS-LCZ dataset over the default WPS MODIS dataset. By specifying `geog_data_res = "cglc_modis_lczi+default"` in the WPS namelist, users can generate land cover and Local Climate Zone (LCZ) data for their study domains, including relative fractions and dominant land types for each grid. For areas not covered by CGLC-MODIS-LCZ (e.g., oceanic or polar regions), the system fills in data using the default MODIS land cover map. This functionality, officially released in WRF/WPS version 4.5, integrates the 100-m global CGLC-MODIS-LCZ dataset archived at NCAR and available online as CGLC-MODIS-LCZ\_100m (UCAR,2023).

The CGLC-MODIS dataset was utilized for the analysis of Urban Heat Island (UHI) effects in Nepal by carefully preprocessing and refining the data to suit the study's requirements. Using tools like ArcGIS, the dataset was cropped to focus on the specific region of interest, ensuring that only relevant geographical and land cover data were included. The refined dataset was then integrated into the WRF (Weather Research and Forecasting) model to facilitate detailed simulations and analyses of UHI dynamics within Nepal. This approach allowed for high-resolution modeling of land cover and climate zones, enabling a more accurate representation of urbanization impacts and thermal patterns critical to understanding UHI effects in the study region.

## **2.9. Computational Requirements and Challenges of running WRF simulations in High Terrain**

Running Weather Research and Forecasting (WRF) model simulations over high topography regions, such as the Nepal and Tibet Himalayas, poses significant computational and technical challenges. These challenges arise from the intricate dynamics of steep terrain and the high-resolution requirements needed to capture atmospheric processes accurately. High-resolution WRF runs, often at scales of 1 km or less, are essential in mountainous regions to resolve localized meteorological phenomena and complex terrain-induced flows. However, finer resolution increases the computational cost exponentially due to the greater number of grid points, vertical levels, and data inputs required. This also leads to longer simulation times and a higher demand for storage and memory (Skamarock et al., 2019).

One of the most persistent issues in high-terrain simulations is numerical instability. The steep gradients in topography can produce excessive vertical velocities and erroneous pressure gradients, which frequently result in model crashes. These problems are further exacerbated by Courant-Friedrichs-Lowy (CFL) violations, where large wind speeds over small grid intervals require extremely small time steps to maintain stability. Techniques such as reducing the time step, enabling vertical damping (`w_damping`), and modifying terrain-following vertical coordinates with settings like `etac=0.02` have been used to address these issues. Advanced options, such as using hybrid vertical coordinates (`hybrid_opt=2`), can also help by smoothing terrain effects near the surface. However, these solutions often require extensive trial and error to optimize, consuming valuable computational resources (Hong & Kanamitsu, 2014).

The computational demands of WRF simulations over high terrain also necessitate access to high-performance computing (HPC) systems. Fine-scale simulations require parallelization over a large number of cores to reduce runtime. Even then, smaller time steps and increased vertical levels add to the already significant computational burden. The need for high-resolution input data, such as terrain data and meteorological boundary conditions from global models, further amplifies memory and storage requirements (Chen et al., 2011).

## Chapter III: Data Description

### 3.1. Geographic and Climatic Overview

#### 3.1.1. Kathmandu

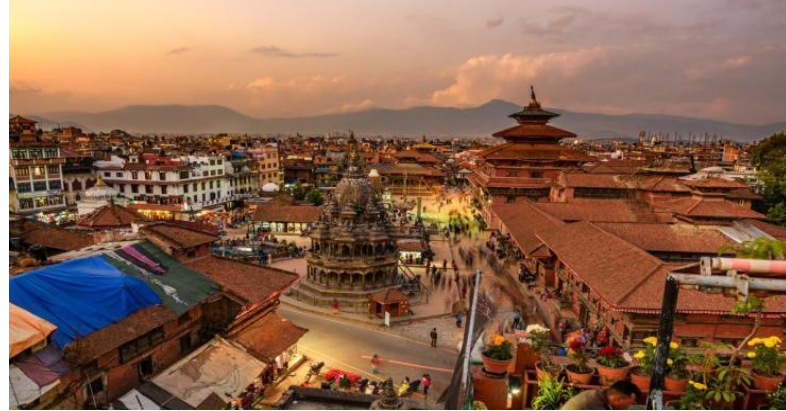


Figure 16: Kathmandu City (Wikipedia, 2020)

Kathmandu is located in the northwestern part of Kathmandu Valley, to the north of the Bagmati River and has an area of 50.7 km<sup>2</sup>. It is bordered by several municipalities within the valley, to the south of Bagmati River lies Lalitpur Metropolitan city, forming a continuous urban zone encircled by a ring road. To the southwest, Kathmandu is Bordered by Kirtipur, and to the east by Madyapur Thimi. Kathmandu consists of eight rivers, the main river of the valley is Bagmati and its tributaries. The mountains from which these rivers are originated are in the elevation range of 1500-3000 meters. Kathmandu is surrounded by Deciduous Monsoon Forest.

Table 2: minimum temperature (°C/°F), maximum temperature (°C/°F), precipitation/rainfall (mm/in), humidity, and rainy days from 1991 to 2021, along with the average sun hours for 1999 to 2019, sourced from Climate-Data.org (n.d.).

	January	February	March	April	May	June	July	August	September	October	November	December
Avg. Temperature °C (°F)	9.2 °C (48.6) °F	11.3 °C (52.4) °F	14.6 °C (58.3) °F	17.9 °C (64.2) °F	19.1 °C (66.4) °F	20.5 °C (68.8) °F	20.3 °C (68.6) °F	20.3 °C (67) °F	19.5 °C (62.2) °F	16.8 °C (56.4) °F	13.6 °C (51.2) °F	10.7 °C (50.7) °F
Min. Temperature °C (°F)	4.9 °C (40.9) °F	6.4 °C (43.5) °F	9.1 °C (48.4) °F	12.2 °C (54) °F	14.8 °C (58.6) °F	17.6 °C (63.6) °F	18.4 °C (65.2) °F	18.2 °C (64.8) °F	17 °C (62.7) °F	13.4 °C (56.2) °F	10 °C (50.1) °F	7 °C (44.6) °F
Max. Temperature °C (°F)	14.2 °C (57.5) °F	16.3 °C (61.4) °F	19.7 °C (67.5) °F	23 °C (73.4) °F	23.5 °C (74.3) °F	23.9 °C (75) °F	23.2 °C (73.7) °F	23.4 °C (74.1) °F	22.8 °C (73) °F	20.7 °C (69.3) °F	17.8 °C (64.1) °F	15.2 °C (59.4) °F
Precipitation / Rainfall mm (in)	44 (1)	56 (2)	59 (2)	79 (3)	205 (8)	460 (18)	778 (30)	643 (25)	334 (13)	98 (3)	30 (1)	26 (1)
Humidity(%)	73%	69%	57%	54%	72%	85%	92%	91%	88%	80%	75%	76%
Rainy days (d)	5	7	8	10	16	19	22	22	20	12	6	4
avg. Sun hours (hours)	7.1	7.6	9.3	10.0	8.6	6.0	4.3	4.8	5.6	7.0	6.5	6.5

The portions of the city with lower elevation (1300-1400m) have a humid subtropical climate (CWA) under Koppen's classification system. The portion of city with higher elevation have a subtropical highland climate (Cwb). The average summer temperature varies from 28°C to 30°C and winter temperature is 10°C. Unpredictable weather is expected, given that temperatures can drop to 0°C (32°F) or less during the winter.[31] The lowest ever temperature of -3.5 °C was recorded in 1978.[31] While snowfall is generally confined to the hills surrounding the city,[32] there have been a few instances of snowfall in city most notably in 1945 and 2007 (Wikipedia, 2025).

### 3.1.2. Pokhara



Figure 17 : Pokhara City (Wikipedia, 2022)

Pokhara is the tourism capital of Nepal. It is second most populous city after Kathmandu. Pokhara is situated almost 200km west from Kathmandu. Pokhara is relatively flat and fertile land surrounded by hills and mountains. The valley is the part of Seti Gandaki river basin and has mild slope which increases gradually towards the north. A major section of Himalayas above 8000m can be seen from the city. The urban core of Pokhara is concentrated around Phewa lake, with mix of hotels, cafes , restaurant and residential buildings. In recent years, the city has expanded into surrounding areas, where both residential and commercial development has increased. Residential areas are emerging as the population grows and urbanization accelerates.

Table 3: minimum temperature (°C/F), maximum temperature (°C/F), precipitation/rainfall (mm/in), humidity, and rainy days from 1991 to 2021, along with the average sun hours for 1999 to 2019,sourced from Climate-Data.org (n.d.).

	January	February	March	April	May	June	July	August	September	October	November	December
Avg. Temperature °C (°F)	11 °C (51.8) °F	12.7 °C (54.9) °F	15.8 °C (60.4) °F	19.3 °C (66.7) °F	21.4 °C (70.5) °F	23.1 °C (73.6) °F	23.1 °C (73.5) °F	23.1 °C (73.5) °F	22.2 °C (72) °F	19.4 °C (66.9) °F	15.8 °C (60.4) °F	12.9 °C (55.2) °F
Min. Temperature °C (°F)	4.6 °C (40.3) °F	5.7 °C (42.3) °F	7.9 °C (46.2) °F	11.3 °C (52.3) °F	15.7 °C (60.2) °F	19.9 °C (67.9) °F	21.4 °C (70.6) °F	21.3 °C (70.3) °F	19.7 °C (67.4) °F	14.6 °C (58.3) °F	11.2 °C (52.1) °F	8.2 °C (46.8) °F
Max. Temperature °C (°F)	15.6 °C (60) °F	17.7 °C (63.9) °F	21.2 °C (70.2) °F	24.6 °C (76.3) °F	25.2 °C (77.4) °F	25.7 °C (78.2) °F	25 °C (77.1) °F	25.1 °C (77.2) °F	24.6 °C (76.3) °F	22.7 °C (72.9) °F	19.4 °C (66.9) °F	16.6 °C (61.9) °F
Precipitation / Rainfall mm (in)	131 (5)	176 (6)	166 (6)	164 (6)	393 (15)	693 (27)	1114 (43)	967 (38)	587 (23)	200 (7)	151 (5)	109 (4)
Humidity(%)	72%	72%	68%	65%	74%	83%	90%	88%	84%	76%	75%	75%
Rainy days (d)	12	14	14	12	17	20	22	21	20	14	12	11
avg. Sun hours (hours)	6.6	6.8	8.5	9.4	8.5	7.1	5.7	6.1	6.6	7.8	5.7	5.7

The climate in Pokhara is warm and temperate. The summer have more rainfall compared to Kathmandu. The mean yearly temperature is 18.2°C and under Koppen classification it falls in humid subtropical climate CWA. Pokhara receives the highest amount of rainfall in the country. The highest temperature recorded in Pokhara was 38.5°C in 2013 while the lowest temperature recorded was 0.5°C in 2012.

### 3.2. Selection of Cities

For the analysis of Urban Heat Islands (UHI) in Nepal, two major cities were chosen: Kathmandu and Pokhara. Kathmandu is located at approximately 27.7172° N latitude and 85.324° E longitude, while Pokhara lies at 28.2095° N latitude and 83.9856° E longitude. The average elevation of Kathmandu is around 1,400 meters (4,600 feet) above sea level, whereas Pokhara is at a lower elevation of approximately 827 meters (2,713 feet).

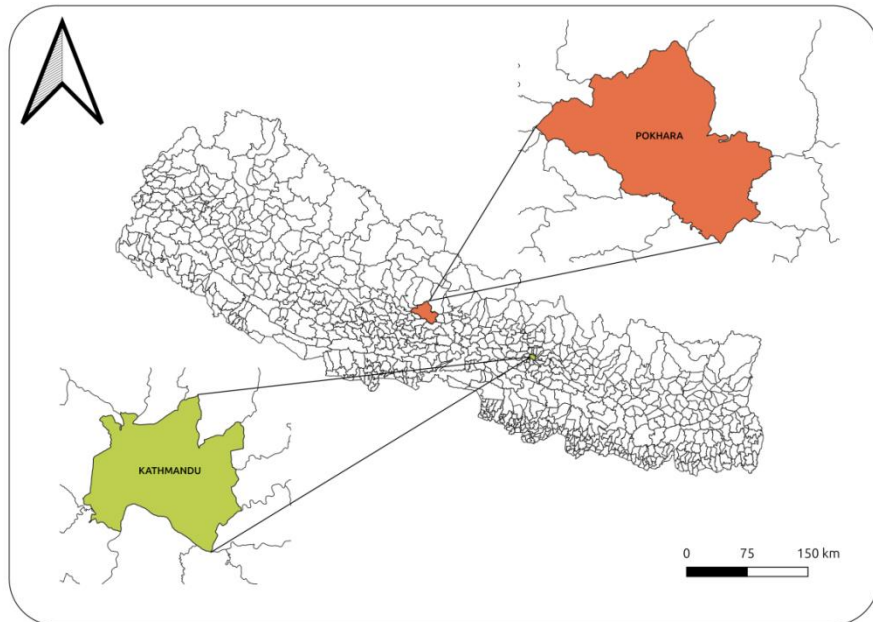


Figure 18 : Selected Cities for the Analysis of Urban Heat Island

#### Criteria for Selection

Both cities are situated in different geography within Nepal. Kathmandu, being the capital and a densely populated urban center, presents a case for urbanization effects on local climate. Pokhara, which is in comparatively Lower elevation offers insight into different urban development patterns. Kathmandu is one of the most densely populated cities in Nepal. This high density leads to significant heat generation and usage of more heat absorbent materials. Pokhara is less populated than Kathmandu and is experiencing rapid urbanization and growth in tourism, which makes it an interesting comparison point.

The urbanization of both cities has substantially increased over the few decades. The differing elevations and climatic conditions of the two cities are significant. Kathmandu's higher elevation leads to different climatic influence compared to lower altitude Pokhara. Also, the availability of historical temperature records and satellite imagery provides a suitable ground for choosing these cities for analysis of Urban heat Island in Nepal.

### 3.3. Synoptic Stations

The limited number of synoptic stations within the city posed a challenge for conducting an analysis on urban heat islands (UHI), which requires temperature measurements from various locations across the city. Additionally, the data obtained from the Ministry of Hydrology and Meteorology was purchased, and acquiring data from all the stations would have been prohibitively expensive. Furthermore, the incomplete availability of data for certain time periods in international exchanges created additional obstacles for the analysis. Solving big problems like climate change and public health needs open access to information, not expensive paywalls. Science works best when knowledge is shared, not sold. It's time to treat data as something for everyone, not just those who can afford it.

*Table 4 : Location of Synoptic Stations obtained from Ministry of Hydrology and Meteorology, Nepal.*

Station Index	Name	District	Latitude	Longitude	Elevation
0804	Pokhara Airport	Kaski	28.188621	84.0169252	804
1030	Kathmandu Airport	Kathmandu	27.703825	85.35624722	1337

The raw synoptic data collected from the Ministry of Hydrology and Meteorology, Nepal, spanning the years 2000 to 2023, was further processed to generate the plots.

#### Pokhara Airport (0804)

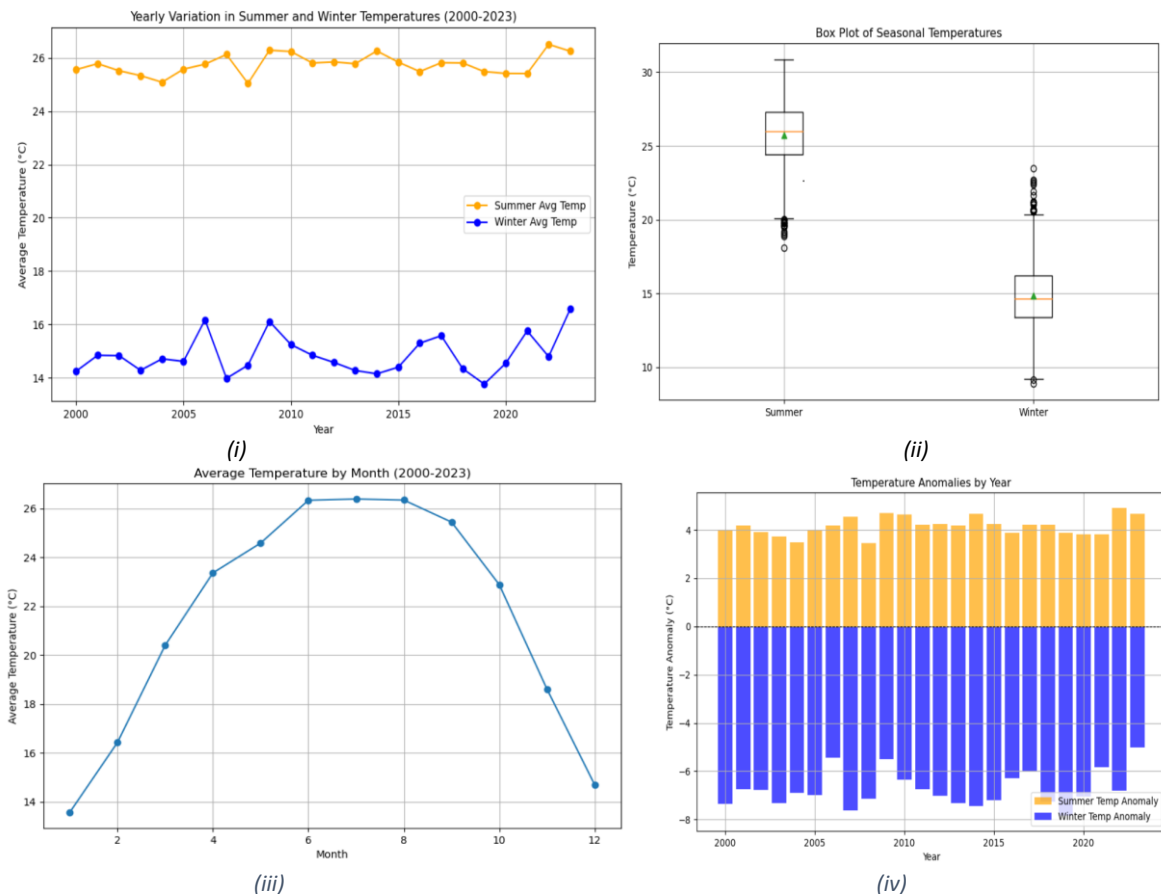


Figure 19 : (i) Yearly Variation of Temperature in Winter and summer, (ii) Box-Plot of Seasonal Temperature ,(iii) Average Temperature by Month, (iv) Temperature Anomalies by year.

Figure 18 reveals distinct seasonal and long-term temperature patterns from 2000 to 2023. The yearly temperature trends demonstrate that summer temperatures have remained relatively stable, consistently averaging around 26°C, while winter temperatures show greater variability, fluctuating between 14°C and 18°C. The box plot underscores these seasonal differences, with summer temperatures exhibiting a higher median and a broader spread, along with some extreme outliers, indicating occasional heat spikes. Winter temperatures, on the other hand, have a narrower range and lower median, reflecting their cooler and more consistent nature. The monthly temperature profile illustrates a typical seasonal cycle, with temperatures peaking during the summer months (June-August) and reaching their lowest in winter (December-February). The temperature anomaly chart highlights a warming trend in summer, with persistent positive deviations from the baseline, while winter anomalies are mostly negative, suggesting cooling or less consistent warming. Together, these observations suggest a stable but warming summer climate and more pronounced variability and anomalies in winter.

### Kathmandu Airport (1030)

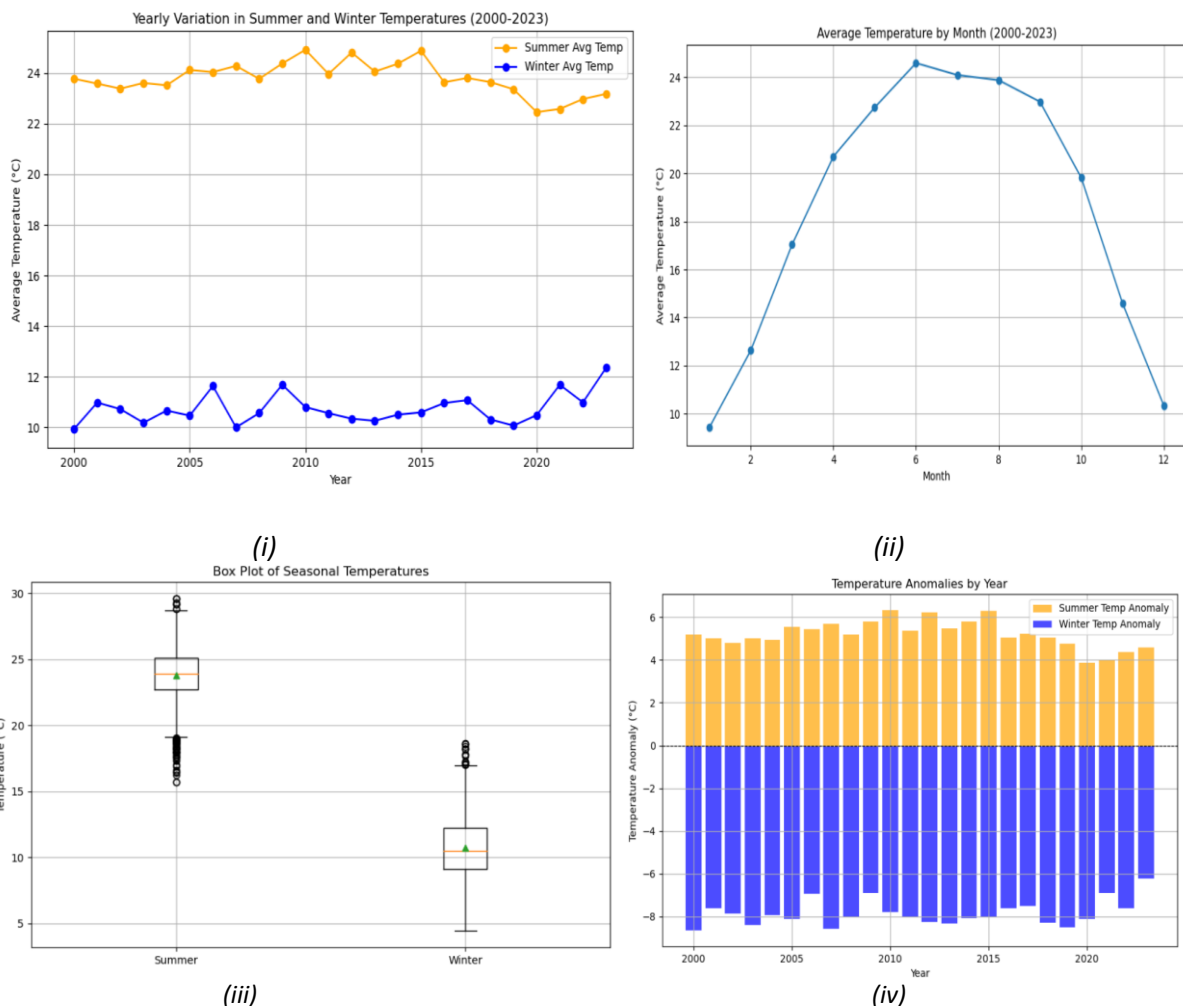


Figure 20 : (i) Year Variation of temperature in Winter and Summer (2000-2023), (ii) Average Temperature by Month , (iii) Box Plot of Seasonal Temperatures, (iv) Temperature Anomalies by Year

The analysis of Synoptic data of Kathmandu represents the annual and monthly temperature patterns from 2000 to 2023. The first figure demonstrates the yearly variation in summer and winter temperatures. Summer temperatures remain relatively stable around 23°C to 24°C, reflecting consistency over the years, while winter temperatures fluctuate more prominently, ranging between 10°C and 13°C, showing some long-term variability. The monthly temperature curve vividly depicts the seasonal cycle, with temperatures peaking in mid-summer (June) at approximately 24°C and bottoming out in winter (January and December) at around 10°C. The cyclical nature of the monthly temperatures reflects the predictable pattern of seasonal weather variations. Together, these figures indicate stable summer trends with consistent peaks and significant variability in winter temperature.

### **3.4 Data description for Analysis based on remote sensing**

**Landsat 8-9 OLI/TIRS**

Landsat Collection 2 Level 1 (Landsat 8-9 OLI/TIRS C2 L1) was used for generating Land use and Land Cover Classification. Band Composites were made using band 4,5 and 6 .

**Table 5 : Band Number and Range of Bands used for the false band composite from Landsat 8-9 OLI/TIRS C2 L1.**

Band Number	Band Description	Band Range (nm)
4	Red (OLI)	636-673
5	Near- Infrared (NIR)(OLI)	851-879
6	Short Wavelength Infrared (SWIR) 1 (OLI)	1566-1651

The combination of bands 4 (Red), 5 (Near-Infrared), and 6 (Shortwave Infrared 1) from Landsat 8-9 OLI/TIRS Collection 2 Level 1 is often used for surface characteristics such as built up areas, vegetation and soil. The classes were filtered to retain only the green areas and concrete (built-up areas) for simplified visualization. All classifications that are not built-up areas were combined into the green area.

Hybrid 100-m global land cover dataset with Local Climate Zones

World Urban Database and Access Portal Tools (WUDAPT, Ching et al., 2018) level-0 Local Climate Zone (LCZ, Stewart and Oke, 2012) maps are widely used in Weather Research and Forecasting (WRF) model. Injection of this LCZ used to be done using W2W python tool. After WRF 4.3 this data set has been enabled in the WRF model . This datasets represents the year 2018 and uses classes from 51 -61 as Urban categories.

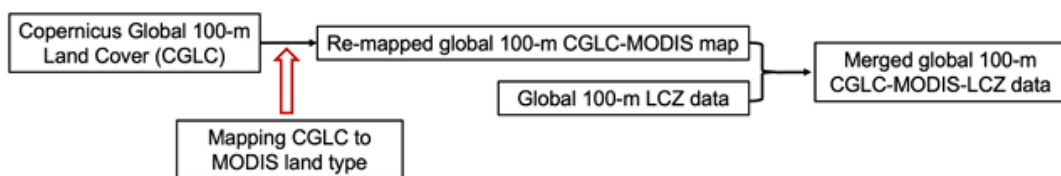


*Figure 21 : Workflow to Develop CCGLC-MODIS-LCZ (NCAR,2023)*

The analysis focused on visualizing these two datasets to assess urban changes in Pokhara and Kathmandu between 2010 and 2023. Additionally, the global land cover dataset, incorporating local climate zones, further classifies urban regions based on building types such as compact high-rise, compact mid-rise, open high-rise, and open low-rise. This classification provides a foundation for understanding the intensity and distribution of different types of built-up areas within the city.

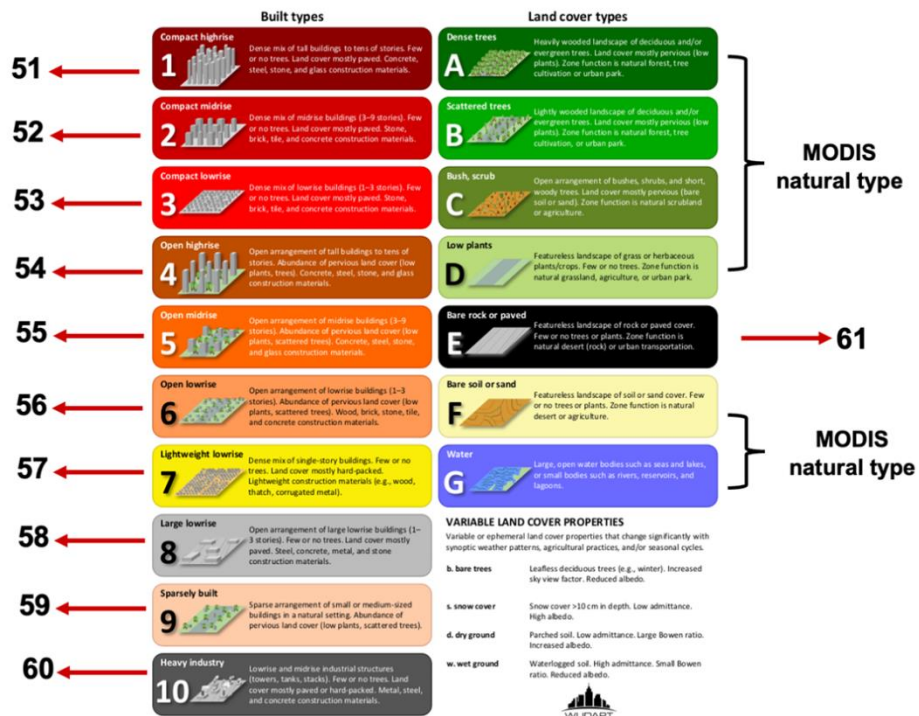


Figure 22 : LCZ numbering classification used in WRF . ( Stewart and oke,2023 ; Demuzere et al., 2020)

### MODIS (Moderate Resolution Imaging Spectroradiometer)

The data used in this study were sourced from MODIS (Moderate Resolution Imaging Spectroradiometer) products to analyze Land Surface Temperature (LST) and vegetation indices, specifically the Normalized Difference Vegetation Index (NDVI). The MOD11A1 dataset, which provides Land Surface Temperature and Emissivity data, was obtained in HDF (Hierarchical Data Format) for analysis. Similarly, MOD09A1, a surface reflectance product from MODIS, was utilized for NDVI calculations. Regional shapefiles, such as the Kathmandu shapefile, were also incorporated to focus the analysis on the area of interest.

The preparation of these datasets involved several processing steps to ensure they were accurately formatted and geo-referenced for the study. First, specific subdatasets were extracted from the HDF files, such as temperature bands and surface reflectance bands. These extracted rasters were then reprojected into the required spatial reference system for consistency with the study area. Using the Kathmandu shapefile, the data was clipped to the region of interest, removing unnecessary geographic information. For LST, raster calculations were conducted to convert raw values into meaningful temperature data, while NDVI values were derived using surface reflectance data through scaled calculations. Additionally, resampling was applied to standardize the resolution of the raster data, ensuring compatibility and comparability between datasets. The final prepared datasets included temperature rasters in degrees Celsius and scaled NDVI values, ready for detailed analysis of Urban Heat Island dynamics and vegetation patterns within the study area. These preparation steps provided a robust foundation for subsequent analysis.

### **3.5. Data Description for WRF-UCM ( Urban Canopy Model)**

#### **Meteorological Global Analysis Data for WRF**

The simulation was run in one of the clusters of National Research Institute, Department of Atmosphere and climatic Modelling, Poland. It was conducted using the GDAS Final Analysis data, which are available at a 0.25-degree spatial resolution and prepared every three hours. These data are derived from the Global Data Assimilation System (GDAS), which integrates observational data collected from the Global Telecommunications System (GTS) and other sources to produce detailed and comprehensive analyses. The GDAS Final Analysis is closely related to the operational Global Forecast System (GFS), as it uses the same underlying model. However, the GDAS Final Analysis incorporates additional observational data and is processed later than the GFS initialization to provide enhanced accuracy .Vtable for GFS Pressure-Level Data from the NCEP Server has been used. This Vtable defines the parameters, levels, units, and descriptions for pressure-level data retrieved from the NCEP server. The data is critical for initializing and driving models such as the **Weather Research and Forecasting (WRF)** model for atmospheric simulations.

Hybrid 100-m global land cover dataset with Local Climate Zones was used as geodata in WRF model which specifically separates the different type of Urban Variations found in the Area of Interest. The same geodata is used in Remote Sensing method of obtaining Land surface Temperature to compare the calculated value over different local climatic Zones.

## **Chapter IV: Methodology**

### **4.1. Supervised / Unsupervised land use classification**

Land use classification involves categorizing the Earth's surface into various types such as forest, agriculture, water bodies, urban using satellites data or any form of remote sensing methodologies. The foundation of urban climate lies on the change of urban architecture and landscapes. To understand how the urban climate is evolving, it is necessary to track the rate and pattern of settlement changes over the years within cities, region or country. This can provide results on how human settlements are influencing the environment.

#### **4.1.1 Unsupervised Classification**

It is a process where classification algorithm groups the pixel into different classes based on their spectral characteristics, without having to provide training data from the users. This type of classification works on the basic theory of Spectral clustering which uses the classification algorithm like K-means. It is an algorithm that groups the data points into a distinct cluster based on similarities. It partitions the dataset into K-distinct or simply non-overlapping clusters, where each point belongs to the cluster with the nearest mean. Since no training data is required, it is useful when there is no prior information of land types or a very less number of classes are required.

#### **4.1.2 Supervised Classification**

Supervised Classification Depends upon the training data where samples of different categories of land type are provided and trained prior to the classification. The user has to identify the land types manually. The algorithm finds the spectral signatures and classify all the pixels accordingly. Common algorithms that are used for supervised classification are Maximum Likelihood classifier and Random Forests. Supervised classification needs higher accuracy of training data in order to accurately distinguish between spectral pixels. The results are completely based on the training dataset and sometimes it could be time consuming and expensive if the area of interest is large.

### **4.2. Normalized Difference Vegetation Index (NDVI)**

Normal Difference Vegetation Index (NDVI) is a remote sensing Index which is used to measure and observe the health and the density of green vegetation in a particular area. Healthy plants reflect the near-infrared radiation, and it absorbs the red reflectance band during the process of photosynthesis. The ratio of its difference gives an indication of vegetation health.

$$NDVI = \frac{NIR - Red}{NIR + Red}$$

Where,

NIR = Reflectance in near-infrared band.

Red = Reflectance in the red band.

The value of NDVI ranges from -1 to 1 , where positive values indicates the dense vegetation and negative values indicates waterbodies ,snow and concreted surfaces. Built Environments may absorb more NIR radiation and reflect more red light, they generally have NDVI values close to zero or slightly negative.

#### **4.2.1. Application of NDVI for analysis of Urban Heat Island**

Vegetations play role in cooling urban areas through process like shading, evapotranspiration, and absorption of solar radiation. Healthy and dense vegetation which is indicated by higher NDVI , lowers the surface temperature and reduces the UHI effect. Areas that are dominated by concrete, asphalts and other materials which has higher albedo that absorbs more solar radiation and retain heat has lower NDVI values. “Urban locations generally exhibited greater values of surface temperature and lower values of a vegetation index than rural locations. The difference in the NDVI between urban and rural regions appears to be an indicator of the difference in surface properties (evaporation and heat storage capacity) between the two environments responsible for the differences in urban and rural minimum temperatures (the urban heat island effect) (Owen, Carlson and Gillies, 1998).NDVI maps can be used to identify green zones in the map . By overlapping or comparing the NDVI maps with thermal maps, one can identify how the surface temperature changes depending on the NDVI values.

#### **4.2.2. Advantages and Disadvantages of remote sensing for analysis of Urban Heat Island.**

Using remote sensing for the analysis of remote sensing has several advantages and disadvantages. Remote Sensing allows us to do analysis over extensive area, which would be time consuming and labour intensive to measure using ground-based techniques. Modern Satellites generally give high resolution data for identification of various land types which serve as a foundation for analysis of Urban heat Island. Moreover, the changes in the land occupancy and settlements can be easily monitored and understood. The thermal bands provided by various satellites such as landsats8-9 OLI-TIRS , provides the direct measure of land temperature in higher resolution. This could easily serve as a firsthand data which anyone can make use of for free for research and analysis.

Remote sensing data are dependent on atmospheric conditions, such as humidity, clouds and haze which can effect the accurate temperature and vegetation assessment. One must be very selective when deciding which satellites to use. Not all satellites provide high resolution data, and some are very case sensitive. Sometimes it can be very time consuming to tally the results between various satellites to come to a conclusion. In the summer months the satellite images from landsat 8-9 OLI/TIRS were very cloudy over Nepal , thus as an alternative MODIS observation which were much clearer was used .

#### **4.2.3. Correlation between NDVI and LST and categorization of LST based on Local Climate Zones**

Correlation between NDVI and LST is used to evaluate the relationship between vegetation cover and Land Surface temperature (LST) in the context of Urban Heat Island (UHI) , NDVI serves as an indicator for vegetation density and health ,whereas LST quantifies the thermal properties of the landsurface . The multispectral bands from sensor such as Landsat 8-9 OLI/TIRS and MODIS are used to find LST and NDVI. The raw metadata is processed in geospatial tools such as QGIS and ArcGIS which allows calculation of raster and pixels. The data can further be processed using tools like fishnet to figure out the necessary correlations

The Land Surface temperature which is calculated using the raw data and MODIS metadata is georeferenced to the The Hybrid 100-m global land cover dataset of Local Climate Zones. To quantify the changes in Land Surface temperature over different zones . The same hybrid 100m global land cover dataset is also implemented as geo resolution in WRF simulation.

### 4.3. Methodology for WRF Simulation

#### 4.3.1 Geogrid

Geogrid.exe transforms the geographic coordinates of raw datasets into the specified map projection, ensuring the model grid aligns correctly with real-world coordinates. For nested domains, it ensures proper grid alignment and boundary buffering to minimize errors and maintain numerical stability. In this study, the utility outputs domain-specific files (geo\_em.d0X.nc), which form the foundation for subsequent preprocessing steps.

**Implementation of MODIS land Categorization in WRF geogrid.**

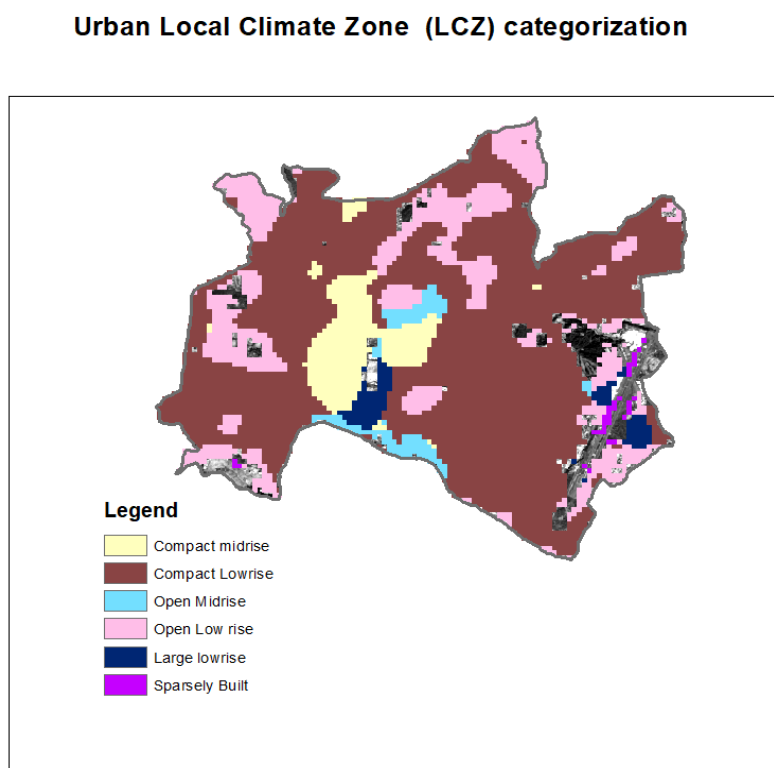


Figure 23 : MODIS LCZ dataset injected to WRF

The provided map illustrates the Urban Local Climate Zone (LCZ) categorization, which was generated using MODIS land categorization data(hybrid 100-m global land cover dataset). The gridded land-use data was carefully classified into distinct LCZ categories, such as compact midrise, compact lowrise, open midrise, open lowrise, sparsely built, and large low-rise zones. These categorizations injected to WRF provides a detailed representation of urban land characteristics within the WRF simulations.

### 4.3.2 Domain Configuration

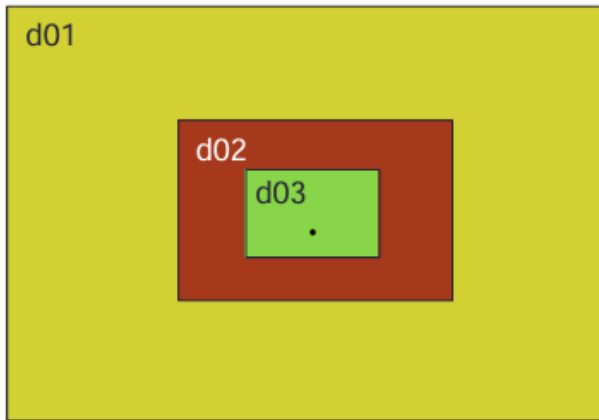


Figure 24: Nested Domain in WRF

A three-level nesting structure is used , where each layer is enclosed within the previous one, and feedback is maintained at a value of 1 across all levels. At the outermost level, d01 serves as the largest container, encompassing the entire structure and providing a foundational boundary for the subsequent layers. Nested within d01 is d02, a smaller region entirely contained within the boundaries of d01, representing a secondary level in the hierarchy. Finally, the innermost layer, d03, is entirely nested within d02, forming the deepest level of the structure. Each layer maintains feedback of 2 , which is a two way feedback , The use of a two-way feedback mechanism at each level enhances the system's adaptability and stability. It allows for the propagation of information in both directions adjustments and responses at every layer of the hierarchy. This ensures that all levels are interdependent yet function cohesively to maintain the integrity and efficiency of the nested system.

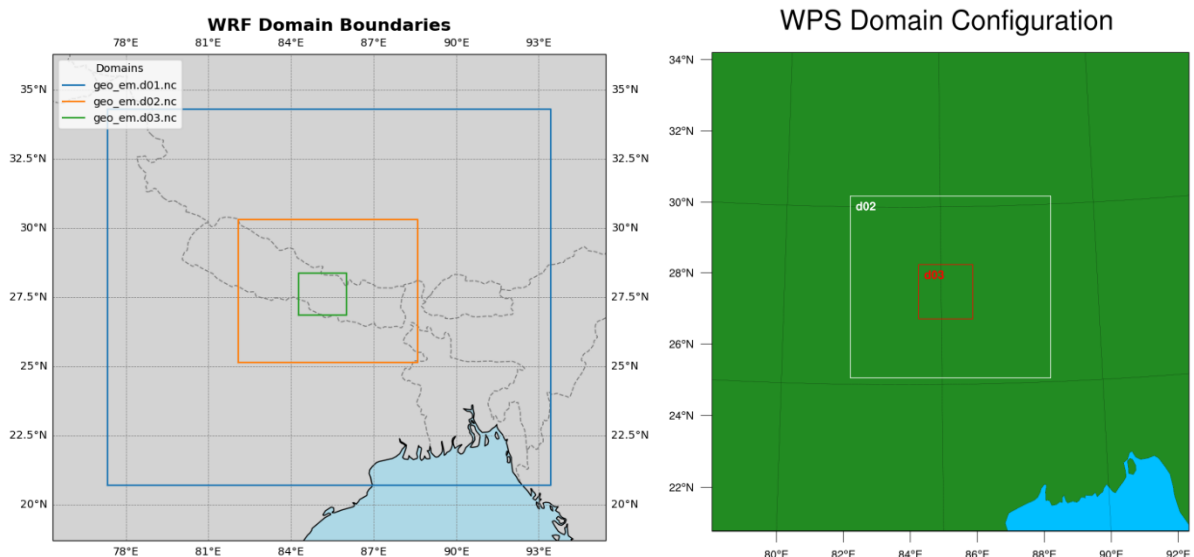


Figure 25:Domain Configured on WPS-4.5 with innermost nested domain over Kathmandu

The parent-child relationship in the domain configuration illustrates a nested structure, where progressively finer resolutions are applied to specific areas of interest. Domain 1, being the outermost or coarsest domain, encompasses the largest area with a grid spacing of 15 km (**dx = 15000** and **dy = 15000**). Nested within this domain is Domain 2, which operates at a finer resolution of 5 km grid

spacing, achieved by applying a grid refinement factor of 3 ( $15 \text{ km} \div 3$ ). Further refinement occurs with Domain 3, which is nested within Domain 2 and features a resolution of 1.67 km grid spacing, derived by dividing Domain 2's 5 km grid spacing by 3. This hierarchical nesting allows for increasingly detailed simulations as one moves inward through the domains, culminating in high-resolution analysis over the focal area of Kathmandu. Such an approach ensures computational efficiency by concentrating the finest resolution only where it is most needed while maintaining broader coverage in the outer domains. The location and projection configuration utilizes the Lambert conformal conic projection (map\_proj = 'lambert'), which is particularly well-suited for mid-latitude regions such as Nepal.

The domain grid dimensions for each nested level are carefully designed to adhere to the rules of nesting and grid refinement. Each domain's grid dimensions must satisfy the condition  $(e_{\text{we}} - i_{\text{parent\_start}} + 1) \bmod \text{parent\_grid\_ratio} = 0$ ,  $e_{\text{we}} - i_{\text{parent\_start}} + 1 \bmod \text{parent\_grid\_ratio} = 0$ , ensuring compatibility between parent and child domains. For Domain 1, the outermost and coarsest grid, the dimensions are  $e_{\text{we}} = 101$  and  $e_{\text{sn}} = 101$ , providing coverage at a resolution of 15 km. Domain 2, nested within Domain 1, has dimensions  $e_{\text{we}} = 127$  and  $e_{\text{sn}} = 125$ , refined to a 5 km resolution. This domain includes a buffer of grid cells around its edges, following the approximate 1/3 rule, which ensures that at least one-third of the parent domain's grid points surround the child domain. This buffer helps maintain stability and proper boundary conditions between domains. Domain 3, nested within Domain 2, focuses on Kathmandu with dimensions  $e_{\text{we}} = 103$  and  $e_{\text{sn}} = 103$ . This grid achieves the highest resolution of  $\sim 1.67 \text{ km}$ , allowing detailed simulations in the area of interest.

Nepal's steep topography and high-altitude terrain necessitate meticulous domain configuration to ensure the accuracy and stability of simulations. Special care has been taken to avoid placing domain boundaries over rugged mountainous areas to minimize errors and maintain numerical stability. Boundaries over steep terrain can result in interpolation errors in lateral boundary conditions, potentially destabilizing the simulation. To mitigate this, a buffer zone of approximately one-third of the domain width is maintained around the edges of nested domains. This buffer helps avoid edge effects that arise from sharp gradients in terrain, ensuring smoother and more reliable boundary transitions.

#### Vtable for GFS pressure-level data from the ncep server

(domain_env)		[bdipson@bd01 WPS-4.5]\$ cat Vtable					
GRIB1	Level	From	To	metgrid	metgrid	metgrid	
Param	Type	Level1	Level2	Name	Units	Description	[GRIB2][GRIB2][GRIB2][GRIB2]
							[Discp][Catg][Param][Level]
11	100	*	*	TT	K	Temperature	0   0   0   100
33	100	*	*	UU	m s-1	U	0   1   2   100
34	100	*	*	VV	m s-1	V	0   1   2   3   100
52	100	*	*	RH	%	Relative Humidity	0   1   1   100
7	100	*	*	HGT	m	Height	0   1   3   5   100
11	105	2	TT	K	Temperature	at 2 m	0   0   0   103
52	105	2	RH	%	Relative Humidity	at 2 m	0   1   1   103
33	105	10	UU	m s-1	U	at 10 m	0   2   2   103
34	105	10	VV	m s-1	V	at 10 m	0   1   2   3   103
1	1	0	PSFC	Pa	Surface Pressure	0   1   3   0   1	
130	102	0	PSL	Pa	Sea-level Pressure	0   1   3   192   101	
144	112	0	SM008010	fraction	Soil Moist	0-10 cm below grn layer (Up)	2   0   0   192   106
144	112	10	SM010040	fraction	Soil Moist	10-40 cm below grn layer	2   0   0   192   106
144	112	40	SM041010	fraction	Soil Moist	40-100 cm below grn layer	2   0   0   192   106
144	112	100	SM100200	fraction	Soil Moist	100-200 cm below gr layer	2   0   0   192   106
144	112	100	SM010200	fraction	Soil Moist	10-200 cm below gr layer	2   0   0   192   106
11	112	0	10	ST000010	K	T 0-10 cm below ground layer (Upper)	0   0   0   0   106
11	112	10	10	ST000040	K	T 10-40 cm below ground layer (Upper)	0   0   0   0   106
11	112	40	100	ST041010	K	T 40-100 cm below ground layer (Upper)	0   0   0   0   106
11	112	100	200	ST0100200	K	T 100-200 cm below ground layer (Bottom)	0   0   0   0   106
85	112	0	10	ST000010	K	T 0-10 cm below ground layer (Upper)	2   0   0   2   106
85	112	10	40	ST010040	K	T 10-40 cm below ground layer (Upper)	2   0   0   2   106
85	112	40	100	ST041010	K	T 40-100 cm below ground layer (Upper)	2   0   0   2   106
85	112	100	200	ST0100200	K	T 100-200 cm below ground layer (Bottom)	2   0   0   2   106
11	112	10	200	ST010200	K	T 10-200 cm below ground layer (Bottom)	0   0   0   6   106
91	1	0	SEACIE	proptn	Ice flag	10   2   0   0   1	
81	1	0	LANDSEA	proptn	Land/Sea flag (1=land, 0 or 2=sea)	2   0   0   0   1	
81	1	0	LANDN	proptn		2   0   0   218   1	
7	1	0	SOLHGT	m	Terrain field of source analysis	0   3   5   1	
11	1	0	SKINTEMP	K	Skin temperature	0   0   0   0   1	
65	1	0	SNOW1	kg m-2	Water equivalent snow depth	0   1   13   1	
1	0	0	SNOWH	m	Physical Snow Depth	0   1   1   1	
33	6	0	UMMAX	m s-1	U	at max wind	0   2   2   2   6
34	6	0	VMAXX	m s-1	V	at max wind	0   2   2   3   6
2	6	0	PMAXX	Pa	Pressure of max wind level	0   3   0   0   6	
1	6	0	PMAXXNN	Pa	PMAXX, used for nearest neighbor interp	0   3   0   0   6	
2	6	0	TMXX	1K	Temperature at max wind level	0   0   0   0   6	
7	6	0	HGTMAXX	m	Height of max wind level	0   3   5   6	
33	7	0	UTROP	m s-1	U	at tropopause	0   2   2   2   7
34	7	0	VTROP	m s-1	V	at tropopause	0   1   2   3   7
2	7	0	PTROP	Pa	Pressure of tropopause	0   3   0   0   7	
1	7	0	PTROPN	Pa	PTROP, used for nearest neighbor interp	0   3   0   0   7	
2	7	0	TTROP	K	Temperature at tropopause	0   0   0   0   7	
7	7	0	HGTROP	m	Height of tropopause	0   3   5   7	

### **4.3.3. Ungrib**

ungrib.exe is utilized as a preprocessing tool within the WRF Preprocessing System (WPS) to extract and decode meteorological data from global datasets. Its primary function is to convert raw meteorological data files into a format that is compatible with the WRF model. This step involves reading GRIB-formatted data files (commonly used for global atmospheric datasets) and converting them into intermediate binary files (FILE:\*) that are processed in subsequent steps.

The Variable Specification File (VTable) plays a critical role in this process. The VTable is a configuration file that maps variables in the input GRIB dataset to the variables required by the WRF model. It ensures that the correct meteorological fields, such as temperature, wind, pressure, and moisture, are identified, extracted, and appropriately formatted. In this study, I use a VTable specific to the selected global meteorological dataset, ensuring consistency between the data source and the WRF model requirements.

### **4.3.4. Metgrid**

metgrid.exe program, it serves as a critical step in the WRF preprocessing workflow. The purpose of this step was to interpolate meteorological data onto the model's simulation domains. Using the six-hourly GRIB2 files from the NCEP FNL dataset, metgrid.exe processed the intermediate files generated by ungrib.exe and aligned the data with the defined domain configuration.

During the execution, metgrid.exe applied the geographic and grid specifications set in the WRF domain configuration, ensuring that the input meteorological data was accurately mapped to the nested domains. This included handling the Lambert conformal conic projection used for Nepal's mid-latitude region and accounting for the grid refinement ratios between the domains.

## **4.4. WRF Physics Configurations**

The physics schemes used in WRF simulations are described along with their corresponding short forms, as specified in the **namelist.input** file.

- Turbulence/Diffusion (diff\_opt, km\_opt)
- Radiation Longwave (ra\_lw\_physics)
- Shortwave (ra\_sw\_physics)
- Surface
- Surface layer (sf\_sfclay\_physics)
- Land/water surface (sf\_surface\_physics)
- PBL (bl\_physics) Cumulus parameterization
- (cu\_physics)
- Microphysics (mp\_physics)

The use\_wudapt\_lc = 1 setting enables the utilization of high-resolution geodata derived from the MODIS 100m hybrid dataset. This approach leverages the detailed spatial resolution of MODIS data to enhance urban modeling accuracy. By activating this feature, the system incorporates urban parameterization tailored to Local Climate Zone (LCZ) classifications through the application of an LCZ-specific URBPARM file. This file provides critical urban parameters, such as surface roughness, albedo, thermal properties, and anthropogenic heat fluxes, calibrated for each LCZ type. The integration of the WUDAPT (World Urban Database and Portal Tools) LCZ framework with MODIS geodata ensures a precise representation of urban environments, facilitating more accurate simulations of urban climate

and surface-atmosphere interactions. This configuration is particularly valuable for studies involving urban heat island effects, urban microclimates, and city-scale weather or climate modeling.

The provided &physics configuration in the WRF namelist.input file is optimized for simulations involving high terrain and urban areas. It uses WUDAPT (World Urban Database and Portal Tool) Local Climate Zones to enhance urban representation and employs the Thompson microphysics scheme (mp\_physics = 10) to accurately simulate cloud and precipitation processes. The Grell-Freitas cumulus scheme is applied in the parent domain, while explicit convection is used for higher-resolution nested domains. Longwave and shortwave radiation are handled by the RRTMG schemes, with a radiation update frequency of 12.5 minutes for all domains. The Yonsei University (YSU) PBL scheme, paired with the Monin-Obukhov surface layer scheme, is used to represent atmospheric boundary layer processes, while the Noah land surface model (LSM) manages surface energy and moisture fluxes. The setting sf\_surface\_physics = 2 couples NOAH land Surface Model with Urban canopy Model and sf\_urban\_physics=1 enables WRF-SLUCM (Single layer Urban Canopy Model) within the WRF (Weather Research and Forecasting) modeling framework. By selecting this configuration, the model integrates the Noah Land Surface Model (LSM) with urban parameterization. Time steps for cumulus and PBL schemes ensure frequent updates to capture terrain-induced variability. This configuration balances physical accuracy and computational efficiency, making it suitable for complex terrain and urban simulations. It employs a hybrid sigma-pressure vertical coordinate system (hybrid\_opt = 2) with a low blending value (etac = 0.02) to improve model performance in regions with steep topography, ensuring smoother transitions between terrain-following and pressure-based coordinates. Vertical velocity damping (w\_damping = 1) reduces numerical noise from strong vertical motions often observed in mountainous areas.

## 4.5. Urban Parameterization

*Table 6: ZR (Roof level / Building Height) used for Urban Parameterization for running WRF-SLUCM (Single Layer Urban Canopy Model)*

Index	Type	ZR (Roof Level/Building Height) [m]
1	Compact High-Rise	30
2	Compact Mid-Rise	15
3	Compact Low-Rise	7
4	Open High-Rise	30
5	Open Mid-Rise	15
6	Open Low-Rise	7
7	Lightweight Low-Rise	4
8	Large Low-Rise	7
9	Sparsely Built	7
10	Heavy Industrial	12
11	Asphalt	10

The roof levels (ZR) specified for various urban types, such as Compact High-Rise (30 m), Compact Mid-Rise (15 m), and Compact Low-Rise (7 m), were determined based on municipal drawings and urban planning data from the Kathmandu region. These ZR values represent the average building heights for the respective urban categories, providing an accurate representation of the city's urban morphology. Additionally, other parameters such as Anthropogenic Heat (AH), Anthropogenic Latent Heat (ALH), and the AKANDA\_URBAN coefficient were incorporated using parameterization techniques outlined by I.D. Stewart and T.R. Oke in their work on Local Climate Zones (LCZs) for urban temperature studies.

## Chapter V: Analysis and Observations

### 5.1. Calculation of Land Surface Temperature using Landsat

The calculation of LST was performed using ArcGIS by extracting metadata from Landsat OLI/TIRS data, leveraging ArcGIS tools to crop the area of interest and performing the necessary calculations to produce the LST raster file, ensuring a high-resolution and geographically specific outcome. The Top of Atmospheric (TOA) spectral radiance and brightness temperature are calculated using band-specific rescaling factors and thermal constants provided in Landsat metadata, as outlined in the Landsat User Handbook by the U.S. Geological Survey (USGS). Vegetation indices, such as the Normalized Difference Vegetation Index (NDVI), derived from near-infrared and red reflectance bands, follow methods established by Rouse et al. (1973). Proportion of vegetation and land surface emissivity are estimated through empirical relationships, like those described by Sobrino et al. (2004), linking NDVI to emissivity. Finally, the LST is derived by integrating emissivity and TOA brightness temperature, applying corrections based on Planck's radiation law, as detailed in studies such as Weng et al. (2004)

#### 1. Top of Atmospheric (TOA) Spectral Radiance

$$L\lambda = M_L * Q_{CAL} + A_L - O_i$$

Where,

$L\lambda$  = Top of Atmospheric (TOA) Spectral Radiance.

$M_L$  = Band-specific multiplicative rescaling factor from metadata. (RADIANCE\_MULT\_BAND\_x)

$Q_{CAL}$  = Quantized and calibrated standard product pixel values (Band 10)

$A_L$  = Band-specific additive rescaling factor from Metadata (RADIANCE\_ADD\_BAND\_x)

$O_i$  = Correction for Band 10

#### 2. Calculation of top of atmosphere brightness temperature

$$BT = \frac{K_2}{\ln \left[ \left( \frac{K_1}{L\lambda} \right) + 1 \right]} - 273.15$$

Where,

$BT$  = Top of atmosphere brightness temperature (C)

$K_1$  = Band-specific thermal conversion constant from Metadata (K1\_CONSTANT\_BAND\_x)

$K_2$  = Band-specific thermal conversion constant from the Metadata (K2\_CONSTANT\_BAND\_x)

$L\lambda$  = Top of Atmospheric (TOA) Spectral Radiance

#### 3. Calculation of NDVI

$$NDVI = \frac{NIR(BAND5) - R(BAND4)}{NIR(BAND5) + R(BAND4)}$$

Where,

NIR = Near Infrared

R = Red

#### 4. Calculating Proportion of Vegetation (PV)

$$PV = \left( \frac{NDVI - NDVI_{mean}}{NDVI_{max} + NDVI_{mean}} \right)^2$$

#### 5. Calculation of Land Surface Emissivity (E)

$$E = 0.004 * PV + 0.986$$

#### 6. Calculation of Land Surface Temperature .

$$LST = \frac{BT}{1 + \frac{(W * BT)}{14380} * \ln(E)}$$

Where,

LST =Land Surface Temperature in Celcius

W = Wavelength of emitted radiace

BT = Top of atmosphere brightness temperature (C)

E = Land Surface Emissivity (LSE)

### 5.2. Workflow process in MODIS Metadata.

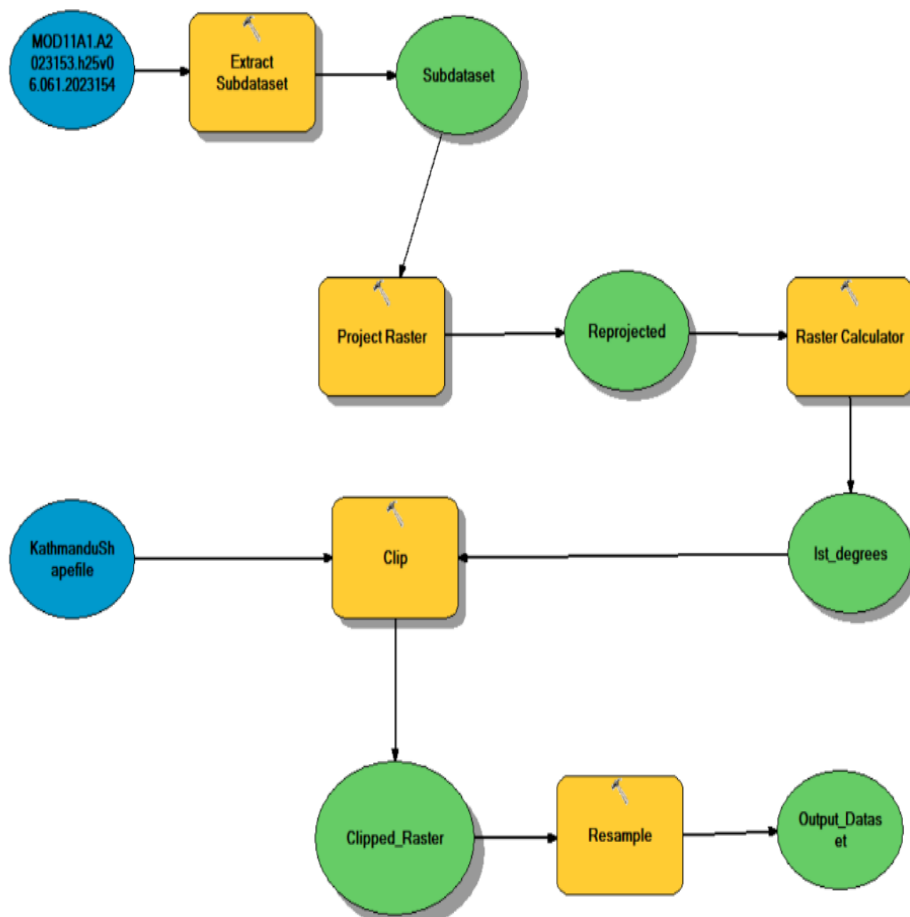


Figure 26 : Model Setup in ArcGIS for Processing the MODIS products for Summer cases

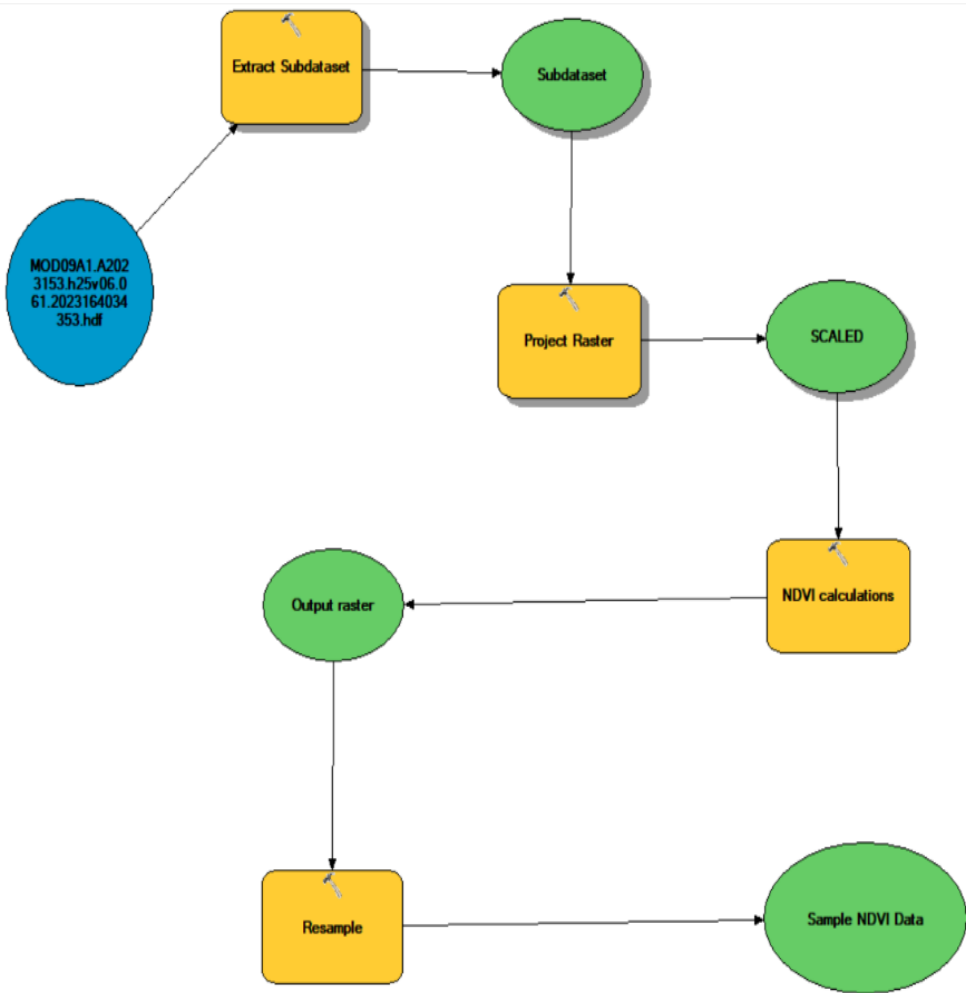


Figure 27 : Model Setup in ArcGIS for Calculation of NDVI from MODIS products for Summer Case .

The MOD11A1 data was processed to derive land surface temperature (LST) for the Kathmandu region. The process began by extracting a subset of the dataset (sub dataset) from the HDF file, which was then reprojected to align with the desired coordinate system. A raster calculator was used to convert the LST values into degrees, ensuring the data was in a usable format. The data was further clipped using a shapefile of Kathmandu to isolate the area of interest. Finally, the clipped raster was resampled to achieve uniform spatial resolution, resulting in an output dataset that was ready for analysis. The MOD09A1 data was processed to calculate the NDVI for the study area. Similar to the first workflow, the sub dataset was extracted and reprojected. The scaled data was then used in an NDVI calculation to generate vegetation indices, which highlighted vegetation health and cover. The resulting raster was resampled for consistent resolution, and the NDVI data was sampled further to prepare it for detailed analysis.

### **5.3. Computational Environment for WRF Simulation**

The simulation employed the Advanced Research WRF (ARW) core, using the Eulerian Mass Coordinate dynamics for atmospheric modeling. Preprocessing was conducted using WPS V4.5 to prepare input data and WRFV4.5.2 was used to run the simulation in Intel Environment. The simulation was configured with three nested domains of increasing resolution: the parent domain at 15 km grid spacing, the first nested domain at 5 km, and the second nested domain at approximately 1.67 km, enabling high-fidelity local modeling.

The system operated on a Linux-based operating system with Little Endian byte order. Parallelization was implemented using a hybrid MPI strategy. The simulation utilized 36 MPI tasks, distributed across 6 tasks in the X-direction and 6 tasks in the Y-direction. A 1D-Y tiling strategy was applied, splitting the computational grid along the Y-dimension for parallelization. Each domain was processed using a single tile, with Domain 1 configured as WRF TILE 1 IS 68 IE 84 JS 1 JE 17 and Domain 2 as WRF TILE 1 IS 85 IE 105 JS 1 JE 19. This configuration ensured efficient load balancing and optimal use of computational resources.

The hardware resources included an x86\_64 processor architecture with an Intel(R) Xeon(R) Silver 4216 CPU operating at a base clock speed of 2.10 GHz and a maximum clock speed of 3.2 GHz. The system had 16 physical cores with Each physical core consisting of two threads (Hyper-Threading enabled). resulting in 32 logical CPUs distributed over a single NUMA node (Node 0: CPUs 0-31). The total RAM was sufficient to support the simulation. Disk space requirements were managed effectively, The frames\_per\_outfile is set to 48, indicating that each output file contains 48 frames of data. As a result, each file represents 24 hours of simulation, with 30-minute intervals between each recorded frame.

To determine the optimal number of processors for the simulation, I used the provided equations tailored for the smallest and largest-sized domains. For the smallest domain, the equation  $((e_{we})/25) \times ((e_{sn})/25)$  was applied, where  $e_{we}$  and  $e_{sn}$  represent the domain dimensions in the west-east and south-north directions, respectively. This calculation provided the maximum number of processors that can effectively be utilized for this domain, ensuring computational efficiency without excessive overhead.

Similarly, for the largest domain, the equation  $((e_{we})/100) \times ((e_{sn})/100)$  was used to compute the minimum number of processors that should be employed. This ensures that the domain size is adequately distributed among processors while avoiding inefficiencies from underutilizing computational resources. These calculations guides in selecting an appropriate range for the number of processors, balancing the computational workload across domains efficiently

#### 5.4. Land Used Land Covered (LULC) using Unsupervised Classification

LULC UNSUPERVISED CLASSIFICATION OF KATHMANDU

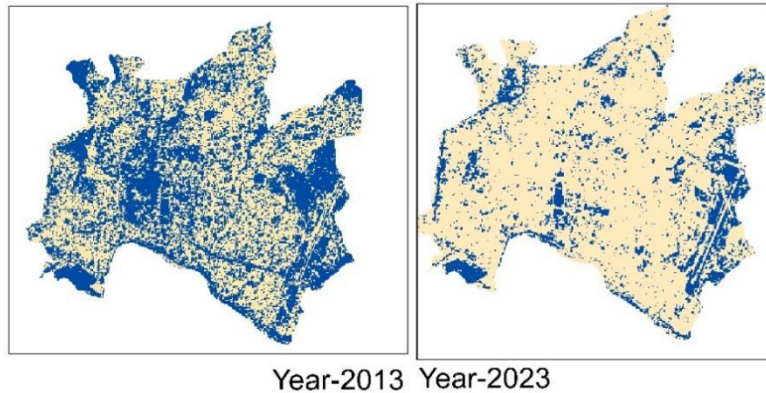


Figure 28 : LULC Unsupervised Classification of Kathmandu

LULC UNSUPERVISED CLASSIFICATION OF POKHARA

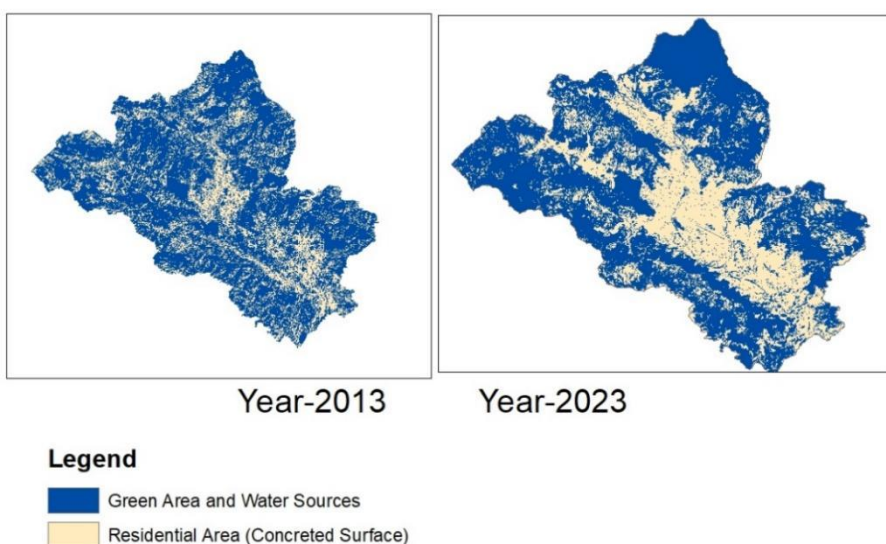


Figure 29 : LULC Unsupervised Classification of Pokhara

Using the ArcGIS platform, geospatial analysis was conducted within the boundaries of two cities—Kathmandu and Pokhara—focusing on the years 2013 and 2023. The results revealed that Kathmandu has experienced rapid urbanization over the past decade. In contrast, in Pokhara, there has been a noticeable shift in settlements toward the center of the valley. This is likely influenced by Pokhara's unique topography, which forms a cup-like shape surrounded by high hills. Given the region's heavy monsoon rainfall, there is a higher risk of landslides and other slope-related natural disasters. As a result, people have migrated toward the central plains. Despite this, the density of the urban area in Pokhara remains lower compared to Kathmandu.

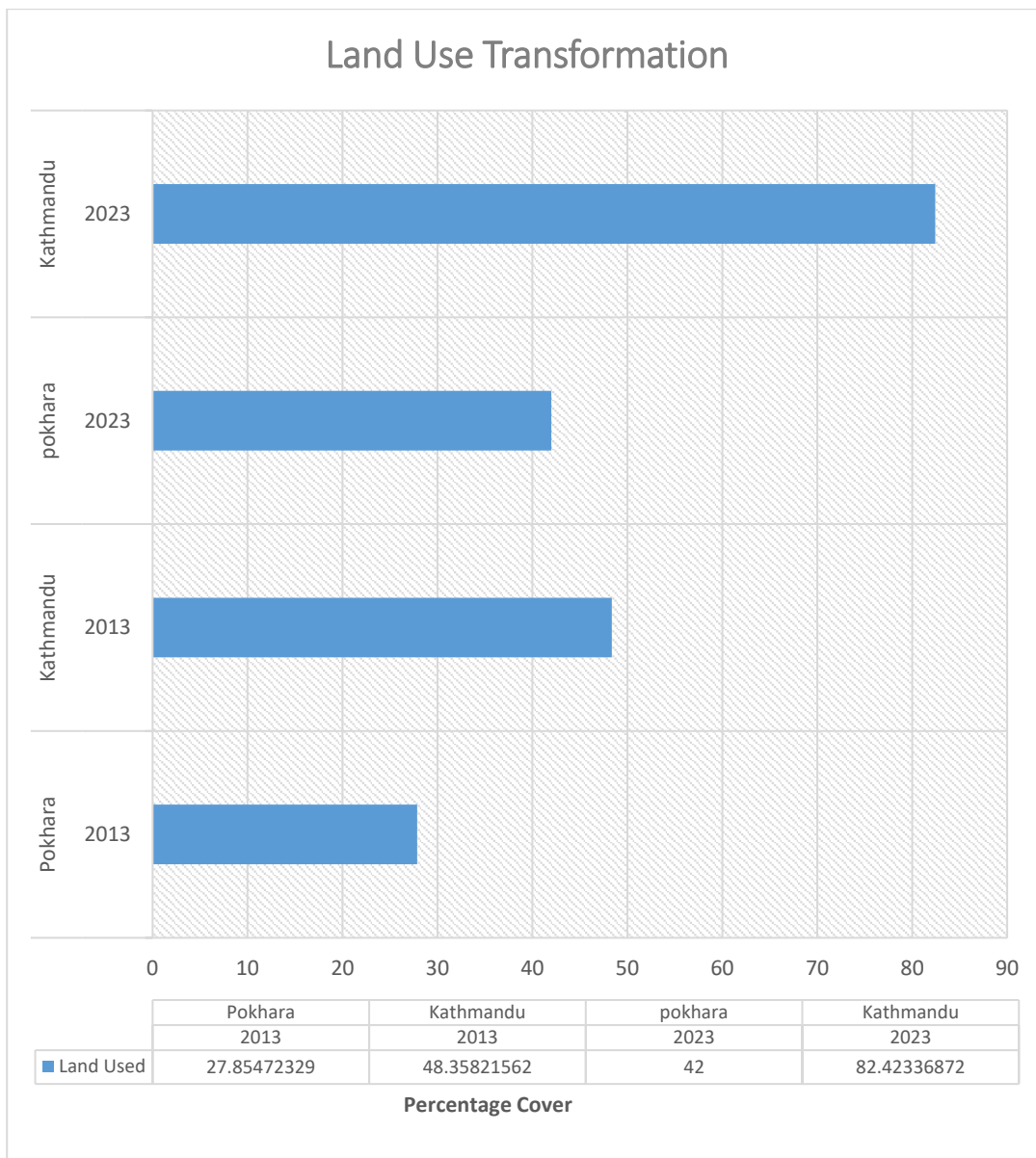


Figure 30 : Land Use Transformation from 2013 -2023

Fig reflects rapid urbanization in Kathmandu, with a notable rise of approximately **34%** over the 10-year period. This indicates a major shift in land use, likely driven by urban expansion and population growth. Although Pokhara also saw a significant increase in land use (around **14%**), the rate of urbanization is much slower compared to Kathmandu. This is likely due to Pokhara's unique geography, including the cup-shaped topography and higher risk of landslides, which may restrict urban sprawl to some extent. These results are approximates and were generated using pixel values of built-up areas derived from GIS software. The raster data were converted to polygons to quantify the changes in land area. It is important to note that the approach for calculating land use and land cover can vary depending on the research objectives and classification methods. In this case, to simplify the quantification process, built-up areas (concreted surfaces) were grouped as a single entity, while the rest of the land characteristics were categorized as green areas. This method provides a clear picture of the changes in land use over the past decade in both cities, offering valuable insights into urban expansion and spatial development.

## 5.5. Preparation of Local Climate Zone (LCZ) Map for Area of Interest

### Urban Local Climate Zone (LCZ) categorization

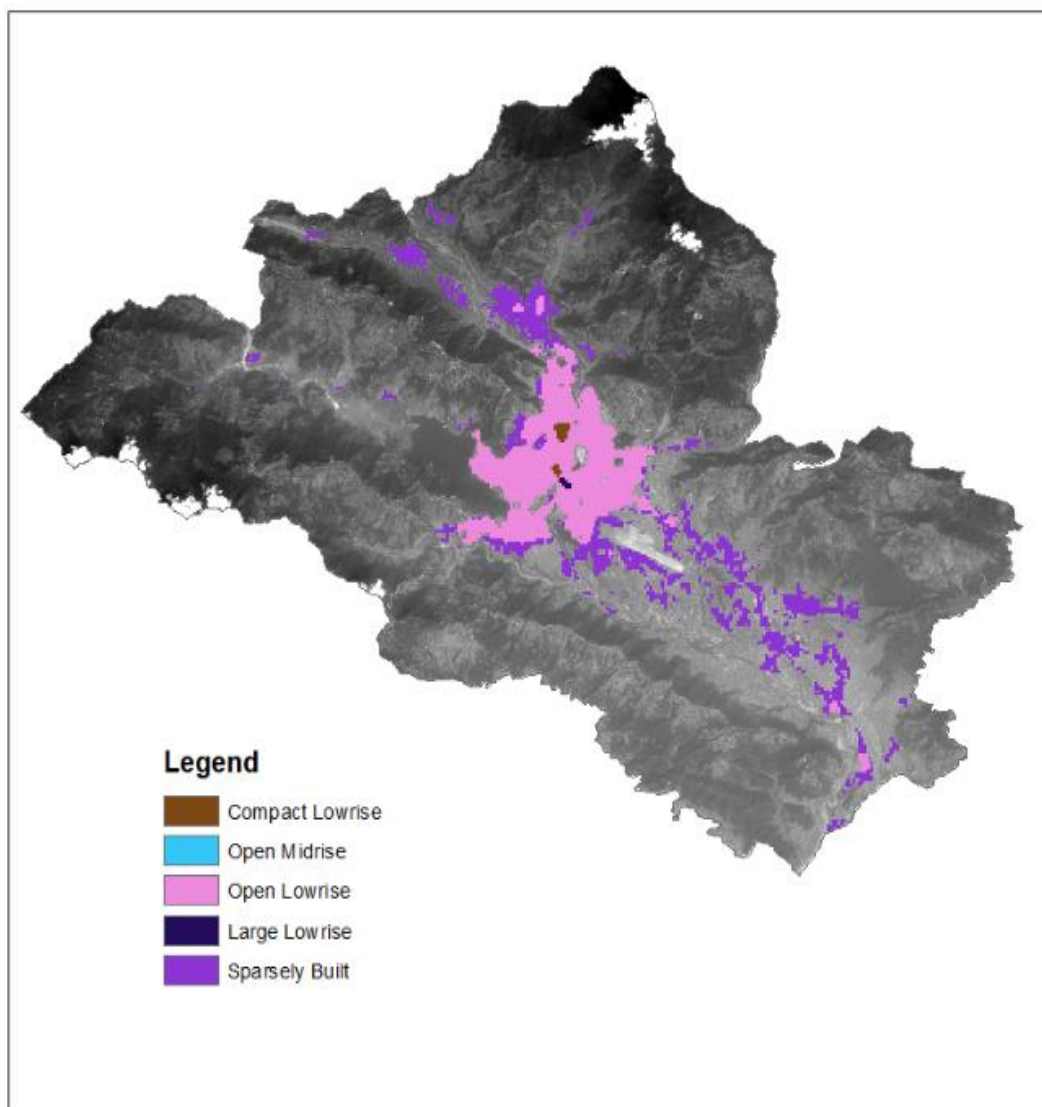


Figure 31 : Local Climate Zone (LCZ) Classification of Pokhara

## Urban Local Climate Zone (LCZ) categorization

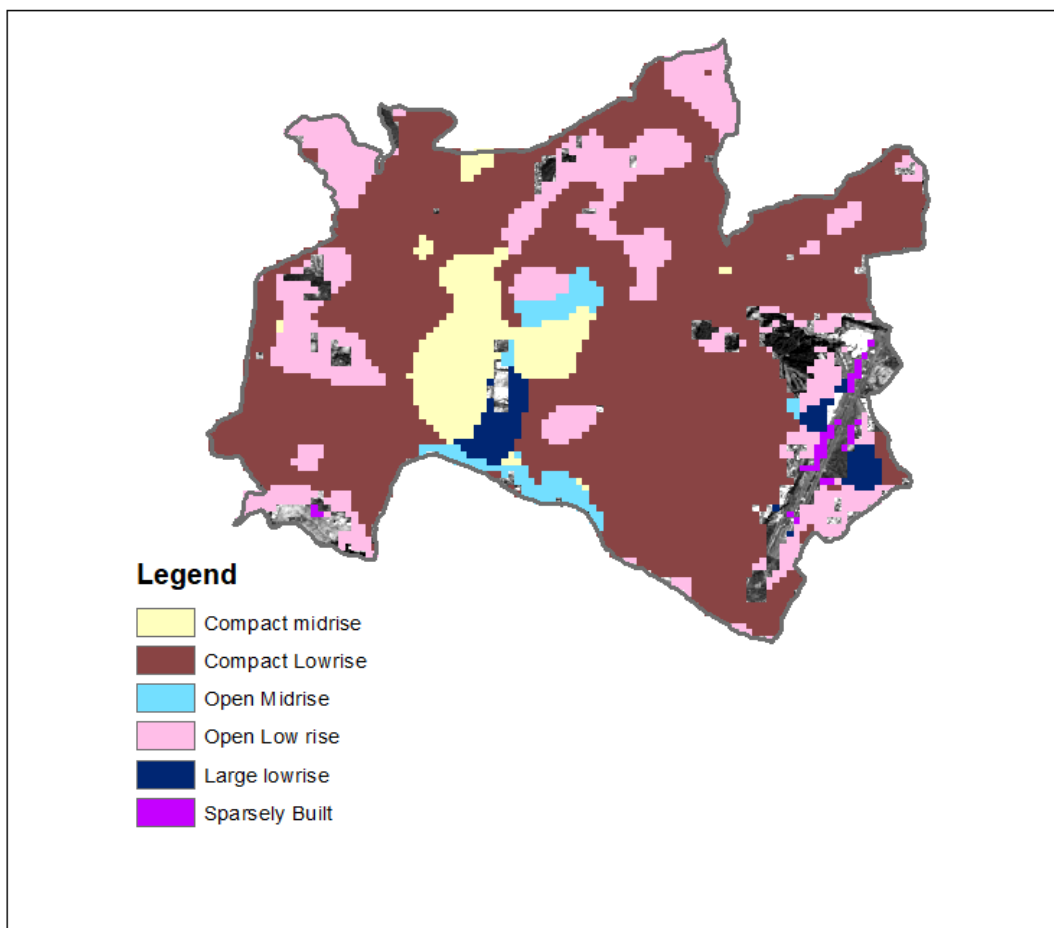


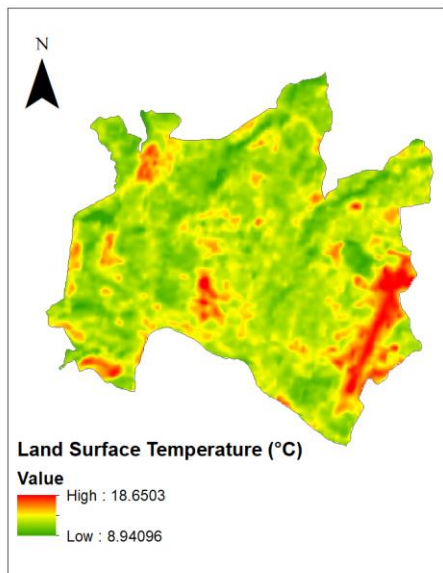
Figure 32 : Local Climate Zones (LCZ) classification of Kathmandu

The Hybrid 100-m global land cover dataset with Local Climate Zones is a large-resolution dataset. It was processed using the pyramid method, which enhances display performance by downsampling the original raster dataset. Each successive layer in the pyramid is downsampled at a 2:1 ratio. Figures included in the analysis depict the categorization of built-up areas based on characteristics such as compact midrise, compact lowrise, open lowrise, open midrise, and others. From these figures, it is evident that Pokhara has a significant concentration of open lowrise buildings in its center, particularly near Phewa Lake, a well-known tourist destination with numerous hotels and residential areas. Beyond this zone, the data shows large expanses of sparsely built areas, while compact lowrise and large lowrise buildings appear in smaller sections. In contrast, Kathmandu demonstrates a higher density of building types. The city is predominantly covered by compact lowrise structures, followed by open lowrise, open midrise, and large lowrise buildings. The notable differences in the built-up characteristics between the two cities suggest that the urban heat island (UHI) effects would vary accordingly, leading to findings that reflect these variations in urbanization patterns.

## 5.6. Observation of Land Surface Temperature (LST) of Kathmandu

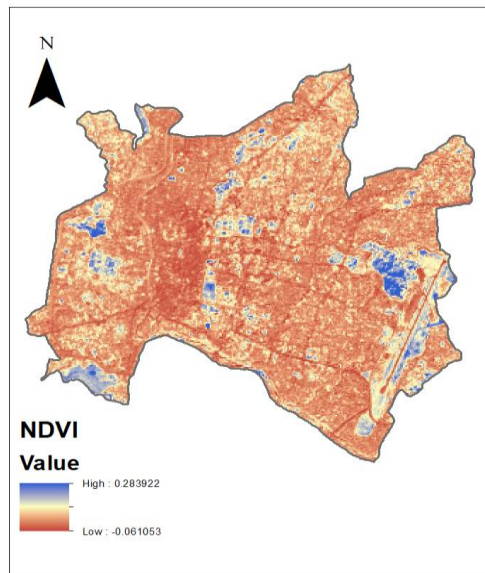
### 5.6.1. Winter Season

Land Surface Temperature (LST) of Kathmandu in Winter.



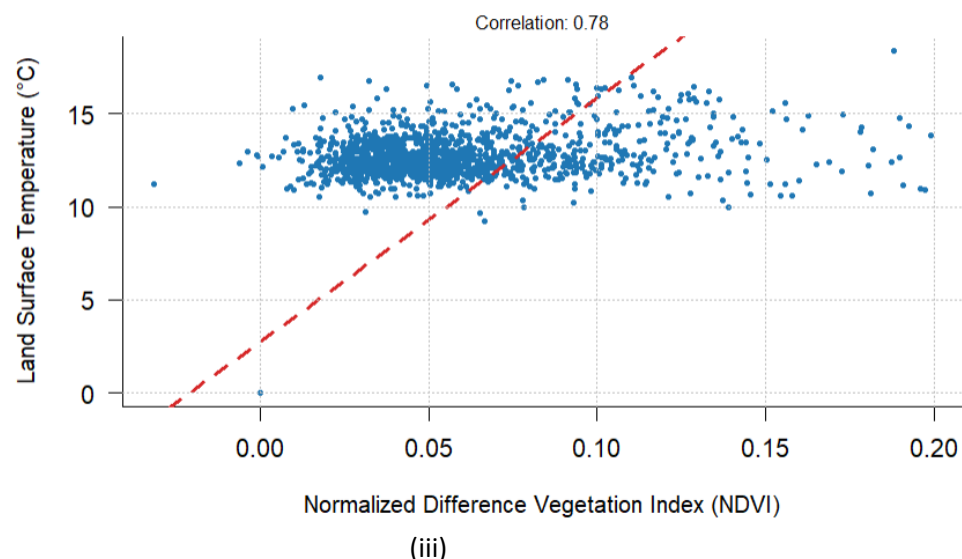
(i)

NDVI of Kathmandu in Winter.



(ii)

Relationship Between NDVI and LST of Kathmandu in Winter



(iii)

Figure 33 : (i) Land surface temperature of Kathmandu in Winter, (ii) NDVI of Kathmandu in Winter. (iii) Relationship between NDVI and LST of Kathmandu in Winter.

The figures illustrate the relationship between land surface temperature (LST) and vegetation cover, as represented by the Normalized Difference Vegetation Index (NDVI), within the urban area of Kathmandu during winter. The figure(iii) displays a scatter plot showing the correlation between NDVI and LST in Kathmandu during winter, with a moderate positive correlation of 0.78. This positive relationship indicates that areas with higher vegetation (higher NDVI values) tend to have slightly lower LST values, but in winter, this relationship is less pronounced due to lower overall temperatures and reduced vegetation activity. It suggests that even in winter, vegetation plays a role in moderating land surface temperatures in urban areas. Figure(i) a heat map of LST, reveals spatial variations in temperature across Kathmandu, with warmer zones (in red) mainly concentrated in areas likely dominated by urban structures, such as densely built-up regions. The temperature in these areas ranges between approximately 8.94°C to 18.65°C. The third image, representing NDVI, shows vegetation distribution, with higher NDVI values (blue areas) corresponding to vegetated or open spaces, while lower NDVI values (reddish areas) indicate built-up zones. Comparing the two maps, it is evident that areas with higher LST correspond with lower NDVI values, supporting the UHI phenomenon where urbanization and lack of vegetation lead to elevated surface temperatures. In summary, these images collectively demonstrate the spatial relationship between vegetation cover and temperature in Kathmandu. In winter, while the temperature variations are less intense, the presence of vegetation still correlates with cooler surface temperatures, underscoring the mitigating role of green spaces in urban thermal regulation.

### 5.6.2 Summer Season

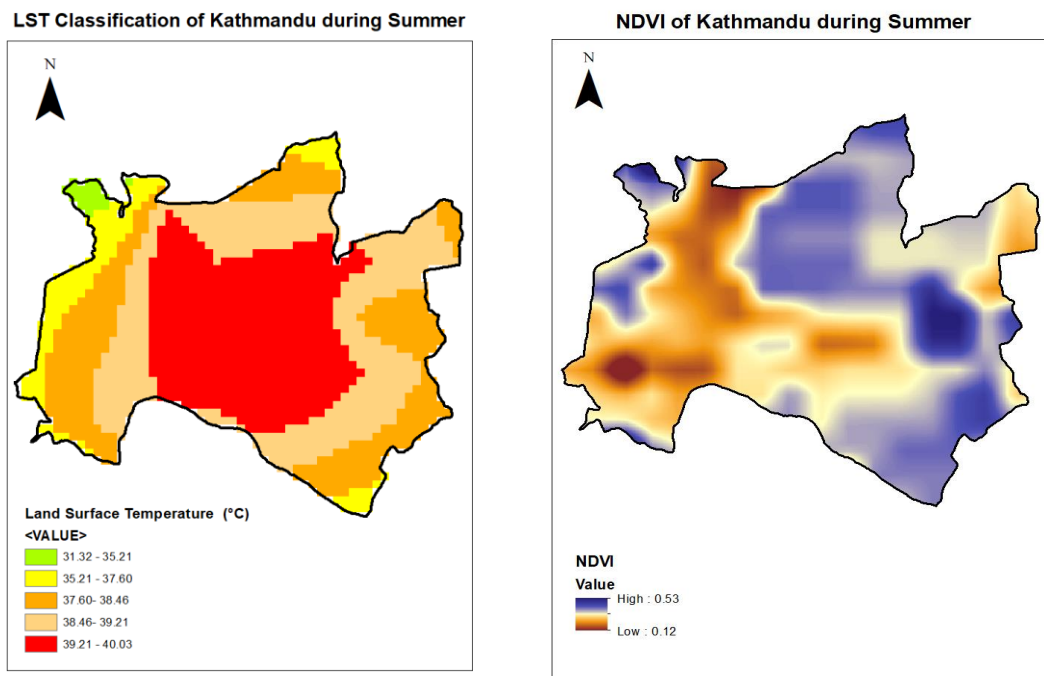


Figure 34: LST and NDVI classification of Kathmandu during summer.

The heat map of LST classification visualizes the temperature distribution across Kathmandu in summer. The map highlights a temperature gradient, with the highest temperatures (39.21–40.03°C, shown in red) concentrated in central urban areas. This pattern aligns with urban structures that intensify heat retention, especially under high summer temperatures. In comparison to winter, the

summer temperatures are much higher, with the peak LST exceeding 40°C. Figure.28 also displays the NDVI distribution across Kathmandu in summer, with higher NDVI values (blue) indicating vegetated areas, likely open green spaces or parks, and lower NDVI values (orange) pointing to densely built-up regions. Compared to winter, NDVI values in summer are higher overall, reflecting active vegetation growth that can offer more pronounced cooling effects.

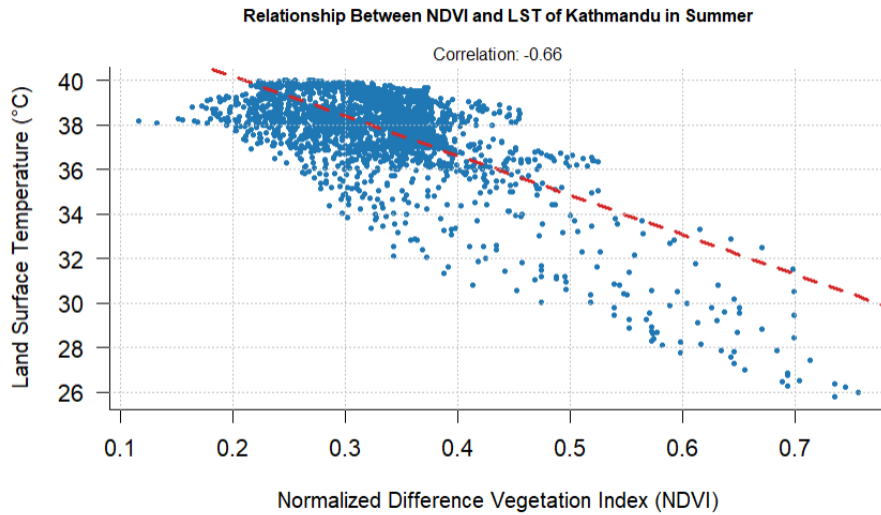


Figure 35 : Relationship Between NDVI and LST of Kathmandu in Summer

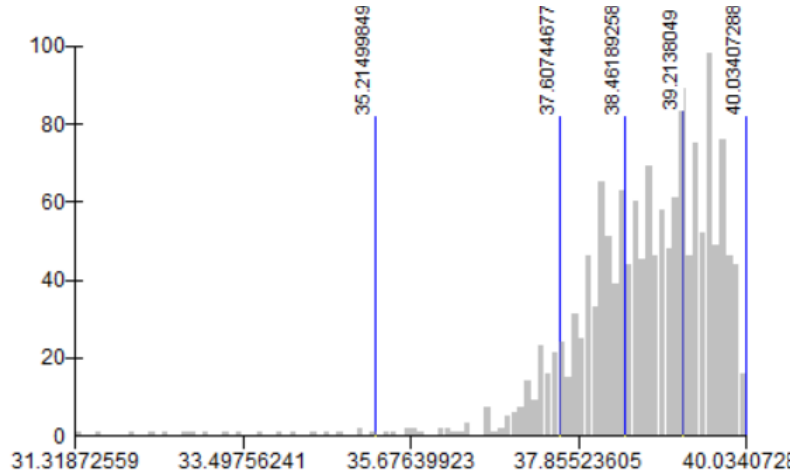


Figure 36 : Temperature Distribution (Skewed Right)

The scatter plot showing a negative correlation (-0.66) between NDVI and LST in Kathmandu during summer, indicating that areas with more vegetation (higher NDVI) experience lower surface temperatures. This negative correlation is stronger than in winter, likely due to the increased influence of vegetation on cooling during the warmer season, when evapotranspiration from plants contributes significantly to temperature moderation. The fourth image shows the distribution of LST values in summer, indicating a right-skewed distribution where the majority of LST values fall between 37.85°C and 40.03°C, reflecting the hot conditions typical of Kathmandu's summer.

## Comparison of Summer and Winter Data

In comparing summer and winter, there are notable differences in the relationship between NDVI and LST, as well as in the spatial patterns of LST. The correlation between NDVI and LST is positive in winter (0.78) but negative in summer (-0.66), suggesting that vegetation has a greater cooling effect in summer than in winter. This season-dependent effect likely reflects increased evapotranspiration during warmer months, which actively cools the land surface.

The spatial distribution of LST also varies significantly: summer LST values are notably higher, with peak values exceeding 40°C, while winter LST ranges only between 8.94°C and 18.65°C. In both seasons, the highest LST values are found in areas with low NDVI, reinforcing the impact of urbanization on temperature elevation.

These seasonal differences underscore the significance of vegetation in mitigating UHI effects, especially during summer when temperature extremes are most pronounced. Implementing more green spaces within urban zones could help to alleviate high LSTs, enhancing thermal comfort and reducing UHI intensity, particularly during the warmer season.

## 5.7. Observation of Land Surface Temperature (LST) of Pokhara

### 5.7.1. Winter Season

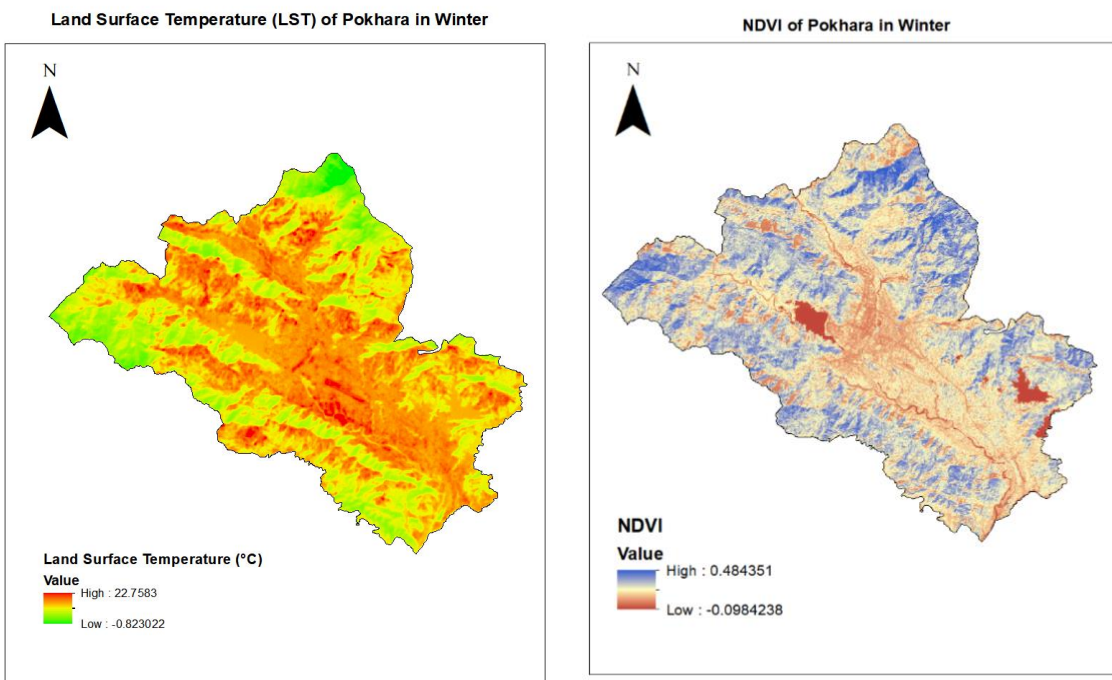


Figure 37 : Land Surface Temperature (LST) and NDVI of Pokhara during Winter.

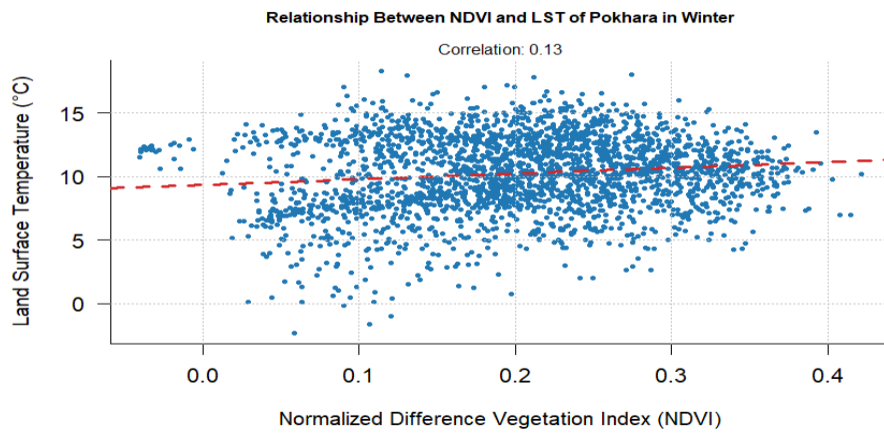


Figure 38 : Relationship Between NDVI and LST of Pokhara in Winter.

The relationship between NDVI and LST in Pokhara during winter, as shown in the scatterplot, reveals a weak positive correlation ( $r = 0.13$ ), suggesting that vegetation has a limited impact on moderating surface temperatures in this season. This could be attributed to seasonal vegetation dormancy, sparse vegetation cover, or the prevalence of other surface types, such as built-up or barren areas, that influence land surface temperature. The NDVI map supports this, highlighting regions with low NDVI values in urban and built-up areas (indicated in red), which are likely contributing to higher LSTs. In contrast, areas with higher NDVI values (in blue), representing vegetated zones, exhibit cooler surface temperatures due to the cooling effects of vegetation. The spatial variability in NDVI values underscores the role of land cover in urban heat dynamics, where urban and sparsely vegetated areas exacerbate heat, emphasizing the need for urban greening to mitigate UHI effects in Pokhara.

### 5.7.2. Summer Season

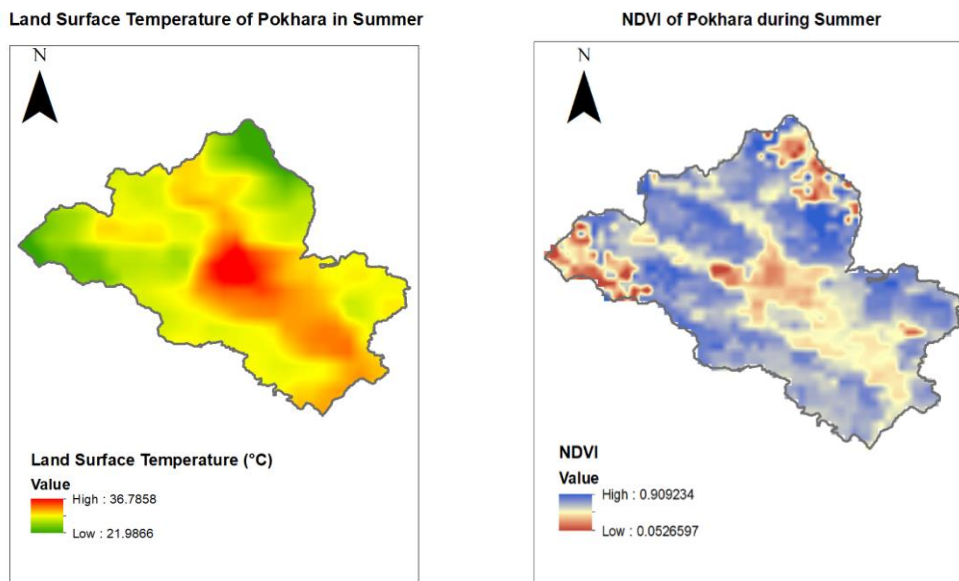
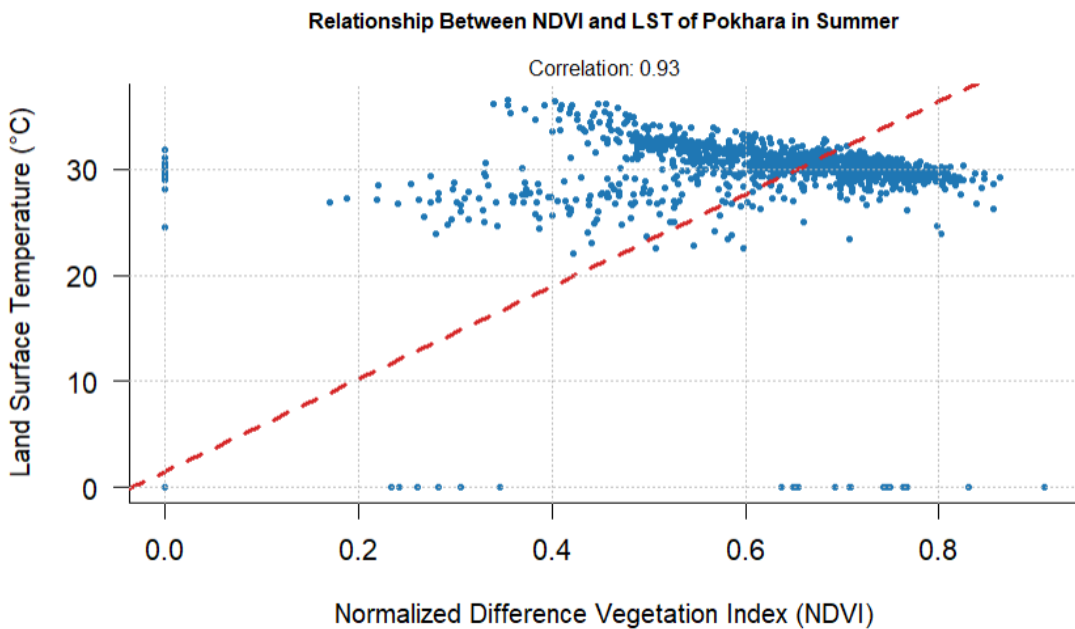


Figure 39: Land Surface Temperature (LST) and NDVI of Pokhara during summer.



*Figure 40 : Relationship Between NDVI and LST of Pokhara during summer.*

The LST map shows land surface temperature values ranging from 21.99°C to 36.79°C, with the hottest areas (red zones) concentrated in urban or built-up regions. These hotspots correspond to areas with low NDVI values in the NDVI map, signifying potential urban heat islands (UHIs). Cooler regions (green areas) align with vegetated zones or higher elevations, but this cooling effect seems limited given the strong positive correlation in the scatterplot.

The unexpected positive correlation ( $r = 0.93$ ) between NDVI and LST in summer suggests that the cooling effects of vegetation in Pokhara might be overshadowed by local climatic, geographic, or land-use factors. While the maps confirm the presence of urban heat islands (UHIs) in urban zones with low NDVI, the scatterplot indicates that some vegetated areas also experience high temperatures. This finding emphasizes the complexity of UHI dynamics and the need for further analysis to understand the interaction between vegetation, terrain, and land surface temperatures in Pokhara.

### **3.13. Zonal classification of the Land Surface Temperature.**

The Zonal Classification of Land Surface Temperature is Based on the CGLC MODIS dataset , which is a hybrid 100-m global land cover dataset specially created for its implementation in Weather Research and Forecastinf (WRF) model. This dataset is based on the Copernicus Global land serivice Land Cover (CGLC) products resampled to MODIS IGBP classes (CLGC-MODIS) and glbal map of Local Climate Zone (LCZ). The remaining areas are filled eith the MODIC land cover classes.

For the analysis of Urban Heat Island in Two cities, The Raw data set of CGLC MODIS dataset were extracted into ARCGIS using Pyramid appoach, this method optimize the performance of raster dataset by creating the pyramids and generating the lower resolution version of original raster making it more efficient for working with the raster file. The Land Surface temperature of two cities, which were obtained using LANDSAT and MODIS satellite were averaged according to the Local Climatic Zones using the Zonal Statistcs tools in ArcGIS. This provided the mean temperature accross various Clamtic Zones which is defined by the CGLC MODIS LCZ raster file.

*Table 7: Mean Land Surface Temperature Based on the Distribution of Local Climatic Zones define by CGLC-MODIS-LCZ dataset of Kathmandu and Pokhara in Summer*

Local Climate Zone (LCZ)	Mean Land Surface Temperature (Pokhara)	Mean Land Surface Temperature (Kathmandu)
Green/Remote	30.03	35.34
Compact Mid-Rise	-	39.59
Compact Low-Rise	35.49	38.82
Open Mid-Rise	31.62	39.39
Open Low-Rise	34.18	37.98
Large Low-Rise	36.21	39.09
Sparsey Built	32.20	38.41

*Table 8: Mean Land Surface Temperature Based on the Distribution of Local Climatic Zones define by CGLC-MODIS-LCZ dataset of Kathmandu and Pokhara in Winter.*

Local Climate Zone(LCZ)	Mean Land Surface Temperature of Pokhara (°c)	Mean Land Surface Temperature of Kathmandu (°c)
Green/Remote	8.55	8.34
Compact Mid-Rise	-	12.42
Compact Low-Rise	13.48	12.63
Open Mid-Rise	12.66	12.76
Open Low-Rise	13.12	12.57
Large Low-Rise	14.96	13.99
Sparsey Built	13.16	11.91

Tables 6 and 7 provide a comprehensive overview of the mean land surface temperature (LST) values categorized according to the Local Climate Zone (LCZ) classification for the cities of Pokhara and Kathmandu during both the summer and winter seasons. These classifications are based on the application of the CGLZ-MODIS-LCZ framework, that combines satellite-derived data from the MODIS (Moderate Resolution Imaging Spectroradiometer) platform with the Local Climate Zone classification system. This enables analysis of urban thermal patterns and variations in land surface temperatures across different climatic zones.

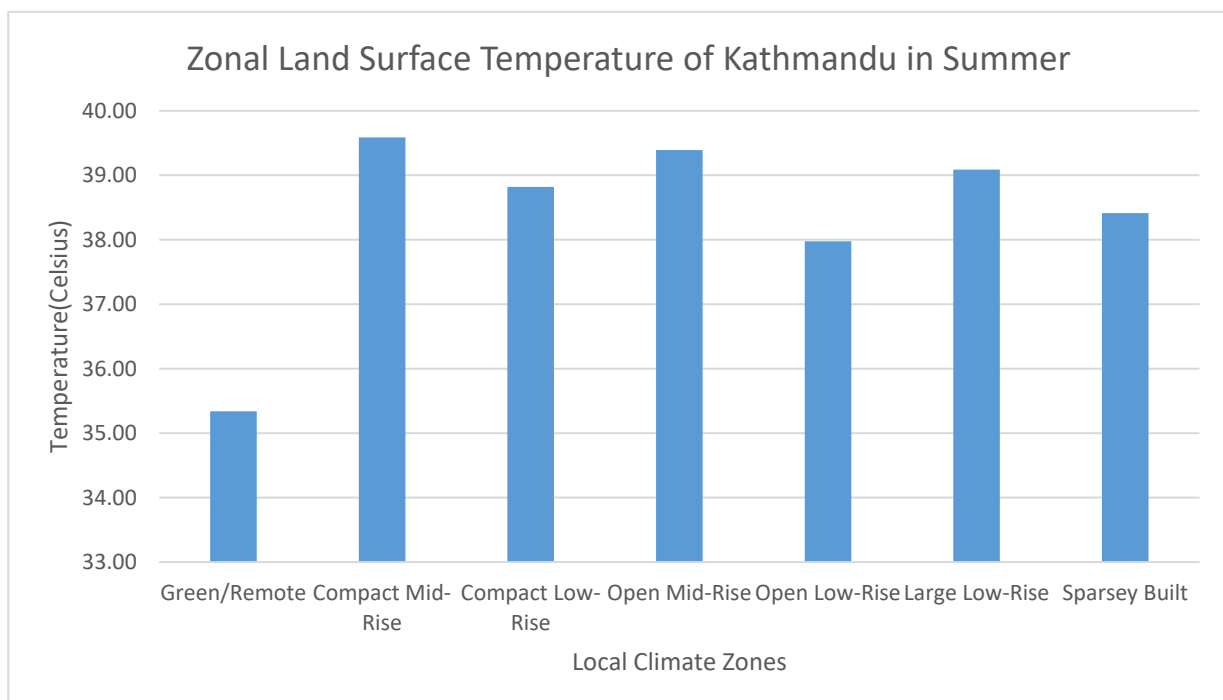
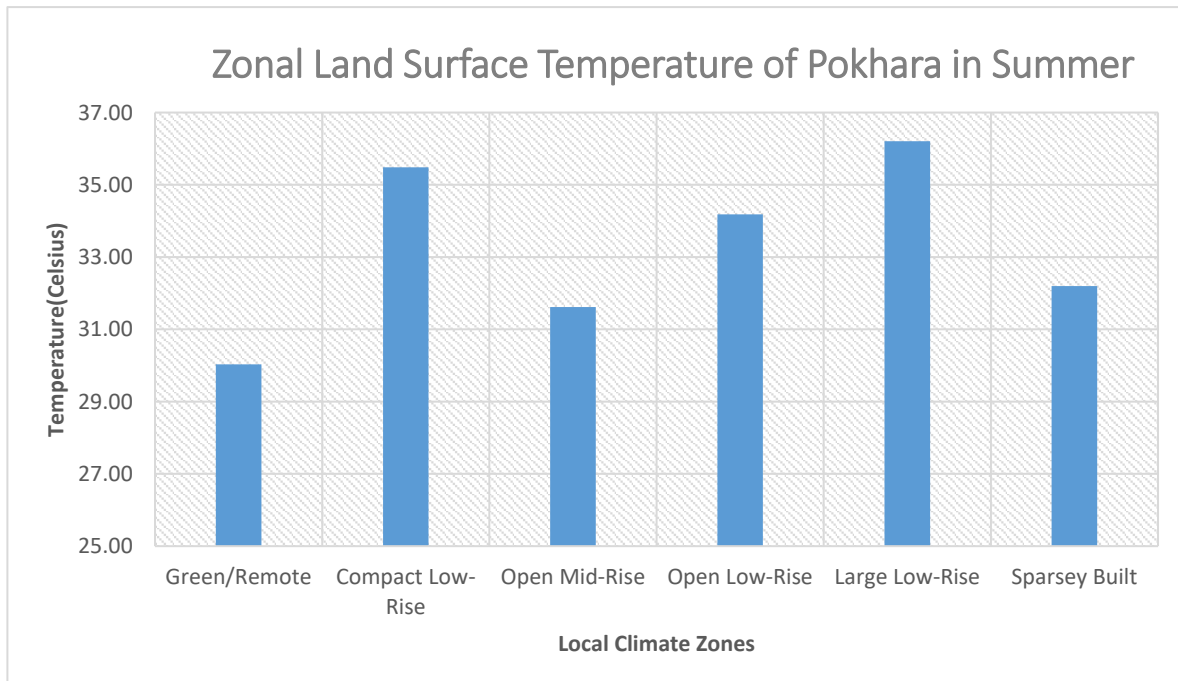


*Figure 41:Zonal Land Surface Temperature of Pokhara (Top) and Kathmandu (Bottom) in Summer*

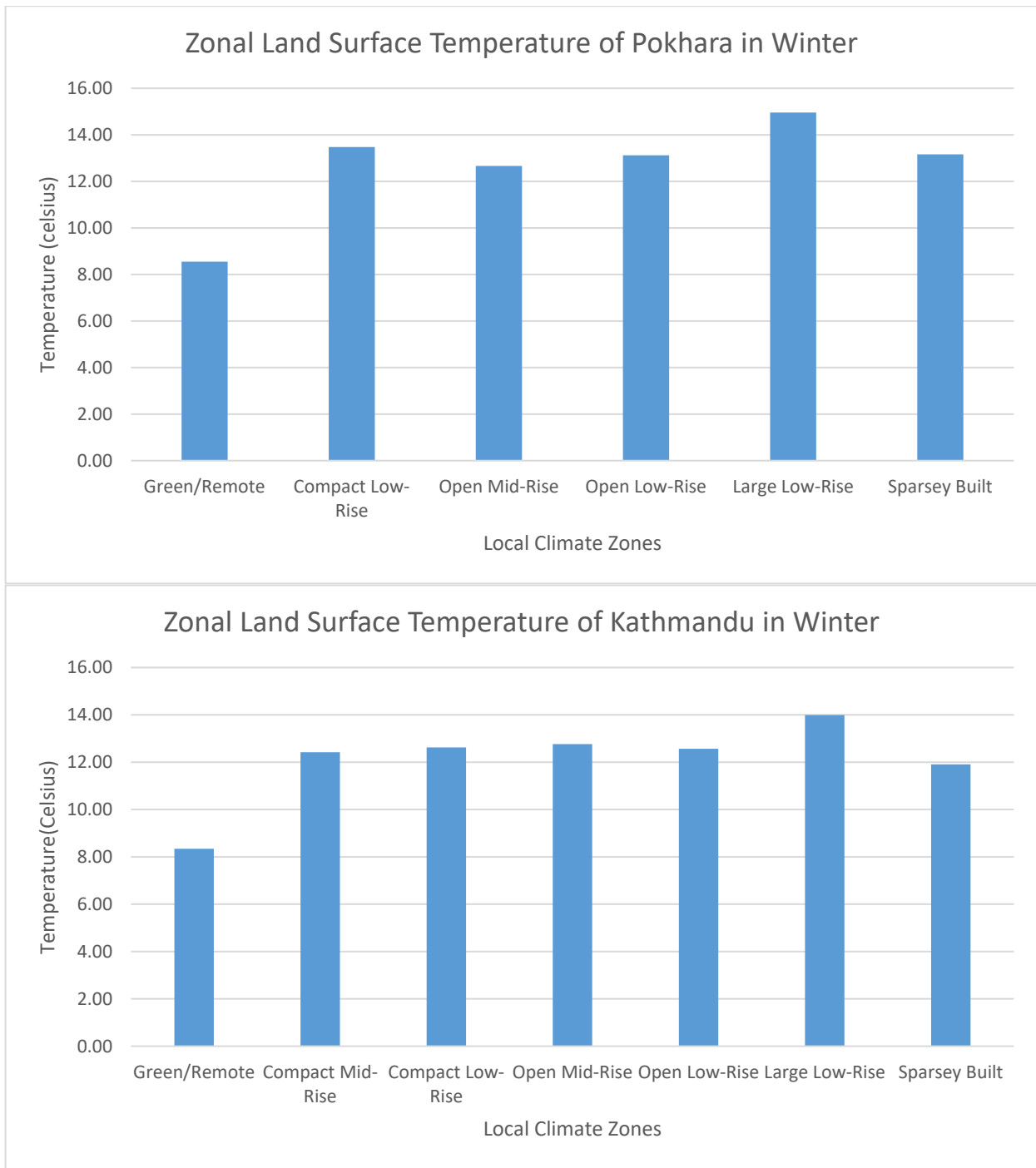


Figure 42 : Zonal Land Surface Temperature of Pokhara (Top) and Kathmandu (Bottom) in Winter

The table presents an analysis of the Mean Land Surface Temperature (LST) for various Local Climate Zones (LCZs) in the cities of Pokhara and Kathmandu, based on the CGCLCG MODIS dataset. Notably, this dataset does not include data for the *Compact Mid-Rise* zone in Pokhara, likely due to the absence or limited extent of this specific urban form in the city. Each LCZ category represents a distinct type of urban environment, from natural or green areas (remote zones) to varying densities of built-up zones (compact, open, large, and sparsely built), each of which has distinct temperature characteristics.

The analysis of Mean Land Surface Temperature (LST) across different Local Climate Zones (LCZs) in Pokhara and Kathmandu reveals key insights into the Urban Heat Island (UHI) effect in these cities.

Green or remote areas in both cities register the lowest LSTs, with Pokhara at 30.03°C and Kathmandu higher at 35.34°C, indicating that natural landscapes help mitigate urban heat, though Kathmandu's green areas are still warmer, likely due to the overall urban density. Compact zones, especially compact mid-rise areas in Kathmandu (39.59°C), display the highest temperatures due to dense buildings and limited vegetation, which trap and radiate heat, intensifying the UHI effect. Open zones, both mid-rise and low-rise, show slightly lower LSTs than compact zones, as increased spacing between buildings improves airflow and reduces heat retention; however, Kathmandu's open zones (39.39°C for mid-rise) are still warmer than Pokhara's (31.62°C). In large low-rise zones, where buildings are typically expansive and include suburban or industrial areas, both cities show substantial heat retention, with Kathmandu at 39.09°C and Pokhara slightly cooler at 36.21°C. Sparsely built areas, characterized by low-density development and more vegetation, moderate the heat somewhat, with Pokhara at 32.20°C and Kathmandu again warmer at 38.41°C. These temperature patterns underscore the more intense UHI effect in Kathmandu, where high urban density, extensive infrastructure, and fewer green spaces elevate LST across all LCZs compared to Pokhara. These findings highlight the need for urban planners to increase green spaces and employ reflective building materials, particularly in compact and large low-rise zones, to mitigate the UHI effect and promote more sustainable and heat-resilient urban environments in both cities.

## 5.8. Findings based on Satellite based Remote Sensing

The analysis of land surface temperature (LST) and vegetation cover, derived through remote sensing, provides insight into the urban thermal dynamics and the Urban Heat Island (UHI) effect in Kathmandu and Pokhara. Kathmandu consistently demonstrates higher LSTs across all Local Climate Zones (LCZs) compared to Pokhara, reflecting its denser urban fabric, extensive infrastructure, and limited vegetation. The Compact Mid-Rise zone in Kathmandu records the highest summer LST (39.59°C), highlighting the role of dense urban development and impervious surfaces in exacerbating heat retention. In contrast, Pokhara, characterized by lower urban density and more distributed vegetation, exhibits comparatively lower LSTs across all zones, with the highest summer LST of 36.21°C in the Large Low-Rise zone. This variation between the cities underscores the significant influence of urban form and vegetation distribution on thermal patterns.

In both cities, Green/Remote areas demonstrate the lowest LSTs during summer, with Pokhara at 30.03°C and Kathmandu at 35.34°C, emphasizing the cooling benefits of natural landscapes. However, the higher temperatures in Kathmandu's green areas suggest that even these zones are influenced by the surrounding urban heat. Open zones, both mid-rise and low-rise, show slightly lower LSTs than compact zones, as the spacing between structures improves ventilation and reduces heat accumulation. However, Kathmandu's Open Mid-Rise and Open Low-Rise zones still exhibit high summer LSTs of 39.39°C and 37.98°C, respectively, compared to Pokhara's 31.62°C and 34.18°C. Similarly, sparsely built areas in Kathmandu show elevated temperatures (38.41°C) relative to Pokhara (32.20°C), further underscoring the intensified UHI effect in Kathmandu. Seasonal differences are evident in the analysis. In winter, the correlation between vegetation (NDVI) and LST weakens, with a positive correlation of 0.78 in Kathmandu and a much weaker correlation of 0.13 in Pokhara. This reflects the limited influence of vegetation during colder months due to reduced plant activity and overall lower temperatures. The LST range during winter is significantly lower, with Kathmandu exhibiting temperatures between 8.34°C and 18.65°C, while Pokhara's winter LST ranges from 8.55°C to 14.96°C. These findings suggest that while vegetation moderates surface temperatures in winter, its impact is less pronounced than in summer.

During summer, the role of vegetation becomes more critical, as indicated by the strong negative correlation between NDVI and LST (-0.66) in Kathmandu. Areas with higher NDVI values

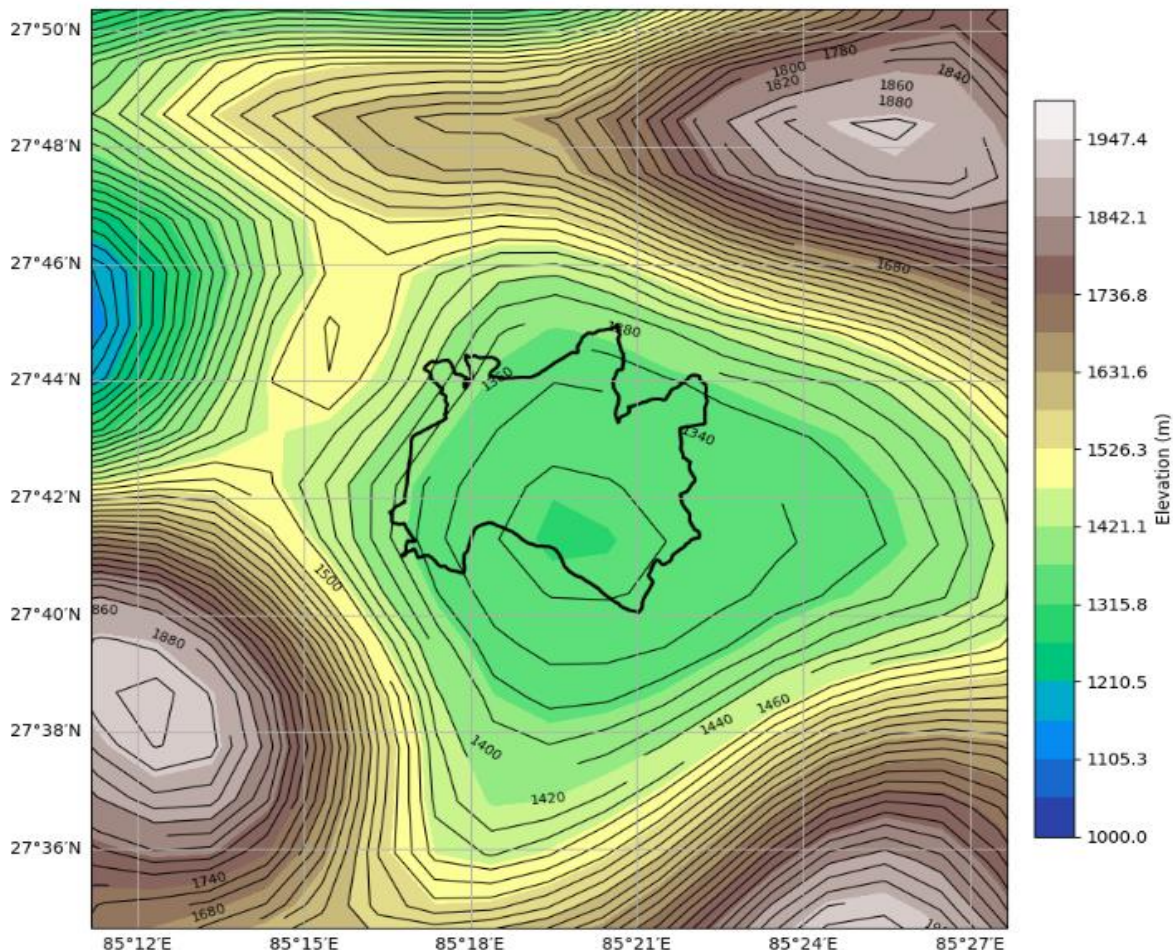
(indicative of more vegetation) exhibit significantly lower LSTs, demonstrating the cooling effects of vegetation through processes like evapotranspiration. In Pokhara, however, an unexpected positive correlation (0.93) between NDVI and LST in summer suggests complex interactions between vegetation, terrain, and land use that may override the typical cooling effect of vegetation. This warrants further investigation to understand localized factors influencing this relationship.

The comparison of both cities highlights the pronounced UHI effect in Kathmandu, driven by its dense urbanization, extensive impervious surfaces, and limited green spaces. Pokhara, while exhibiting some UHI characteristics, benefits from lower urban density and more widespread vegetation, resulting in less intense heat accumulation. The findings underscore the critical importance of green spaces in mitigating the UHI effect, particularly during summer when temperature extremes are most pronounced. Enhancing urban greenery, incorporating reflective building materials, and adopting sustainable urban design practices are essential strategies for reducing LST and improving thermal comfort in rapidly urbanizing cities like Kathmandu and Pokhara.

## 5.9. Post processing of WRF Model output

The post-processing of WRF (Weather Research and Forecasting) model output was performed using Python scripts, CDO (Climate Data Operators), and NCL (NCAR Command Language) scripts, along with visualization tools such as Panoply.

### Topography of Kathmandu

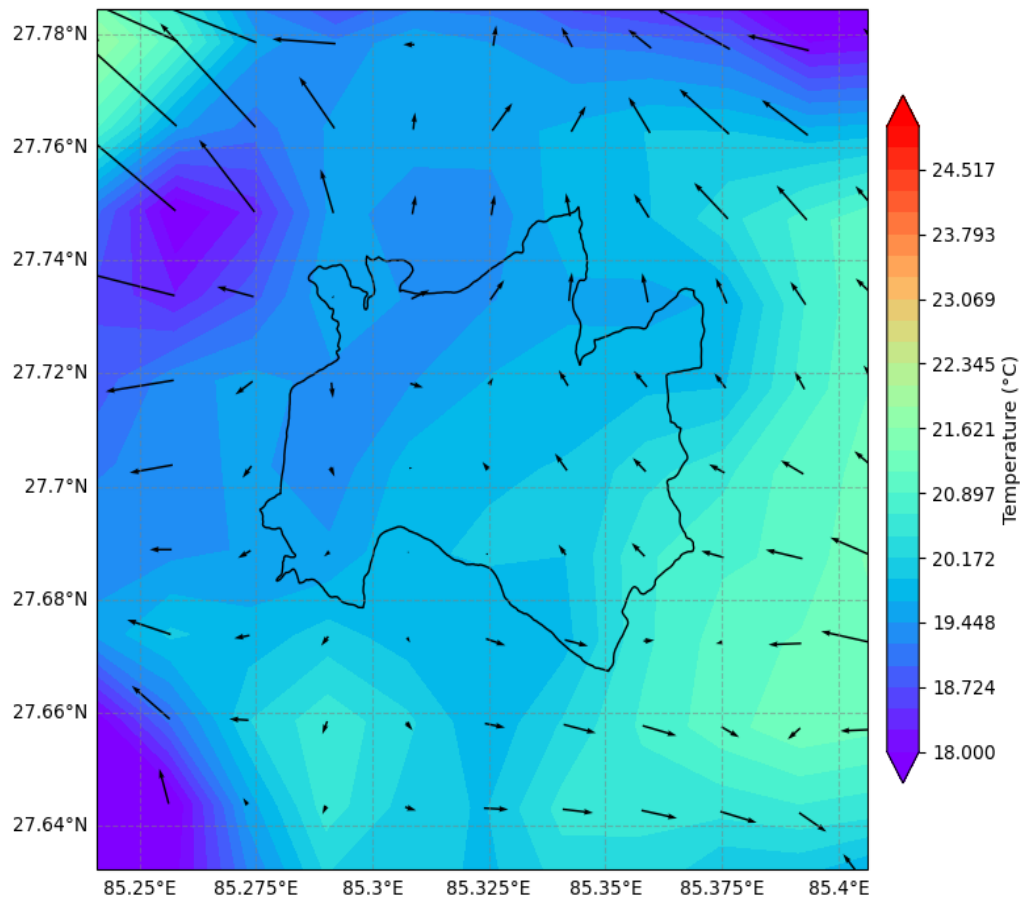


The topography of Kathmandu is characterized by a basin-like structure, with the valley floor surrounded by steep ridges and hills. The elevation in the region ranges from approximately 1100 meters to 1947 meters above sea level, with the average elevation of Kathmandu being around 1400 meters. The central part of the valley is relatively flat or gently sloping, as indicated by the wider spacing of contour lines in the green-colored areas. However, the terrain becomes significantly steeper near the edges of the valley, where closely spaced contour lines mark the abrupt rise of ridges and highlands. The steepness across the region varies between 300 and 500 meters per 3 kilometers.

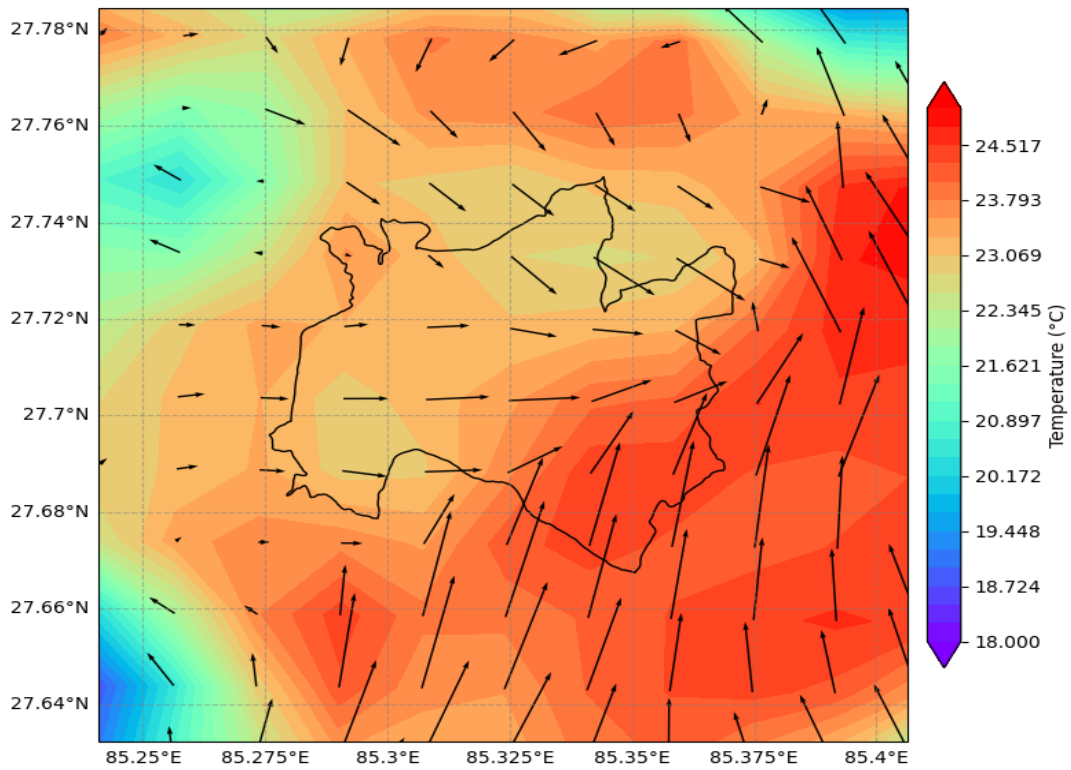
### 3.15.1. Initial Test Run:

- 2023/07/01 6:00 AM (Morning), 2023/07/02 12:00:00 (Noon), 2023/07/01 20:00:00(Night)

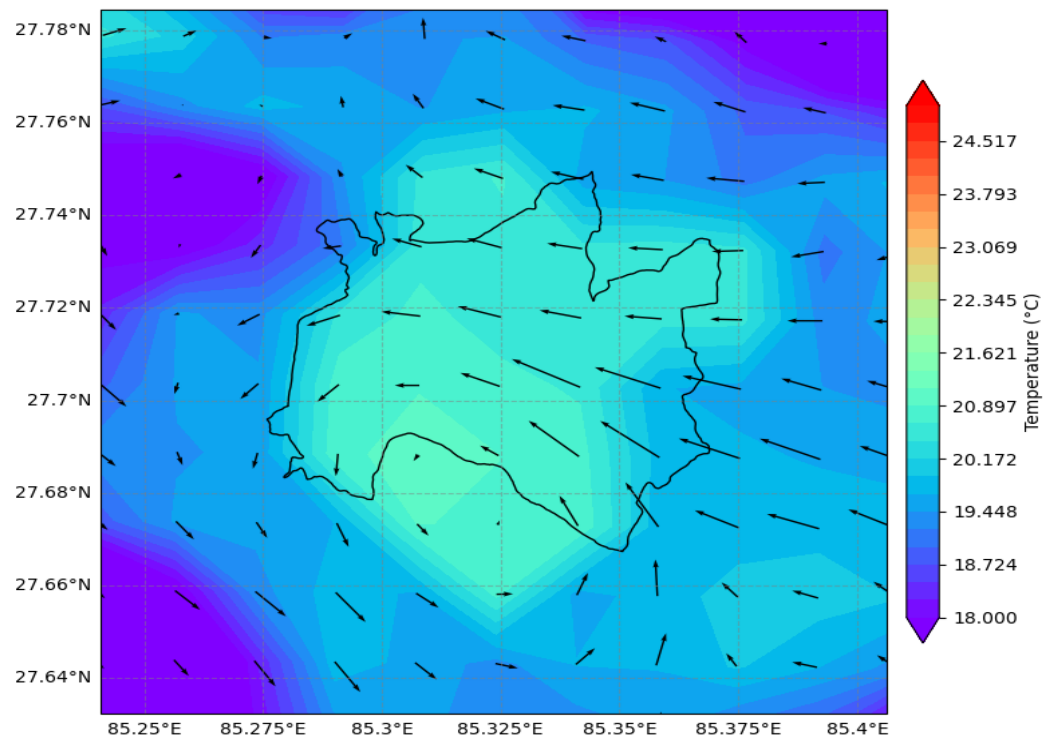
Temperature and Wind Vector Magnitude Map for 2023-07-01 06:00:00



Temperature and Wind Vector Magnitude Map for 2023-07-01 12:00:00



Temperature and Wind Vector Magnitude Map for 2023-07-01 20:00:00



The three initial test runs show temperature maps overlaid with 10 m/s wind vectors magnitude and highlight diurnal variations: cooler mornings with calm winds, midday heating with stronger convection-driven winds, and nighttime cooling with subdued wind activity. This reflects the classical pattern of temperature and wind dynamics for this instance of time.

### 5.9.1. Summer Season (Kathmandu)

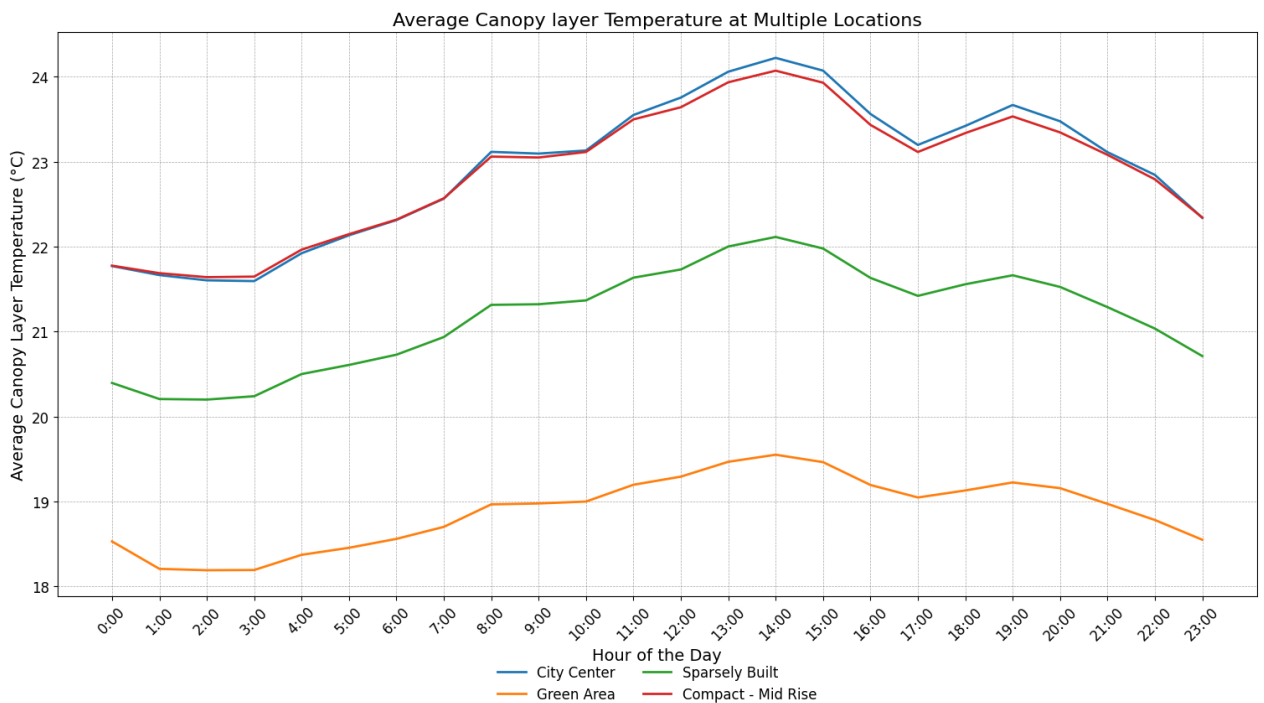


Figure 43: Average Canopy Layer Temperature at Multiple Locations of Kathmandu in Summer-Season

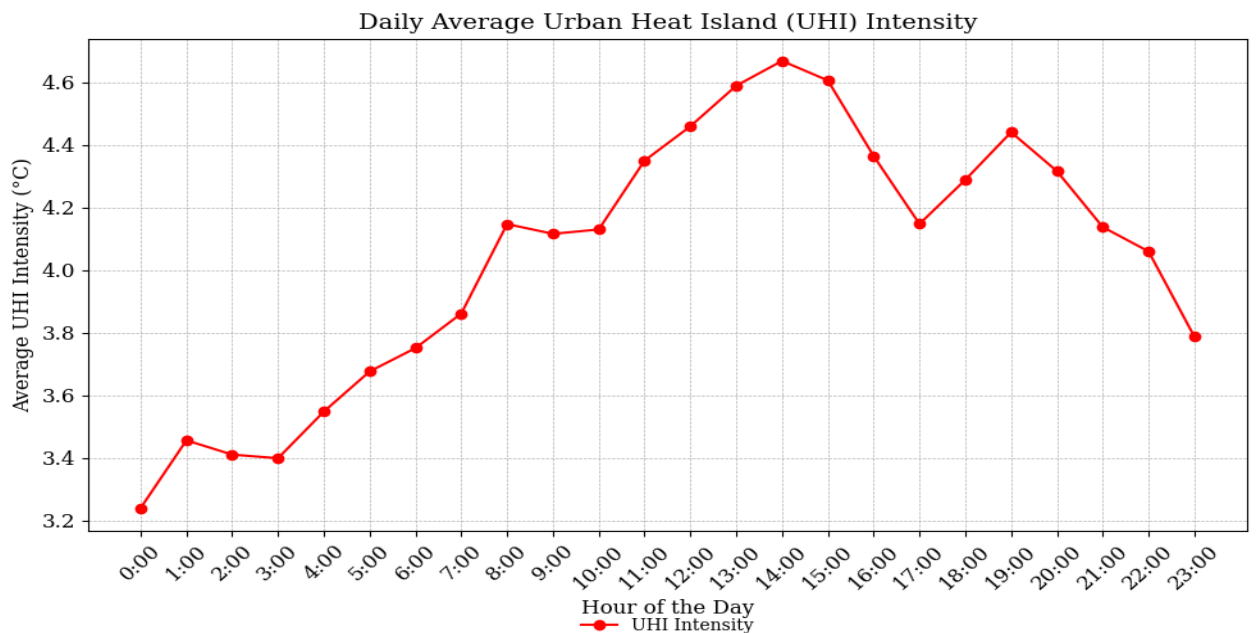


Figure 44 : Daily Average Urban Heat Island (UHI) Intensity in Summer-Season

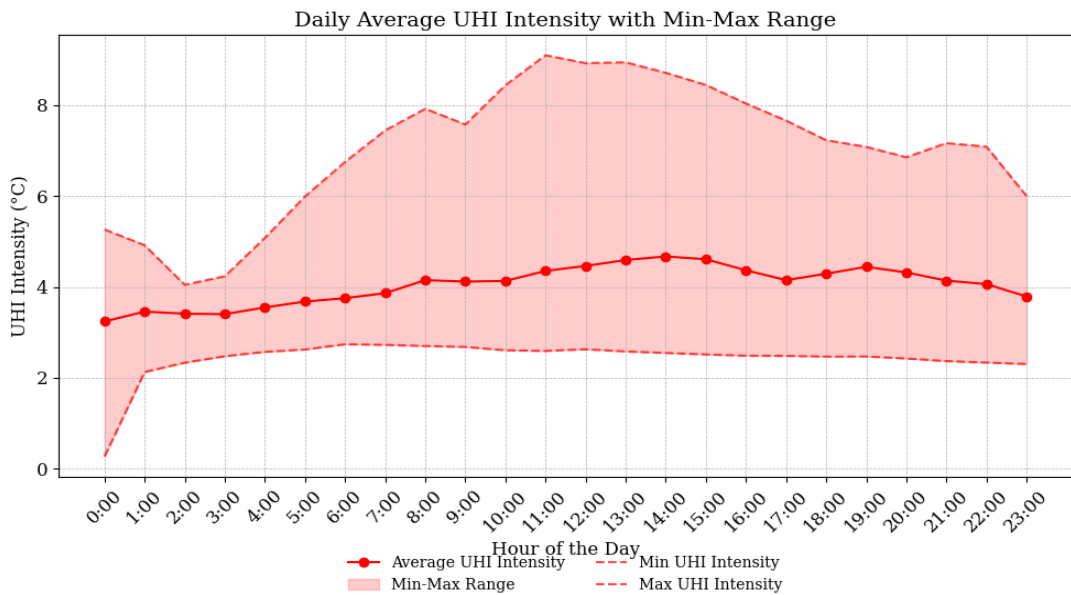


Figure 45 : Daily Average UHI Intensity with Min-Max range in Summer-Season.

7-day simulation was conducted in July 2023 using the Weather Research and Forecasting (WRF) model to study the Urban Heat Island (UHI) phenomenon in Kathmandu. The simulation incorporated MODIS land categorization data to accurately represent urban land-use patterns within the geogrid, ensuring a realistic depiction of various urban and non-urban areas. Figure 43 illustrates the diurnal variation of the average canopy layer temperature across multiple locations in Kathmandu. Key locations such as the city center, green areas, sparsely built regions, and compact mid-rise zones were selected for analysis. The results reveal distinct temperature patterns influenced by land use. For example, the city center and compact mid-rise areas exhibited higher average temperatures due to increased urbanization and reduced vegetation, while green areas demonstrated lower temperatures, reflecting their cooling effect.

Figure 43 presents the daily average UHI intensity over the simulation period, showing how temperature differences between urban and non-urban areas vary throughout the day. The UHI effect was most pronounced during the afternoon and evening hours, peaking around 2:00 PM to 3:00 PM, which aligns with increased solar heating and urban surface heat retention.

Figure 44 further explores UHI intensity, displaying its average, minimum, and maximum values over the course of the day. The shaded region indicates the range of UHI intensities, highlighting variability influenced by meteorological and land-use factors. This figure emphasizes the persistence of the UHI effect, with its impact being significant even during the night due to heat release from urban surfaces.

These results collectively provide a comprehensive understanding of the UHI effect in Kathmandu, illustrating its temporal dynamics and spatial variability. This study contributes to urban climate research by quantifying the influence of land-use patterns on UHI intensity, with implications for urban planning and climate adaptation strategies in the region.

### 5.9.2. Winter Season (Kathmandu)

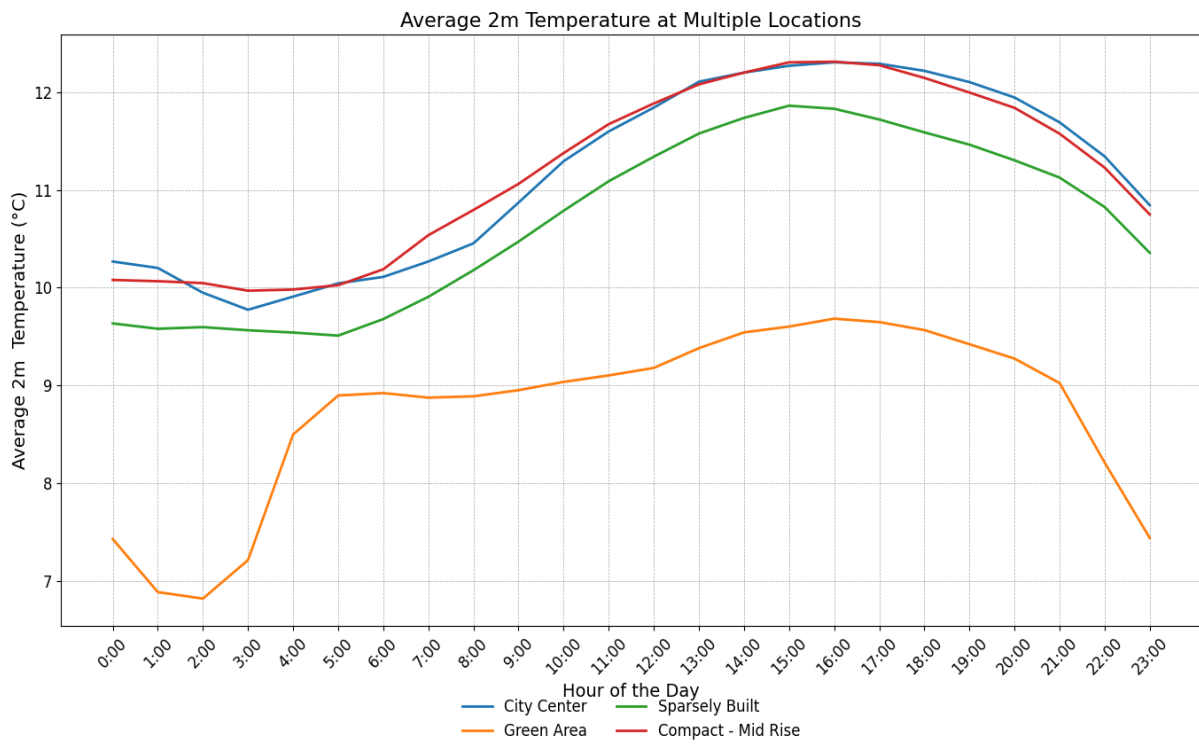


Figure 46 : Average 2m Temperature at Multiple Locations of Kathmandu in Winter

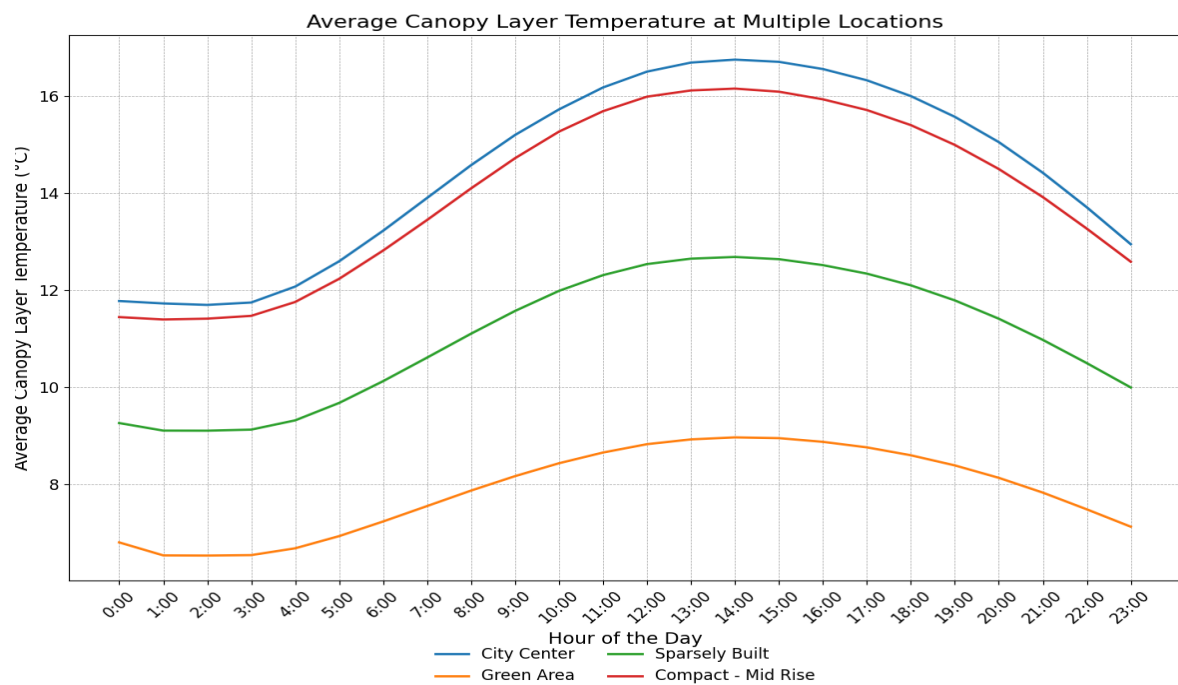


Figure 47: Average Canopy Layer Temperature at Multiple Location of Kathmandu in Winter.

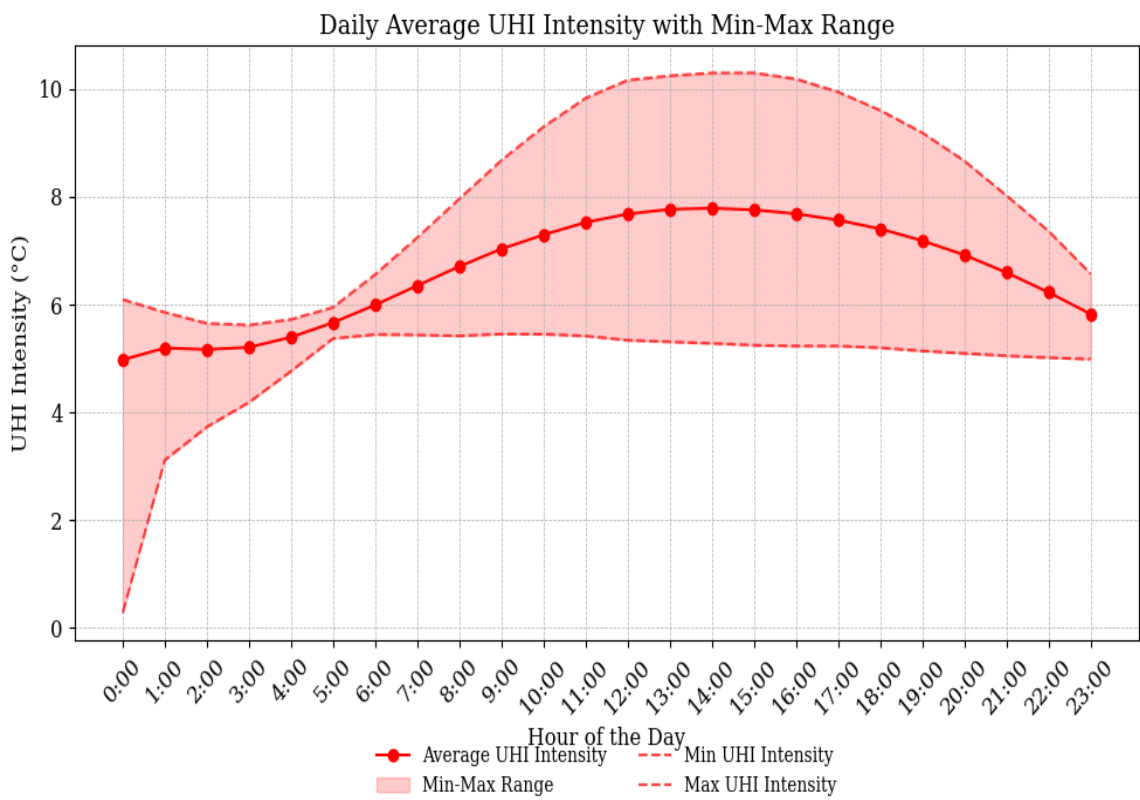


Figure 48 : Daily Average UHI Intensity with Min-Max Range of Kathmandu during Winter

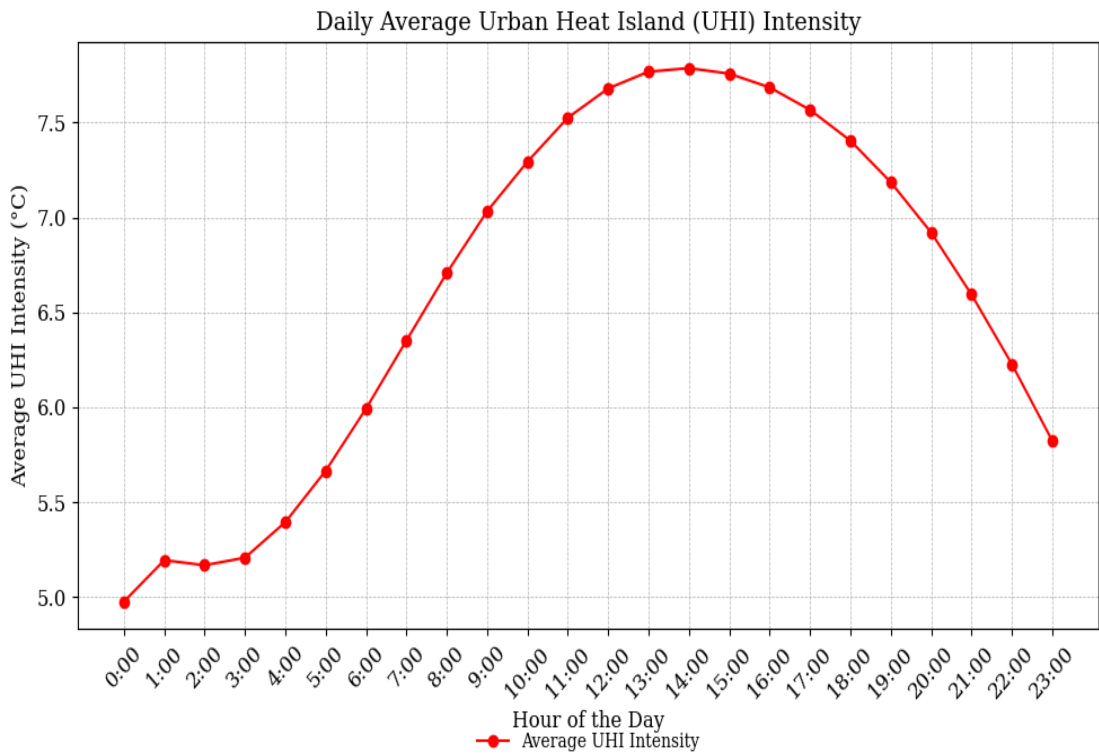


Figure 49 : Daily Average Urban Heat Island (UHI) Intensity

Figure 46 shows the diurnal variation of 2-meter temperatures across four land-use types: city center, sparsely built areas, green areas, and compact mid-rise regions. Urban areas, including the city center and compact mid-rise zones, exhibit higher temperatures throughout the day due to heat retention by urban surfaces and reduced vegetation. Green areas maintain consistently lower temperatures, illustrating the cooling effect of vegetation and reduced urban heat retention. Sparsely built areas lie in between, reflecting a mix of urban and natural characteristics. This pattern emphasizes the urban heat differences caused by surface properties and land use. The average canopy layer temperature for various land-use types in Kathmandu during winter in city center and compact mid-rise areas consistently exhibit higher temperatures throughout the day, with a peak in the afternoon, reaching values around 16°C. This is due to the urban heat retention and reduced vegetation in these densely built areas. Green areas show lower temperatures, reflecting the cooling effect of vegetation and natural surfaces. Sparsely built regions lie between urban and green areas, displaying moderate temperatures influenced by a mix of urban and natural characteristics. The plot highlights the significant variation in canopy layer temperatures caused by land-use differences, with urban regions experiencing more intense heating compared to green spaces.

Figure 47 highlights the daily variation of Urban Heat Island (UHI) intensity, showing the average, minimum, and maximum values, along with a shaded range of variability. UHI intensity increases steadily from the early morning, reaching its peak in the late afternoon when urban surfaces release the most stored heat. The shaded area indicates the variability of UHI intensity across different urban regions, with the maximum intensity diverging significantly from the minimum during certain hours. This plot underscores how urban morphology and surface properties create variability in urban heat retention and release. Figure 48 and Figure 49 show the daily average UHI intensity, showing a smooth curve of urban heat amplification throughout the day. The UHI intensity rises gradually in the early morning, peaks in the late afternoon or early evening, and declines steadily during the night. This trend aligns with the heating and cooling cycles of urban surfaces, which absorb solar radiation during the day and release stored heat during the evening. The plot captures the overall urban heating pattern, emphasizing the temporal dynamics of UHI effects in Kathmandu during winter.

## Chapter VI: Conclusion

This study provides a comprehensive analysis of the Urban Heat Island (UHI) phenomenon in Kathmandu and Pokhara, utilizing land surface temperature (LST) data and vegetation indices derived from remote sensing, along with advanced simulations using the Weather Research and Forecasting (WRF) model. The findings reveal critical insights into the spatial and temporal dynamics of the UHI effect, emphasizing the significant influence of urbanization and land-use patterns on surface temperatures in both cities.

### 6.1. Urban Heat Island Dynamics in Kathmandu and Pokhara

The analysis shows that Kathmandu experiences a more intense UHI effect than Pokhara, driven by its dense urban fabric, extensive impervious surfaces, and limited green spaces. Across all Local Climate Zones (LCZs), Kathmandu consistently records higher LSTs compared to Pokhara, with the Compact Mid-Rise zone in Kathmandu reaching a summer peak of 39.59°C. In contrast, Pokhara, with its lower urban density and widespread vegetation, exhibits comparatively lower LSTs, peaking at 36.21°C in the Large Low-Rise zone. Green or remote areas in both cities demonstrate the lowest LSTs, highlighting the cooling role of vegetation, though Kathmandu's green zones remain warmer, indicating urban heat spillover effects.

Seasonal variations further illustrate the role of vegetation in moderating surface temperatures. During summer, a strong negative correlation between NDVI and LST (-0.66) in Kathmandu underscores the cooling impact of vegetation through evapotranspiration. However, in Pokhara, an unexpected positive correlation (0.93) suggests complex interactions between local climatic, geographic, and land-use factors. In winter, correlations weaken, reflecting reduced vegetation activity and lower overall temperatures, with LST ranges significantly lower in both cities.

### 6.2. WRF Model Simulations for Kathmandu

The comprehensive analysis of the Urban Heat Island (UHI) phenomenon in Kathmandu, based on a 7-day simulation in July 2023 and evaluations during the winter season (January), underscores the interplay between urbanization, land-use patterns, and atmospheric processes. The study, employing the Weather Research and Forecasting (WRF) model and MODIS land categorization data, provides critical insights into the temporal and spatial variability of UHI intensity and its implications for urban climate dynamics. The simulation results reveal that UHI effects in Kathmandu are most pronounced during summer, driven by the higher solar radiation and heat retention properties of urban materials. Urban areas such as the city center and compact mid-rise zones in Kathmandu exhibit significantly higher canopy layer temperatures throughout the day compared to green and sparsely built areas. The peak UHI intensity occurs during the afternoon, between 2:00 PM and 3:00 PM, when solar heating is at its maximum, and urban surfaces amplify the heat due to their lower albedo and limited vegetation cover. These high temperatures persist into the evening, demonstrating the prolonged heat retention and release from impervious urban surfaces in winter. UHI intensity follows a similar diurnal pattern, albeit with lower overall temperatures. Urban areas retain their characteristic higher temperatures compared to green and sparsely built zones, with the city center and compact mid-rise regions exhibiting daytime peaks around 16°C in winter. The difference in temperature between urban and green areas highlights the impact of urban morphology and land-use patterns, even during colder months when vegetation activity and solar radiation are reduced.

The daily variation of UHI intensity during winter demonstrates a steady increase from early morning, peaking in the late afternoon when urban surfaces release the most stored heat, before gradually

declining at night. This pattern mirrors the heating and cooling cycles of urban surfaces, with maximum UHI intensities occurring during times of peak solar energy absorption and minimum heat dissipation. The shaded variability range indicates that UHI intensity is influenced by localized factors, such as differences in land cover, building density, and atmospheric conditions.

### **6.3. Comparison of UHI intensities in Kathmandu and Pokhara**

The analysis of Urban Heat Island (UHI) intensity in Kathmandu and Pokhara reveals significant differences in the magnitude and spatial distribution of the phenomenon between the two cities. Kathmandu exhibits a higher UHI intensity compared to Pokhara, driven by its denser urbanization, extensive impervious surfaces, and limited vegetation cover. Across all Local Climate Zones (LCZs), Kathmandu consistently records higher land surface temperatures (LSTs), with peak summer temperatures reaching 39.59°C in compact mid-rise areas, compared to Pokhara's peak of 36.21°C in large low-rise zones.

The findings show that Kathmandu's UHI effect is particularly pronounced in densely built zones such as the city center and compact mid-rise areas, where urbanization has significantly altered the natural land cover. The higher temperatures in these zones result from heat retention by impervious surfaces, reduced vegetation, and the thermal properties of urban materials. Conversely, green areas and sparsely built zones in Kathmandu exhibit relatively lower temperatures, although they remain warmer than their counterparts in Pokhara.

## References

1. National Geographic, n.d. Urban Heat Island. [online] Available at: <https://education.nationalgeographic.org/resource/urban-heat-island/>
2. Wikipedia, n.d. Urban heat island. [online] Available at: [https://en.wikipedia.org/wiki/Urban\\_heat\\_island#/media/File:Urban\\_heat\\_island.svg](https://en.wikipedia.org/wiki/Urban_heat_island#/media/File:Urban_heat_island.svg)
3. AccuWeather, n.d. How these 5 cities became the most intense urban heat islands. [online] Available at: <https://www.accuweather.com/en/weather-news/how-these-5-cities-became-the-most-intense-urban-heat-islands/981815>
4. EPA, n.d. Using Green Roofs to Reduce Heat Islands. [online] Available at: <https://www.epa.gov/heatislands/using-green-roofs-reduce-heat-islands#:~:text=Green%20roofs%20provide%20shade%2C%20remove,effect%2C%20particularly%20during%20the%20day>
5. Tomorrow's Cities, 2020. Tomorrow's Cities Working Paper #1. [online] Available at: <https://tomorrowscities.org/sites/default/files/resources/2020-11/Tomorrow's%20Cities%20Working%20Paper%20%231.pdf>
6. NASA, 2022. Fundamentals of Remote Sensing. [online] Available at: [https://appliedsciences.nasa.gov/sites/default/files/2022-11/Fundamentals\\_of\\_RS\\_Edited\\_SC.pdf](https://appliedsciences.nasa.gov/sites/default/files/2022-11/Fundamentals_of_RS_Edited_SC.pdf)
7. Jensen, J.R., 2015. Introductory Digital Image Processing: A Remote Sensing Perspective. 4th ed. Pearson.
8. Lillesand, T., Kiefer, R.W. and Chipman, J., 2015. Remote Sensing and Image Interpretation. 7th ed. Wiley.
9. Planck, M., 1914. The Theory of Heat Radiation. 2nd ed. Philadelphia: P. Blakiston's Son & Co.
10. How Things Work, n.d. Physics: Quantum Mechanics - Black Body Radiation. [online] Available at: <https://howthingswork.org/physics-qm-black-body-radiation>
11. USGS, 2018. Landsat OLI/TIRS. [online] Available at: <https://www.usgs.gov>
12. Owen, T.W., Carlson, T.N. and Gillies, R.R., 1998. The use of a vegetation index for assessment of the urban heat island effect. *International Journal of Remote Sensing*, 19(8), pp.1479-1497.
13. NASA, 2023. MODIS Surface Reflectance (MOD09A1) and MODIS Land Surface Temperature and Emissivity (MOD11A2). [online] Available at: <https://modis.gsfc.nasa.gov/data/>
14. National Weather Service, n.d. Planetary Boundary Layer. [online] Available at: [https://www.weather.gov/source/zhu/ZHU\\_Training\\_Page/clouds/planetary\\_boundary\\_layer/PBL.html](https://www.weather.gov/source/zhu/ZHU_Training_Page/clouds/planetary_boundary_layer/PBL.html)
15. Stull, R.B., 1988. An Introduction to Boundary Layer Meteorology. Dordrecht: Springer.
16. ATPI, n.d. Energy Interactions: Absorption, Reflection, and Transmission. [online] Available at: <http://www.shodor.org/os411/courses/411b/module03/unit03/page09.html>
17. University Corporation for Atmospheric Research (UCAR), 2021. WRF Users Tutorial Presentations 2021. [online] Available at: [https://www2.mmm.ucar.edu/wrf/users/tutorial/tutorial\\_presentations\\_2021.html](https://www2.mmm.ucar.edu/wrf/users/tutorial/tutorial_presentations_2021.html)
18. Skamarock, W.C., Klemp, J.B., Dudhia, J., Gill, D.O., Barker, D.M., Duda, M.G., Huang, X.Y., Wang, W. and Powers, J.G., 2008. A Description of the Advanced Research WRF Version 3. Boulder, CO: National Center for Atmospheric Research (NCAR).
19. Rouse, J.W., Haas, R.H., Schell, J.A. and Deering, D.W., 1973. Monitoring vegetation systems in the Great Plains with ERTS. *Third ERTS Symposium, NASA SP-351*, Washington, DC, pp.309-317.

20. Sobrino, J.A., Jiménez-Muñoz, J.C. and Paolini, L., 2004. Land surface temperature retrieval from Landsat TM 5. *Remote Sensing of Environment*, 90(4), pp.434-440. DOI: 10.1016/j.rse.2004.02.003.
21. Weng, Q., Lu, D. and Schubring, J., 2004. Estimation of land surface temperature–vegetation abundance relationship for urban heat island studies. *Remote Sensing of Environment*, 89(4), pp.467-483. DOI: 10.1016/j.rse.2003.11.005.

## List of Figures

Figure 1: Urban Heat Island Profile, [Wikipedia,n.d.] .....	1
Figure 2 : Earth's Energy Budget [NASA,2022].....	4
Figure 3 : Spectral Irradiance of Blackbody Radiation as a Function of Wavelength for Different Temperatures (howthingswork,n.d.) .....	6
Figure 4 : Example of False-Color Composite for Land Classification. Source: Humboldt State University, Department of Geospatial Sciences.....	8
Figure 5 : Types of Turbulence (National Weather Service, n.d.) .....	9
Figure 6 : Diurnal evolution of the atmospheric boundary Layer (Stull,1998) .....	10
<i>Figure 7 : Variation of temperature with height during (a) Day and (b) Night in the atmospheric boundary layer over land under high pressure system Stull(1998)</i> .....	10
Figure 8: (National Weather Service, n.d.).....	11
Figure 9 : Breakdown of Incoming Solar Energy (ATPI,n.d.).....	12
Figure 10 : WRF Modelling Flowchart (UCAR,2021).....	13
Figure 11 : WRF processing system (UCAR,2021) .....	14
Figure 12 : Defining WRF Domain (UCAR,2021).....	15
Figure 13 : Staggered Grid Structure Showing U, V, and $\theta$ Points in METGRID .....	16
Figure 14 : Schematic of the single-layer urban canopy model.( Kusaka and kimura ,JAM 2004) .....	16
Figure 15 : Radiation of the single-layer urban canopy model (Kusaka and kimura,2004) .....	17
Figure 16: Kathmandu City (Wikipedia,2020) .....	19
Figure 17 : Pokhara City (Wikipedia,2022) .....	20
Figure 18 : Selected Cities for the Analysis of Urban Heat Island .....	21
Figure 19 : (i) Yearly Variation of Temperature in Winter and summer, (ii) Box-Plot of Seasonal Temperature ,(iii) Average Temperature by Month, (iv) Temperature Anomalies by year. ....	23
Figure 20 : (i) Year Variation of temperature in Winter and Summer (2000-2023), (ii) Average Temperature by Month , (iii) Box Plot of Seasonal Temperatures, (iv) Temperature Anomalies by Year .....	23
Figure 21 : Workflow to Develop CCGLC-MODIS-LCZ (NCAR,2023) .....	24
Figure 22 : LCZ numbering classification used in WRF . ( Stewart and oke,2023 ; Demuzere et al., 2020) .....	25
Figure 23 : MODIS LCZ dataset injected to WRF .....	29
Figure 24: Nested Domain in WRF .....	30
Figure 25:Domain Configured on WPS-4.5 with innermost nested domain over Kathmandu .....	30
Figure 26 : Model Setup in ArcGIS for Processing the MODIS products for Summer cases .....	35
Figure 27 : Model Setup in ArcGIS for Calculation of NDVI from MODIS products for Summer Case .	36
Figure 28 : LULC Unsupervised Classification of Kathmandu .....	38
Figure 29 : LULC Unsupervised Classification of Pokhara .....	38
Figure 30 : Land Use Transformation from 2013 -2023 .....	39
Figure 31 : Local Climate Zone (LCZ) Classification of Pokhara .....	40
Figure 32 : Local Climate Zones (LCZ) classification of Kathmandu .....	41
Figure 33 : (i) Land surface temperature of Kathmandu in Winter, (ii) NDVI of Kathmandu in Winter. (iii) Relationship between NDVI and LST of Kathmandu in Winter.....	42
Figure 34: LST and NDVI classification of Kathmandu during summer.....	43
Figure 35 : Relationship Between NDVI and LST of Kathmandu in Summer.....	44
Figure 36 : Temperature Distribution (Skewed Right) .....	44
Figure 37 : Land Surface Temperature (LST) and NDVI of Pokhara during Winter. ....	45
Figure 38 : Relationship Between NDVI and LST of Pokhara in Winter. ....	46
Figure 39: Land Surface Temperature (LST) and NDVI of Pokhara during summer.....	46
Figure 40 : Relationship Between NDVI and LST of Pokhara during summer.....	47
Figure 41:Zonal Land Surface Temperature of Pokhara (Top) and Kathmandu (Bottom) in Summer .	49

Figure 42 : Zonal Land Surface Temperature of Pokhara (Top) and Kathmandu (Bottom) in Winter ..	50
Figure 43: Average Canopy Layer Temperature at Multiple Locations of Kathmandu in Summer-Season .....	55
Figure 44 : Daily Average Urban Heat Island (UHI) Intensity in Summer-Season .....	55
Figure 45 : Daily Average UHI Intensity with Min-Max range in Summer-Season.....	56
Figure 46 : Average 2m Temperature at Multiple Locations of Kathmandu in Winter .....	57
Figure 47: Average Canopy Layer Temperature at Multiple Location of Kathmandu in Winter. ....	57
Figure 48 : Daily Average UHI Intensity with Min-Max Range of Kathmandu during Winter.....	58
Figure 49 : Daily Average Urban Heat Island (UHI) Intensity .....	58

## List of Tables

Table 1 : Band Designations of Landsat OLI /TIRS.....	7
Table 2: minimum temperature (°C/°F), maximum temperature (°C/°F), precipitation/rainfall (mm/in), humidity, and rainy days from 1991 to 2021, along with the average sun hours for 1999 to 2019,sourced from Climate-Data.org (n.d.) .....	19
Table 3: minimum temperature (°C/°F), maximum temperature (°C/°F), precipitation/rainfall (mm/in), humidity, and rainy days from 1991 to 2021, along with the average sun hours for 1999 to 2019,sourced from Climate-Data.org (n.d.) .....	20
Table 4 : Location of Synoptic Stations obtained from Ministry of Hydrology and Meteorology, Nepal. .....	22
Table 5 : Band Number and Range of Bands used for the false band composite from Landsat 8-9 OLI/TIRS C2 L1. ....	24
Table 6: ZR (Roof level / Building Height) used for Urban Parameterization for running WRF- SLUCM (Single Layer Urban Canopy Model).....	33
Table 7: Mean Land Surface Temperature Based on the Distribution of Local Climatic Zones define by CGLC-MODIS-LCZ dataset of Kathmandu and Pokhara in Summer .....	48
Table 8: Mean Land Surface Temperature Based on the Distribution of Local Climatic Zones define by CGLC-MODIS-LCZ dataset of Kathmandu and Pokhara in Winter.....	48

## Appendices

### Appendix 1 : Calculating Appropriate Number of Processor for WRF Simulation

```
# enter the namelist values of e_we and e_sn
e_we = 200
e_sn = 250

# number of cores you want to use per node (Cheyenne has a max of 36/node)
cores = 36

# The value for 'cores' gets incremented later, so we want a static variable for
# the original value
cores_orig = cores

# set upper limit of nodes - the max you want to loop through
node_max = 200

# This is the least number of grid points allowed for each processor.
# Dont' change this value.
smallest_size = 10

x = 1
while x <= node_max:

    # finds the factor pairs for the total number of cores
    def f(cores):
        factors = []
        for i in range(1, int(cores**0.5)+1):
            if cores % i == 0:
                factors.append((i, cores/i ))
        return factors

    factors = f(cores)

    # Of the factor pairs, this finds the closest values (pair) in that array
    closest_factors = factors[-1]

    # Of the set of closest values, assign the i and j values
    i_array_value = closest_factors[0]
    j_array_value = closest_factors[-1]

    # Calculate how the domain will be decomposed
    e_we_decomp = int(e_we / i_array_value )
    e_sn_decomp = int(e_sn / j_array_value )

    # Once the decomposition becomes smaller than the least number of grid points
    # allowed for each processor, the loop will quit and display the max
    # number of processors and nodes you can use for your domain.
    if ((e_sn_decomp < smallest_size) or (e_we_decomp < smallest_size)):

        # test to see if the max number of processors allowed is within the number for a
        # single node
        initial_factor_pair = factors[0]
        initial_factor = initial_factor_pair[-1]
        if initial_factor == cores_orig:
```

```

# start with value of cores_orig and decrease by 1 for each iteration
# until the value is allowed
    y = cores_orig
    while y >= 1:
        processors = y

# finds the factor pairs for the total number of processors
# still testing processor values for a single node
    def f(processors):
        factors = []
        for i in range(1, int(processors**0.5)+1):
            if processors % i == 0:
                factors.append((i, processors/i ))
        return factors

    factors = f(processors)

# Of the factor pairs, this finds the closest values (pair) in that array
# still testing processor values for a single node
    closest_factors = factors[-1]

# Of the set of closest values, assign the i and j values
# still testing processor values for a single node
    i_array_value = closest_factors[0]
    j_array_value = closest_factors[-1]

# Calculate how the domain will be decomposed
# still testing processor values for a single node
    e_we_decomp = int(e_we / i_array_value )
    e_sn_decomp = int(e_sn / j_array_value )

# Once the decomposition becomes larger or equal to the least number of grid
points
# allowed for each processor, the loop will quit and display the max
# number of processors and nodes you can use for your domain.
    if ((e_sn_decomp >= smallest_size) and (e_we_decomp >=
smallest_size)):
        max_procs = (i_array_value * j_array_value)
        print "max # of processors that can be used is: ", max_procs
        print "max # of nodes that can be used is 1 "
        break

# if you haven't reached your limit, the loop continues
# still testing processor values for a single node
    else:
        y -= 1

# if the size of the domain allows multiple nodes
    else:
        max_procs = (i_array_value * j_array_value) - cores_orig
        max_nodes = (max_procs / cores_orig)
        print "max # of processors that can be used is: ", max_procs
        print "max # of nodes that can be used is: ", max_nodes
        break

# If you haven't reached your limit, the loop continues
    x += 1
    cores = (cores+cores_orig)

```

## **Appendix 2** : Bash Scripts for Extracting and combining the required Variables from NetCDF File.

```
#!/bin/bash
# Define the variables to extract (comma-separated)
VARIABLES="XTIME,XLAT,XLONG,LU_INDEX,T2,TH2,Q2,U10,V10,QC_URB,UC_URB,TC_URB"

# Input directory containing NetCDF files
INPUT_DIR="."

# Temporary directory to store intermediate files
TEMP_DIR=".tmp_selected"
mkdir -p ${TEMP_DIR}

# Output file for the combined variables
OUTPUT_FILE="combined_variables.nc"

# Step 1: Extract the variables from each file
echo "Extracting variables: ${VARIABLES}"
for FILE in ${INPUT_DIR}/wrfout_d03_*; do
    BASENAME=$(basename ${FILE})
    cdo -select,name=${VARIABLES} ${FILE} ${TEMP_DIR}/selected_${BASENAME}
done

# Step 2: Merge the selected files along time
echo "Merging extracted files for variables: ${VARIABLES}"
cdo -mergetime ${TEMP_DIR}/selected_* ${OUTPUT_FILE}

# Step 3: Clean up temporary files
rm -rf ${TEMP_DIR}

# Verify the output
if [ $? -eq 0 ]; then
    echo "Successfully created ${OUTPUT_FILE}"
else
    echo "Error: Failed to create ${OUTPUT_FILE}"
fi
```

## **Appendix 3** : Geogrid Configuration

```
&geogrid
parent_id = 1, 1, 2,
parent_grid_ratio = 1, 3, 3,
i_parent_start = 1, 30, 44,
j_parent_start = 1, 33, 38,
e_we = 101, 127, 103,
e_sn = 101, 115, 103,
geog_data_res =
'cgfc_modis_lc+default','cgfc_modis_lc+default','cgfc_modis_lc+default',
dx = 15000
dy = 15000
map_proj = 'lambert'
ref_lat = 27.606
ref_lon = 85.298
truelat1 = 30.109
truelat2 = 30.109
stand_lon = 83.808
geog_data_path = '/home/bdipson/WRF/WPS-4.5/NEW_GEOG/WPS_GEOG_HIGH_RES/>,
```

## **Appendix 4** : Domain Configuration for the use of WRF – Single layer Urban Canopy Model

```
&domains
  time_step = 60,
  time_step_fract_num = 0,
  time_step_fract_den = 1,
  max_dom = 3,
  e_we = 101, 127 ,103,
  e_sn = 101, 115, 103,
  e_vert = 45, 45, 45,
  p_top_requested = 5000,
  num_metgrid_levels = 34,
  num_metgrid_soil_levels = 4,
  dx = 15000, 5000, 1666.66,
  dy = 15000, 5000,1666.66,
  grid_id = 1, 2, 3,
  parent_id = 1, 1, 2,
  i_parent_start = 1, 30, 44,
  j_parent_start = 1, 33, 38,
  parent_grid_ratio = 1, 3, 3,
  parent_time_step_ratio = 1, 3, 3,
  auto_levels_opt = 2,
  max_dz = 1000,
  dzbot = 100,
  dzstretch_s = 1.3,
  dzstretch_u = 1.1,
  rebalance = 1,
  feedback = 1,
  smooth_option = 0,
```

## **Appendix 5:** Physics Setting for the Model

```
&physics
  use_wudapt_lc = 1,
  mp_physics = 10, 10, 10,
  cu_physics = 3, 0, 0,
  ra_lw_physics = 4, 4, 4,
  ra_sw_physics = 4, 4, 4,
  bl_pbl_physics = 1, 1, 1, !11before
  sf_sfclay_physics = 1, 1, 1,
  sf_surface_physics = 2, 2, 2, ! Coupled with Noah
  radt = 12.5, 12.5, 12.5,
  bldt = 0, 0, 0,
  cldt = 5, 5, 5,
  icloud = 1,
  num_land_cat = 61,
  num_soil_layers = 4, ! need to change to a 4 for Noah runs, 2 is for PBL LSM
  sf_urban_physics = 1, 1, 1, ! Urban Canopy Model Call
  pxlsm_smois_init = 0, 0, 0.
/
```